MULTIPLE TRACER BREAKTHROUGH RESOLUTION AT A PUMPING WELL

by

Robert TerBerg

Submitted in Partial Fulfillment

of the Requirements for the Degree of

Master's of Science in Hydrology

New Mexico Institute of Mining and Technology

Socorro, New Mexico

August, 1993

ABSTRACT

The objective of this project is to investigate the separation capability of Strong Anion eXchange - High Pressure Liquid Chromatography (SAX-HPLC) - in resolving multiple arrivals of seven fluorobenzoic acid tracers and bromide at a pumping well. The investigation was complicated by a highly transient flow-field and few differentiated tracers vs. many injection sites. Resolution was accomplished by two approaches. Firstly, various SAX-HPLC analytic methodologies were tested to separate the influences of analytic method instability and background interference effects from tracer recoveries. Secondly, cross verification by a vertically averaged 2D solute transport model, with transient condition input, helped not only to guide interpretation and recognition of errors in analytic methodology, but helped also to resolve the identity, sequence, and character of coalescing arrivals of identical tracers from different injection points.

In testing various SAX-HPLC analytic methodologies on resolving multiple tracer arrivals, three trends were apparent. 1) At low HPLC mobile phase pH conditions, when the acids are for the most part neutral and undissociated, the separation mechanism seemed to be degree of dissociation. 2) As mobile phase pH approached higher tracer pKa values, some other effect, possibly polarity, seemed to influence separation more than degree of ionic dissociation. 3) Retention time drift, or gradual coelution of tracers and background anions, as a function of column deterioration, indicated that SAX-HPLC columns in conjunction with acidic pH mobile phases are susceptible to method instability.

The close correspondence of simulated and observed results for particular arrivals indicated that sample filter retention, in-situ sorption, and sample or in-situ degradation were at best insignificant influences. The most important discrepancies attributable to analytic methodology, between observed tracer behavior and model behavior, were due to the effects of tracer misidentification, background interferences, and detector imprecision. In particular, bromide arrival interpretation was complicated by background interferences that were unresolvable by SAX-HPLC, polyvinyl styrene based ion exchange (IC) columns, or phenol colorometric analytic methods. The main sources of discrepancy, outside of analytic methodology, were geologic heterogeneity, gaps in the acquisition or analysis of samples, and differential migration rates for the tracers. Most of the tracer arrival spreading was due to lateral displacement of layered arrival components due to vertical heterogeneity.

ACKNOWLEDGEMENTS

This independent study received partial financial support from both United States Environmental Protection Agency and the United States Geological Survey. The author would like to thank Dr. John Wilson for securing financial support, and providing optimistic encouragement with critical guidance. Dr. Rob Bowman was very gracious in providing nearly all the HPLC advisory support required for this study; Bill Linderfelt was especially helpful in providing the model, directions, and explanations for the modeling component of the project; and Mark Mansell provided highly appreciated help not only in sample analysis and data processing, but in providing final revisions to this independent study as well. Dr. Charles Mase, Dave Smyth, Youzhi Chen (all of University of Waterloo), Steve Caldwell, and Catherine Lively (both of New Mexico Tech) co-operated tremendously in providing the infrastructure, samples, and preparation of the samples for the project on which this independent study is based. Finally, Jiamin Wan, deserves a special acknowledgement for showing me the power of a positive attitude and a logically organized approach.

TABLE OF CONTENTS

LIST OF FIGURES

LIST OF TABLES

I. INTRODUCTION

Background

A capture zone is defined by the area and associated aquifer volume around a pumping well that contributes to its water supply. The capture zone, or well-head protection area, as defined in the EPA WellHead Protection Area (WHPA) model, released in 1990 by the EPA Office of Groundwater Protection, was introduced by Thiem (1906) and has been clearly outlined in porous media hydraulics texts (Muskat, 1937; Bear, 1979) and in many papers (Keeley and Tsang, 1983; Javendel and Tsang, 1984; Morrisey, 1987; Wilson and Linderfelt, 1991). Although capture zones have been modeled, they have only been measured in terms of hydraulic heads (Bair and Roadcap, 1992; Springer and Bair, 1992), which were converted to flow-lines by the assumption of orthogonality between equipotentials and flow-lines. In the subject of validation and calibration of capture zone models using tracer tests, nobody has previously delineated capture zone extent with a multiple tracer field experiment.

To investigate capture zone extent on the basis of tracer behavior, a field experiment was designed using eight different tracers over a grid of 15 injections points, up-gradient of a fully penetrating pumping well.

Although spatial separation of identical tracers was maximized and combinations of tracers were injected, analyzing samples from vertically discretized intervals of the pumping well yielded two problems in resolving tracer arrivals. Analytic method instability and interference effects by background anions required re-analysis by modified analytic methods. Secondly, an extremely transient flow field complicated efforts at assuring identity and quality of observed tracer arrival data. To that end, preliminary modeling with transient flow field condition input was required to help validate identity, sequence, and character of tracer arrivals.

Objectives

The objective of this thesis was to investigate the separation capability of Strong Anion eXchange - High Pressure Liquid Chromatography (SAX-HPLC) in resolving multiple arrivals of seven fluorobenzoic acid tracers and bromide at a pumping well. This was accomplished by two approaches. Firstly, various SAX-HPLC analytic methodologies were tested to separate the influences of analytic method instability and background interference effects from tracer recoveries. Secondly, cross verification by a vertically averaged 2D solute transport model helped not only to guide interpretation and recognition of gross errors in analytic methodology, but helped also to separate the identity, sequence, and character of coalescing arrivals of identical tracers from different injection points.

Discrepancies between observed tracer behavior and model behavior were discussed in terms of characteristics attributable to analytic methodology. Influences due to model conceptualization and field conditions were acknowledged with explanation for basis of recognition. If sources of data uncertainty due to tracer analytic methodology were over-riding enough to be separately recognizable in end-product data, they were prioritized for consideration in future model conceptualization.

For the benefit of future investigations involving large suites of tracers, such as those used herein, it was imperative that innovations in SAX–HPLC analytic technique be pursued and shared.

II. METHOD AND APPROACH

Field Experiment

The context for the problems in multiple tracer breakthrough resolution was a field experiment conducted at the Camp Borden Canadian Forces Base, Ontario, Canada (see fig.1a). The site had been used for numerous other published experiments, including a long term natural gradient plume experiment (Cherry *et al.*, 1983, and others in Journ. of Hydrol. vol. 63; Sudicky, 1986, and others in Water Resour. Res., 22(13)).

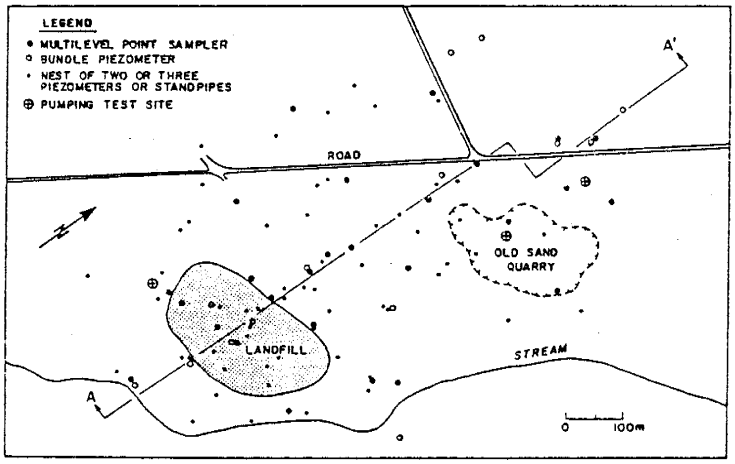

Figure 1a. Site map (from MacFarlane *et al.*, 1983). Field experiment was located near pumping test site (MacFarlane, 1983) in sand quarry. Other instrumentation is from previous experiments.

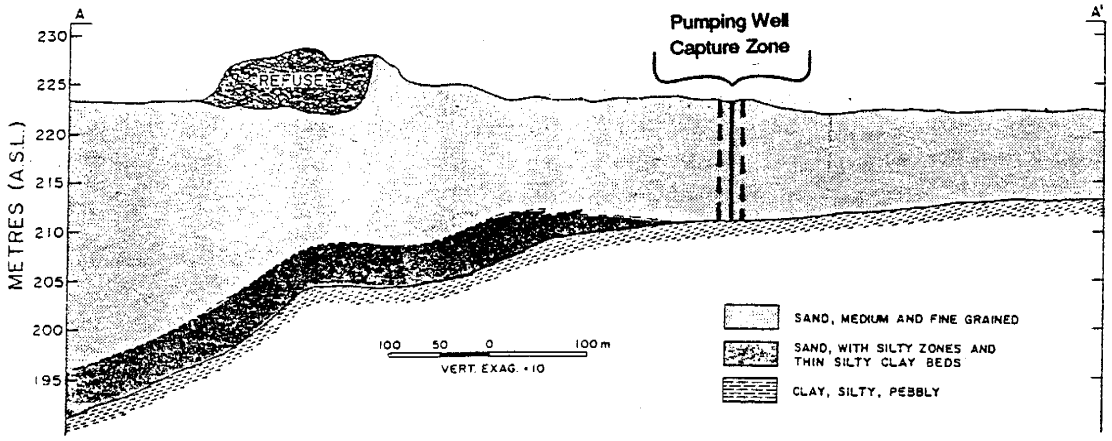

Figure 1b. Site cross-section (from MacFarlane *et al.*, 1983)

The site was in an old flat-bottomed sand quarry where previously overlying material had been used to provide cover material for the landfill at the southern end of the pit. The sand was derived from a glaciofluvial deposit (MacFarlane *et al.*, 1983), but has not yet been characterized to the extent that

a more exact interpretation is available. The sand deposit is 8 m thick, over the area dedicated to our experiment, and overlies an extensive 15–30 m thick clayey silt deposit (MacFarlane *et al.*, 1983). According to Sudicky (1986), the sand deposit was comprised of anastomosing lobes, trending longitudinally north–northeastwards, where the lobes were 1–3 m wide, and 0.2–1.0 m thick, while lengths varied from 1–10 m. The conductivities over the entire deposit varied between 2×10^{-4} m/s and 6×10^{-6} m/s. The most recently calculated geometric mean for those conductivities was 9.23×10^{-5} m/s (Woodbury and Sudicky, 1991).

The experiment took place in an essentially infinite flow domain setting with no nearby effective lateral boundaries and a highly fluctuating ambient flow field. With a water table at 1–2 m depth, the sum of these hydrogeologic features was an ideally unconfined aquifer with minimal leakage. The predominant flow of groundwater was parallel (northeast) to the stream in fig. 1a, but with local bias northwards from the landfill mound to the low-lying area of the pit (see fig.1a & 1b) during the summer. Water level monitoring, at six old piezometers around the test area, revealed that during winter, the ambient groundwater flow was to the north. Through spring, as the snow melted and the ground thawed, groundwater levels rose and created wetlands 50 m east of the pumping well. The flow field subsequently appeared to pivot around the wetlands (area of transient prescribed head), until it was oriented in a northeast direction (Linderfelt, 1993). Least squares surface analysis of the head measurements yielded data on flow direction and gradient from manual water level probe measurements taken about once a week. These data formed key input conditions for modeling (Linderfelt, 1993; see also Appendix II)

The aquifer water quality was a special consideration since interference effects by background anions in tracer sample analyses motivated re-analysis by modified analytic methods. Nicholson *et al.* (1983) found that overall TDS varied from 380 mg/L in uncontaminated water, to 3800 mg/L in a leachate plume, moving northeastwards from the abandoned landfill, along the basal 2.5 m of the aquifer. Chloride and nitrate varied from 1.1 and 0.6 mg/L, respectively, in the uncontaminated water, to 347 and 5.3 mg/L, respectively, in the plume. Other outstanding contaminants included reduced iron, which varied from 0.0022 mg/L in uncontaminated water to 30.3 mg/L in the plume. The reduced iron from the plume intervals of the pumping well caused significant pump clogging problems when it was mixed with shallow zone water and oxidized metabolically by shallow zone bacteria. Nicholson *et al.* (1983) also found the aquifer water pH was 6.8–8.0, and organic carbon level was notably low at 0.8–3.2 millimol/L DOC, thus minimizing the possibility of acidic–organic sorption of the FBA tracers (Boggs *et al.*, 1992).

The spatial distribution of field instrumentation is shown in fig. 2. Given that seven FBAs and bromide were distributed over 15 injection points, the areal locations of the injection points were selected to maximize arrival separation of differently sourced but identical tracer arrivals at the pumping well. At some injection points, in fig. 2 and Table 1, bromide was co-injected as a mass balance check on the accompanying FBA tracer. Tracer injection amounts were set with consideration for HPLC detection limits, modeled dispersivity as a function of travel-time, projected breakthrough at the pumping well, and density induced sinkage. Single pulse injections were used because of tracer expense and our interest in resolving multiple sources of breakthrough concentrations.

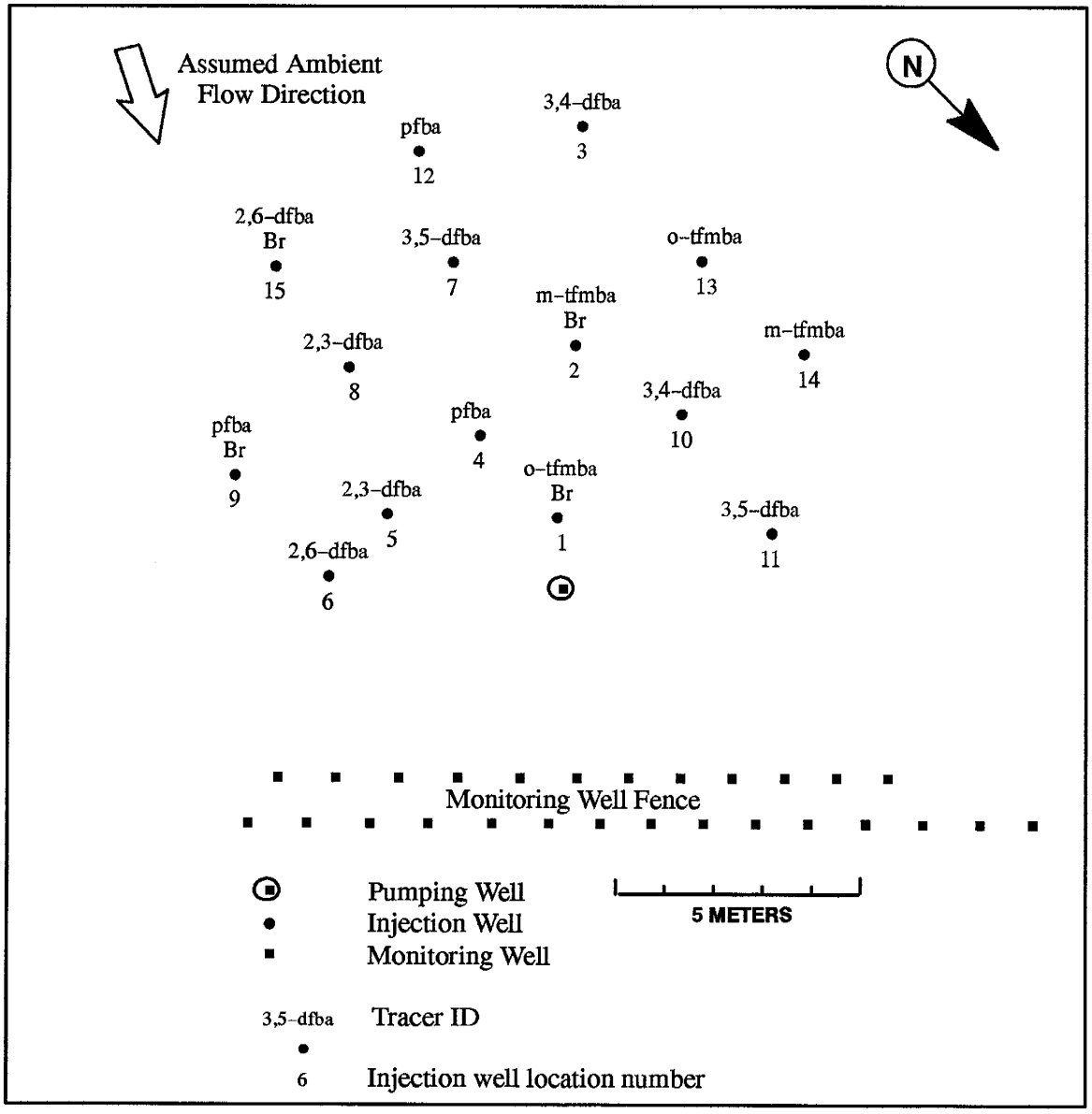

Figure 2. Map view of well network

The injections took place between July 1 and July 6, 1992. According to Linderfelt (1993), at each injection point, a total of 32 L of water, was evenly divided into three different containers. A subset volume of 1 L, from each container, was used to mix the FBA and/or potassium bromide, along with an equimolar amount of potassium hydroxide (see Table 1) to dissociate the acids. Extra potassium hydroxide was used to bring the pH to 7, or near aquifer conditions. The subset volume of prepared solution was poured back into the storage container, mixed, and stored overnight before transport to the field site.

Table 1. Tracer injections (amounts rounded to 0.1 g from field measurements (Linderfelt, 1993))

Inj. well	Injection Date	FBA mass	Bromide mass	KOH mass
I-1	July 1, 1992	o-tfmba 30.1 g	KBr 45.1 g	KOH 10.0 g
I-2	July 1, 1992	m-tfmba 30.2 g	KBr 48.9 g	KOH 9.6 g
I-4	July 1, 1992	pfba 60.3 g	-	KOH 19.0 g
I-5	July 1, 1992	2,3-dfba 60.4 g	-	KOH 23.4 g
I-10	July 1, 1992	3,4-dfba 60.8 g	-	KOH 23.8 g
I-6	July 3, 1992	2,6-dfba 60.4 g	-	KOH 23.8 g
I-8	July 3, 1992	2,3-dfba 60.4 g	-	KOH 24.5 g
I-9	July 3, 1992	pfba 30.2 g	KBr 44.7 g	KOH 9.3 g
I-11	July 3, 1992	3,5-dfba 60.4 g	-	KOH 24.2 g
I-13	July 3, 1992	o-tfmba 60.4 g	-	KOH 20.4 g
I-3	July 6, 1992	3,4-dfba 60.4 g	-	KOH 24.5 g
I-7	July 6, 1992	3,5-dfba 60.3 g	-	KOH 24.4 g
I-12	July 6, 1992	pfba 60.3 g	-	KOH 18.5 g
I-14	July 6, 1992	m-tfmba 60.3 g	-	KOH 20.5 g
I-15	July 6, 1992	2,6-dfba 30.2 g	KBr 44.7 g	KOH 12.6 g

The injection wells had dedicated tubes to three successive 1 m intervals. Air in each injection tube was withdrawn before the solutions were gravity-fed into the aquifer. After injection, 30 ml of deionized (DI) water per meter of tubing length was injected to displace tracer solution from the tube. Containers and valves were rinsed with a liter of DI water three times to prevent cross-contamination from re-use.

Vertically, the tracers were injected through the three 1 m screened intervals from 2.0 to 5.0 m below ground surface. Each 1 m interval had a dedicated 6 mm polyethylene tube with 10 sets of injection holes drilled at 10 cm intervals, using downwardly increasing bit sizes to facilitate uniform injection

over each interval length. To prevent sediment plugging inside the tubing, each perforated interval was wrapped with Nytex screen.

The multi-level pumping well, on which this study of resolving tracer breakthrough is focussed, had seven discrete 1 m sampling intervals from 1 to 8 m depth (see fig. 3). In this form the well provided the following: 1). A fully penetrating line sink over the depth of the aquifer, for theoretical consistency with the investigation of a vertically averaged two-dimensional capture zone. 2). Allowance of smaller injection concentrations since well-bore dilution effects would be reduced. 3). Provision of vertical resolution of tracer arrivals and the governing conductivity distributions.

Like the injection wells, each 1 m interval of the multi-level pumping well had a dedicated 6 mm polyethylene tube with 10 sets of injection holes drilled at 10 cm intervals (see fig. 3). The center stock of the well had the first 2.2 m below ground surface screened from 0.5 m to 2.0 m depth, and the remaining 5.8 m segment separated from the first 2.2 m by a rubber stopper and silicone caulking. In the upper screened interval, a sampling tube was placed in the basal unperforated 0.2 m, so as to keep the pump isolated from water table fluctuations and air intake.

A small pump rate (Q_w=1.5 L/min) was chosen to facilitate an optimal capture zone size that could be covered by available time constraints on tracer reception while minimizing drawdown. Minimal drawdown provided consistency with 2D modeling considerations. The low pump rate also minimized water disposal problems and the potential for interference with other ongoing experiments.

The tubing from the sampling intervals to the pump was routed from the well-head to a heated shed, where a valved header system cycled flow from each line through separate 20 ml sample bottles, before merging the flows into a centrifugal pump. Flow rates for each of the seven individual intervals were monitored with individual visual flow indicators, and regulated for uniformity by needle valves. Upon shifting flow to bypass a sample loop on the valved header system, the respective sample bottle could be removed. Sampling frequency was limited to once a day, in the interests of budget constraints with respect to both sample acquisition and laboratory analysis. Down-stream of the centrifugal pump, a residence tank and a series of in-line filters were used to prevent particulate-induced clogging of total discharge metering equipment. Pump discharge was re-injected down-gradient within the sand pit area, but at distance of 114 m so as to not affect experiment results.

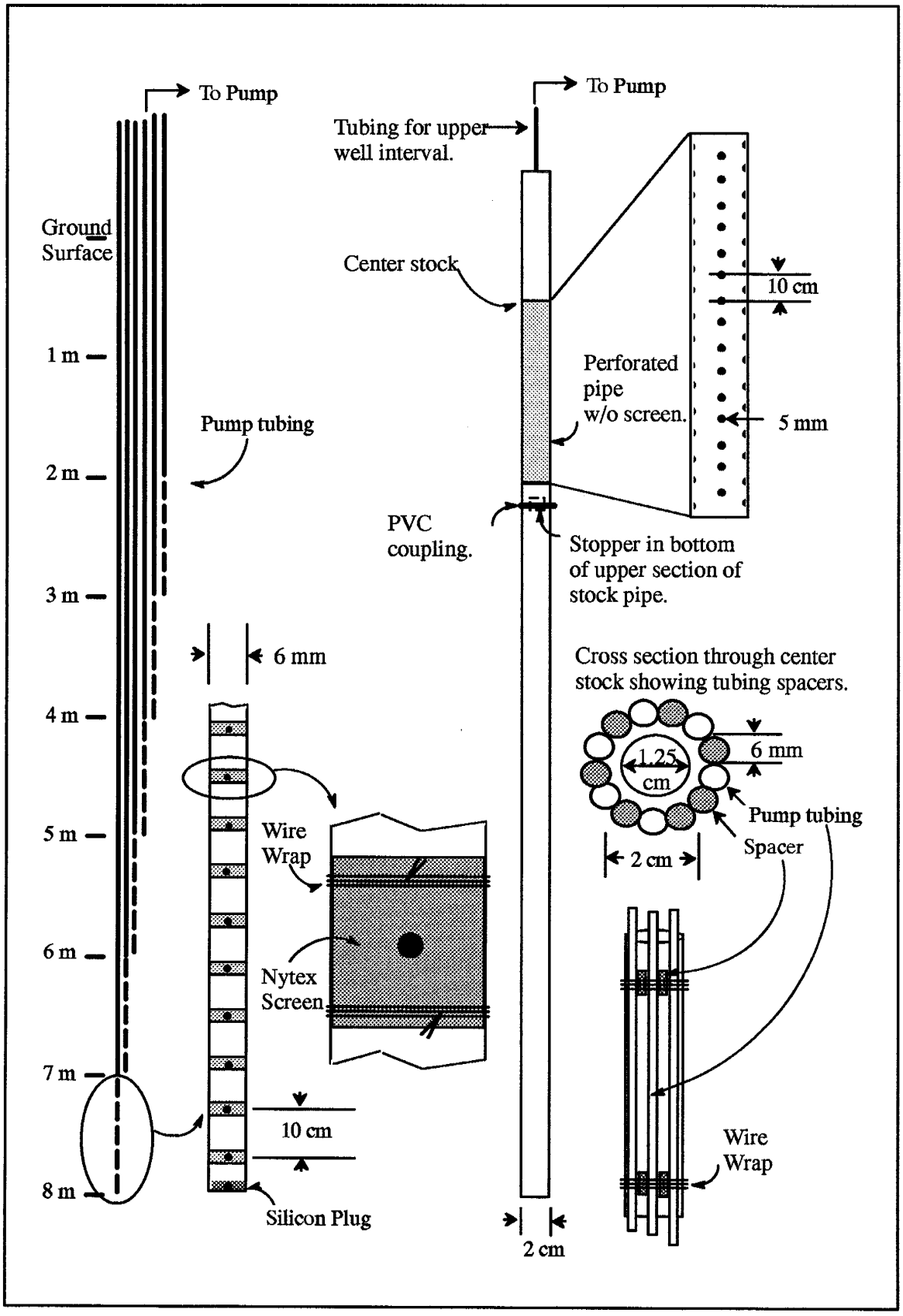

Figure 3. Schematic of pumping well (from Linderfelt, 1993).

Tracer Analysis

The samples were transferred at the field site to HDPE bottles for cold storage purposes and subsequent transport for analysis at New Mexico Tech. Samples received at New Mexico Tech were syringe filtered through disposable 3 mm diameter, 0.45 μm nylon mesh filters (Regis Chemical Co.) into 2 mL glass vials (Sun Brokers), prior to analysis by HPLC methods (see p. 14). The tracers were separated chromatographically by retentive properties on an anion exchange column. A group of elements or compounds with the same retention or elution time in the column, would register coincidentally at the detector. After processing the raw detector signals into chromatograms, sample tracer recoveries were quantified by reference to external calibration standards analyzed between every 10 samples. The calibration suite included three different concentration level standards (approx. 20, 10, and 1 mg/L), and one interference standard consisting of nitrite, nitrate, and chloride, with 2,6-dfba for reference. The quantified tracer recoveries from each interval per day, were weighted by interval pump rate for the given day. Vertical integration of resultant interval contributions yielded a daily value for a depth–averaged breakthrough curve.

The first problem in resolution involved the separation of tracers from each other and from interfering anions resident in the aquifer. Although analytic methods were designed to adequately separate tracers and interfering anions, the methods were unstable. HPLC is a flow–based measuring system and susceptible to drift in retention times, due to variations in temperature, mobile phase conditions, and column conditions. There are long term variations, such as column age, and shorter term variations, such as temperature and individual sample concentration. Retention time drift and resultant coelution of tracers with interference effects could be discerned in the context of chromatograms from individual analyses, sequentially adjacent analyses, replicates, calibration standards, interference standards, and method blanks. Over the course of 1000+ analyses, however, problems had to be prioritized for solution. The most productive approach to quality control was thus to compare actual tracer recoveries to the vertically-averaged predictive simulations in terms of concentration received over time. In this way, discrepancies between expected and received concentration could be quickly isolated to sample dates. Re–analysis of samples with coelution of tracers with interference effects was then undertaken with a mobile phase tailored to maximize separation between the affected tracers and the interfering anions.

The second problem in resolution involved deconvolution of overlapping arrivals. This was made as trivial as possible through the use of a large tracer suite and maximizing space between similar

tracers. Even so, the spreading and coalescence of multiple arrivals due to heterogeneity influences, required that tracer arrival identities and sequences be cross-verified with modeling.

Tracer Breakthrough Modeling

A random walk 2D particle tracker (Linderfelt, 1993), with a random walk module and a histogram module (see p. 26), was used to help identify and verify arrival mass and character. In the random walk module, particles representing tracer mass were given starting coordinates at an injection point in a 2D flow field. The analytic solution, in the random walk module, for the flow field velocities was derived from the superposition of a point sink on a gradient. Each particle was iteratively tracked through the flow field by applying time-step duration to randomized positional velocities derived from the analytic solution. The randomized path-lines of successive particles collectively generated a probabilistic plume of particles. The random walk module output consisted of a report of arrival times for particles breaking through at the pumping well.

The arrivals were sorted and translated to concentration-time arrival coordinates in the separate histogram module. Apparent concentration was derived from the division of total particle mass per time interval by pumped volume per time interval. The pump-rate in the histogram module was assumed to be constant. Thus generated arrival concentrations were subject to dilution error, but arrival times could be used with some confidence to identify and verify observed arrivals.

III. HPLC ANALYSIS

Pumping well samples were analyzed for the tracers using an HPLC separation developed by Bowman (1984; see also Bowman and Gibbens, 1992). The obvious approach to resolving tracer arrivals was to maximize the unique number of tracers involved. Seven fluorobenzoic acids (FBAs) and potassium bromide were used, including four difluorobenzoic acid isomers, two trifluoromethyl-benzoic acids and pentafluorobenzoic acid (see fig. 4 and Table 2). These particular tracers were chosen for their collective attribute of being simultaneously analyzable by the HPLC separation that Bowman and Gibbens (1992) developed. Furthermore, the FBAs are notable for indeterminately low toxicity (as by U.S. federally mandated Material Safety Data Specifications), detectability at low concentrations, absence in nature, and conservativeness outside of areas with high acidic-organic carbon contents (Boggs *et al.*, 1992).

Literature Review on Related Chromatographic Analysis

The basic methodological components of the isocratic HPLC separation, developed by Bowman and Gibbens (1992), included phosphate-based mobile phase, constant pump rate, 25 μL sample injection, silica–packed chromatographic column with Strong Anion eXchange (SAX) bonded phase, and UV detection. The separation mechanism used mobile phase pH, phosphate concentration, and acetonitrile content to differentiate tracer retentiveness, on an anion exchange column, by their degree of deprotonation, or acid dissociation constants (pK_a's). At a mobile phase pH far in excess of the highest tracer pK_a, the FBA tracers were largely deprotonated and, since they were all monovalent in anionic form, largely undifferentiable on an anion exchange column. Thus, effective mobile phase pH was limited to suggested column manufacturer limits for silica-based columns ($2 > pH > 8$) and tracer pK_a range (2.7–3.8).

Pearson *et al.* (1992) used ion chromatography with conductivity detection in the isocratic separation of bromide, a difluorobenzoic acid, a trifluoromethyl-benzoic acid, and a pentafluorobenzoic acid. The methodological components included carbonate/bicarbonate-based mobile phase, constant pump rate, 25 μL sample injection, polyvinyl styrene anion exchange chromatographic column, and UV detection. Although advantages of low detection limit capability were evident, lateral peak resolution suffered from very close elution times and coelution of the trifluoromethyl-benzoic acid with chloride. This method is a standard EPA sanctioned procedure for detecting bromide, since it is very effective in maintaining separation of bromide from chloride and nitrate. In fact, the New Mexico

Bureau of Mines and Mineral Resources (NMBMMR) Chemistry Lab used this method to cross-verify our bromide recoveries (see p. 22).

Howe (1988; see also Boggs and Adams, 1992) used a similar methodology in the isocratic separation of bromide, a difluorobenzoic acid, a trifluoromethyl-benzoic acid, and pentafluorobenzoic acid. Again, a phosphate-based mobile phase was used, in conjunction with a constant pump rate, 25 μL sample injection, a silica-based SAX chromatographic column, and UV detection. Mobile phase pH was 4.0, notably in excess of the highest tracer pK_a. The separation was successful and stable because the tracers were unique enough in polarity to separate in spite of the fact they were largely deprotonated and all monovalent in anionic form. The principle difference between Howe's method (1988) and that of Bowman (1984) was the incorporation of a silica pre-column of the same size as the analytical column. The silica pre-column presaturated the mobile phase with silicate ions so as to protect the analytical column from acidic mobile phase induced dissolution. Both methods incorporated small guard columns packed with the same material as the analytical column. Bowman (personal comm., 1993) found that a silica pre-column did not significantly increase column life.

Stensrud *et al.* (1990) used many of the same methodological components as Bowman (1984) in the evaluation of tracer data from 1988 field experiments at the Waste Isolation Pilot Plant (WIPP) site, near Carlsbad, NM. Four of our fluorobenzoic acids were used including one difluorobenzoic acid, two trifluoromethyl-benzoic acids and pentafluorobenzoic acid. An isocratic separation was invoked by a phosphate-based mobile phase with tetrabutylammonium phosphate to induce ion pairing with the FBA, constant pump rate, 50 μL sample injection, octadecyl silane (C18) chromatographic column, and UV detection. The mobile phase pH was 6.4. The C18 column differentiated ion pairs on the basis of polarity.

Methods and Materials in Chromatographic Analysis

Tracers

The seven fluorobenzoic acids listed in Table 2 were obtained from Yarsley Fluorochemicals Ltd. (UK), while Br^-, in the form of KBr, was obtained from Aldrich Chemical Co. (Milwaukee, WI). The compounds were used without further purification from stock purity, which was 97%. The acid dissociation constants were determined for 0.01M solutions using base titration. Aqueous diffusion coefficients were estimated (Bowman and Gibbens, 1992) from molecular structure using the Hayduk and Laudie method (Tucker and Nelken, 1982).

Figure 4. Tracer molecular structures

2,3-dfba

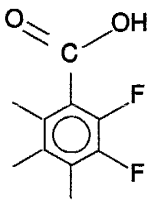

2,3-difluorobenzoic acid

2,6-dfba

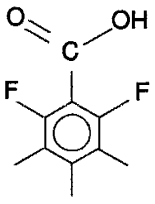

2,6-difluorobenzoic acid

3,4-dfba

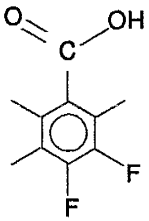

3,4-difluorobenzoic acid

3,5-dfba

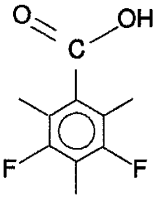

3,5-difluorobenzoic acid

m-tfmba

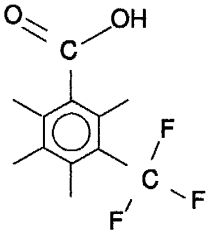

meta-trifluoromethyl benzoic acid

o-tfmba

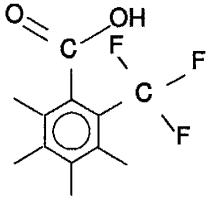

ortho-trifluoromethyl benzoic acid

pfba

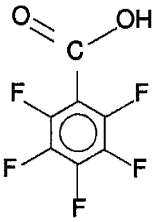

pentafluorobenzoic acid

KBr

potassium bromide

Table 2. Overview of tracer properties

Tracer	pK_a	Dipole Moments (debyes)	Aqueous Diffusion Coefficient ‡ ($10^{-10}m^2/s$)	Molecular Weight (g/mol)	Melting Point (°C)	Cost (US$/100g) July, 1991
2,3-dfba	3.29**	3.05	7.6	158.11 †	161.5-162.5†	236.84 †
2,6-dfba	2.85**	3.16	7.6	158.11 †	158.5 †	22.35 †
3,4-dfba	3.83**	3.05	7.6	158.11 †	120.0 †	346.68 †
3,5-dfba	3.59**	0.24	7.6	158.11 †	120.0-122.0†	236.84 †
KBr	N/A	N/A	18.7	119.01 ♦	734.0 ♦	9.50 ♦
m-tfmba	3.8*	1.93	7.4	190.12 †	111.0 †	105.62 †
o-tfmba	3.0*	3.30	7.3	190.12 †	103.0 †	170.10 †
PFBA	2.72**	1.59	7.2	212.07 †	103.0 †	90.72 †

* Gibbens, 1984

** Benson, 1993

‡ Bowman and Gibbens, 1992

† Yarsley Fluorochemicals Ltd., 1991

♦ Aldrich Chemical Co., 1991

The dipole moments in Table 2 were calculated for the undissociated acid molecules by the Nelken and Birkett (1982) method of dipole moment estimation, based on planimetric tracer molecular structures as displayed in fig. 4. Measured dipole moments can be 10 - 25% different from such estimations. No data was available for the dissociated acid molecules. Hence, the dipole moments are only for purposes of relative comparison in subsequent discussion.

Instrumentation

The instrumentation sequence included the following: Waters Model 501 pump (1.0 to 2.0 mL/min), Perkin-Elmer ISS-200 Autosampler (25 μL sample injections), 4.6mm × 250mm stainless steel SAX column, Waters Model 481 UV variable wavelength detector (wavelength set at 205 nm), HP 3396II integrator, and a real-time linked Chrom-Perfect data management program in an Everex 386 PC. The SAX column brands were: Phenomenex, with Spherex 5-μm SAX particles; and Regis, with 5-μm Spherisorb S5SAX particles. Both the Phenomenex and the Regis SAX packings had 10-nm average pore size and were preceded upstream by an Alltech SAX guard cartridge. The differences between column and guard cartridge packing bonded phases had no distinguishable influence on comparative separation sequences and elution times.

Separation Mechanisms and Methods

The tracers were carried through the instrumentation sequence by a mobile phase with a given molarity of potassium dihydrogen phosphate buffer, a pH adjusted by an equimolar solution of ortho-phosphoric acid, and an addition of acetonitrile as an organic modifier (see Appendix I for exact compositions used). Increased phosphate anion concentration competes with the deprotonated tracers to invoke shorter tracer retention times on the column. Notably, phosphate concentration affects all tracers including bromide in the same way. Thus differences in mobile phase concentration would not rearrange elution sequence, but only have the effect of compressing or expanding the elution sequence. The acetonitrile organic modifier affects FBA retention in a consistent manner, in that higher acetonitrile content quickens FBA elution times but has little affect on bromide. The interaction of pH with the anionic tracers, however, involves degree of acid dissociation. Thus FBA elution is strongly affected by pH while bromide elution is not.

FBA retentiveness in an anion exchange column is related by the Henderson–Hasselbalch (equation 6 and 7) to mobile phase pH and the degree of dissociation for the given FBA. An acid with a pK_a greater than mobile phase pH will remain mostly in undissociated form, while an acid with pK_a less than mobile phase pH will be largely dissociated (see equations 8a and 8b).

$$K_a = \frac{[H][A]}{[HA]} \quad (6)$$

$$pK_a - pH = \log[HA] - \log[A] \quad (7)$$

$pH < pK_a$	$pH = pK_a$	$pH > pK_a$	(8a)
$[A] < [HA]$	$[A] = [HA]$	$[A] > [HA]$	(8b)

In Table 3, the principal variable between different separation methods was mobile phase pH. Acetonitrile content was always held at 18%, while phosphate concentration was tailored to column conditions. For the mobile phases with pH's as follows: 2.60, 2.80, 3.47, and 3.52, the mobile phase molarities were 0.01, 0.02, 0.008, and 0.02. Again, phosphate concentration only had the effect of compressing or expanding the elution sequence.

Table 3. Elution Sequences as a Function of pH (see Appendix I for reference chromatograms)

Tracer	3,4-dfba	m-tfmba	3,5-dfba	2,3-dfba	o-tfmba	KBr	2,6-dfba	PFBA
pK_a	3.83	3.8	3.59	3.29	3.0	N/A	2.85	2.72
pH=2.60	1	2	3	4	5	8	6	7
pH=2.80	1	2	3	4	5	6	7	8
pH=3.47	1	2	3	4	6	5	8	7
pH=3.52	1	2	3	5	7	4	8	6

At a mobile phase pH of 2.60, common ion effects inhibited fluorobenzoic acid dissociation and all of the FBAs were largely undissociated, except pfba. The elution sequence (see Table 3) remained unchanged from pH levels of 2.6 to 2.7, and reflected pK_a progression, in that the tracer with the highest pK_a yielded the earliest elution time. Only bromide could react with the column exclusively by anion exchange, and accordingly, it was the longest retained tracer. The problem with this mobile phase was the lack of adequate separation between 3,4-dfba and m-tfmba. The acidic pH, and possibly hydrolysis, exacerbated this lack of lateral resolution, by dissolving bonded phase. If 3,4-dfba and m-tfmba were initially separated, they would be coeluting after 24 hours of analysis.

Between a pH of 2.70 and 2.80, bromide and 2,6-dfba were very difficult to separate. When mobile phase pH was 2.80, elution order again reflected pK_a progression. Bromide, however, eluted before 2,6-dfba and pfba, with pK_a's of 2.85 and 2.72 respectively. This elution sequence was observed over a pH range of 2.80 to 2.85. The problem with this mobile phase was, again, the lack of adequate separation between 3,4-dfba and m-tfmba. Bromide and nitrate were similarly affected. The acidic pH,

and possibly hydrolysis, dissolved the bonded phase, subsequently inducing coelution of bromide and nitrate after 12 hours and coelution of 3,4–dfba and m–tfmba after 24 hours.

Between a pH of 2.9 and 3.4, bromide and o–tfmba were very difficult to separate. At a pH of 3.47, the pK_a progression was no longer adhered to, except by those tracers with pK_a's greater than 3.0. For the low-pK_a tracers with a high degree of dissociation, the pK_a–related retention mechanism decreased in influence, while it appears that polarity increased in influence. After bromide the elution sequence was o–tfmba, pfba, and 2,6–dfba (see Table 3). From Table 2, it was apparent that the higher polarity of o–tfmba was responsible for it's longer retention time. Similarly, the longer retention of 2,6–dfba vs. pfba indicated that the higher polarity of 2,6–dfba had more influence on the retention mechanism than pK_a. This method was unfortunately used only as a first-time screening method on samples because it coeluted chloride and nitrate over o–tfmba. The separation was found to be considerably more stable than the two previous methods. Identical mobile phases could be used in succession over 48 hours, before bromide would start coeluting with o–tfmba, chloride, and nitrate.

At a pH of 3.52, bromide eluted ahead of 2,3–dfba and the remaining elution sequence was rearranged to the following: 2,3–dfba, pfba, o–tfmba, 2,6–dfba. From Table 2, the dipole moments for the undissociated acids are 3.05, 1.59, 3.30, and 3.16, respectively. This method also coeluted chloride and nitrate over o–tfmba. But, identical mobile phases could be used in succession over 48 hours, before pfba would start coeluting with o–tfmba, chloride, and nitrate. At mobile phase pH's greater than 3.55, bromide and 3,5–dfba coeluted, as well as 2,3–dfba and pfba.

There are three trends apparent in this series of observations. 1) At low mobile phase pH conditions, when the acids are for the most part neutral and undissociated, the retention mechanism appeared to be degree of dissociation. 2) As mobile phase pH approached higher tracer pK_a values, it appears that high polarity serves to increase retention time while degree of dissociation has less influence on retention behavior. 3) Retention time drift, or gradual coelution of tracers and background anions, as a function of column deterioration, indicated method instability, possibly due to hydrolysis or acidic dissolution of the bonded phase by the mobile phase.

One hypothesis for the low pH retention behavior is that the total fraction of dissociated tracer reflects how long the aggregate mass of dissociated [A] and undissociated [HA] tracer is retained by the column. A tracer aggregate with a large fraction of dissociated tracer would be more strongly subject to retention by anion exchange than a tracer aggregate with a small dissociated fraction.

A hypothesis for the higher pH retention behavior is that the tracers may be temporarily bonding and separating according to polarity, especially when tracer pK_a is less than mobile phase pH. This would imply that either the carbon chains holding the quaternary amines to the silica base, or the end-cap methyl groups used to coat leftover silicon-hydroxide sites, were interacting by organic sorptive behavior with the benzoic acid components of the tracers. No long-term pressure increases were noted over the course of column life, indicating that permanent sorption was not a problem. The only indication we had to support organic sorptive interaction as a significant retention mechanism, was that the most highly ionized tracers, bromide, 2,6-dfba, and pfba, had their positions in the elution sequence gradually reordered to reflect the increasing influence of polarity on retention, as pH went above 2.80 (see Tables 2 and 3).

SAX-HPLC Method Optimization

Column deterioration, over extended periods of analysis and exposure to mobile phase, was most evident in gradual coelution of tracers with similar pK_a's, late elution times, or low pK_a's. Specifically, 3,4-dfba and m-tfmba have very similar high pK_a values, while bromide, 2,6-dfba, and pfba had late elution times and low pK_a values. Since the high pK_a tracers adhered to pK_a progression while the low pK_a tracers were the most likely candidates for an organic sorptive retention mechanism, we surmised that column deterioration affected both retention mechanisms equally. The transience of the column conditions demanded different mobile phases over time.

Problems stemming from column deterioration thus included gradual coelution, or retention time drift, method instability, the need for frequent method redevelopment and recalibration, the question of reproducibility between calibrations to new methods, and obviously, high column expenses.

The aspects of retention time drift and method instability were addressed by focussing on flow rate and pH of the mobile phase. At pH's <2 or >8.5, the silica beads and bonded phase in an SAX column break down (Snyder and Kirkland, 1979), the silica beads more so at pH's greater than 8.5. No separations were observed at pH > 3.55, since the FBAs were largely deprotonated and thus undifferentiable (observed) by degree of dissociation, nor, as mentioned earlier, by polarity differences. At pH's of 2.6–2.8, downward adjustments in mobile phase concentration were required after 24 hours of analysis, in order to re-expand shrinking and potentially overlapping retention times. Hence, pH was increased from 2.8 to 3.5. The separations at pH<2.85 were optimized with a flow rate of 2.0 mL/min. A flow rate of 1.0 mL/min or less did not induce appreciable separation between 3,4-dfba and m-tfmba, while increasing analysis time for the complete tracer suite from 15 min to 30 min. Unfortunately, most SAX columns deteriorate prematurely at high flow rates (Phenomenex recommenda-

tion: 0.6 mL/min; Regis recommendation: 0.4 mL/min). At a pH of 3.5, a flow rate of 1.0 mL/min, and a relatively lower starting molarity, downward adjustments in mobile phase concentration were usually required after 48 hours of analysis. As mentioned before, these advantages were nullified by the coelution of chloride and nitrate with o-tfmba. But the acidic pH, high flow rate methods could be set aside for only cross-checking o-tfmba arrivals.

To address the concerns about frequent method redevelopment, recalibration, and the question of reproducibility between calibrations to new methods, single component tracer standards were tested before each mobile phase was used. Secondly, our HPLC analysis involved external calibration. A detector response to a calibration standard suite under one mobile phase condition would thus be exclusively applied to the five samples directly preceding and following that suite. Trying to impose the condition of exact reproducibility at the status quo would have effectively shortened column life to one batch of mobile phase.

To minimize column costs, a discount manufacturer was chosen (Phenomenex) that recycled column bodies. As mentioned previously, differences between column bonded phases had no distinguishable influence on comparative separation sequences or elution times.

Problems in Analysis

Several preliminary measures were undertaken in order to isolate discrepancies between observed tracer behavior and model behavior in terms of characteristics attributable to analytic methodology. Among the aspects considered, before the field experiment started, were: filter retention percentages, peak integration methods, and the sorption and biodegradation of tracers. Other aspects tested over the course of routine analysis were: analytical precision, replicate analyses, and misidentification of tracers.

If sources of data uncertainty due to tracer analytic methodology were over-riding and systematic enough to be separately recognizable in end-product data, they could be considered for incorporation in future model conceptualizations.

Filter Retention Percentages

Sample filtration was necessitated because aquifer samples invariably contained particles in excess of the 0.45 μm maximum threshold permitted in HPLC analysis. Before routine analysis began, a sample of aquifer water from the vicinity of the field experiment was filtered through a 13 mm diameter 0.45 micron nylon mesh filter, which was subjected to scanning electron microscopy (SEM) anal-

ysis. The NMT Materials and Metallurgical Engineering Dept. carried out the SEM analysis on a Hitachi HiScan HHS-2R, at 20 kv accelerating power. After applying a gold-palladium plasma coating to the filter, analysis of the filter element found abundant calcium carbonate, silica particles, as well as flocculated masses of iron hydroxides and clay minerals, all of which corresponded to previous findings (Nicholson *et al.*, 1983). Additionally, early background samples from wells of previous experiments had gelatinous masses of precipitate stained to a rusty brown color, derived from iron-oxidizing bacteria metabolism. The bacterial metabolism and subsequent iron colloid precipitation necessitated the pumped fluid filtration system mentioned in the Introduction chapter (p.9).

In comparing response-peak height-based recoveries of standard and filtered standard solutions, the best response came from positive displacement filtration systems with low dead-volume. A 3 mm diameter syringe filter provided better tracer conservation than an 8.5 mm diameter centrifugal filter (all 0.45 μm nylon mesh). The 3 mm filters were set in hard plastic molds, while the 8.5 mm filters were hand-installed in re-usable flexible translucent polyethylene assemblies. 13 mm - and 25 mm - diameter syringe filters simply had more dead volume to facilitate solute retention upstream of the filter element.

Table 4 shows the mean detector responses, in terms of peak height, to an eight-component standard. One fifth of the milligram amount listed in Table 4 was dissolved in 100 mL of distilled-deionized water. A 25 mL subset was diluted on a 1:1 ratio to make 50 mL. From the 50 mL standard, 2 mL were analyzed without filtration, 2 mL were analyzed after filtration thruough an 8.5 mm centrifugal filter, and 2 mL were analyzed after filtration through a 3 mm syringe filter. An uncalibrated centrifuge was used to spin the centrifugal filter assemblies until all the fluid had passed through the filter membrane. The 3 mm syringe filters were used in conjunction with 2 mL polyethylene syringes. Each of the 2 mL standards was analyzed in triplicate, providing the bases for the reported means. The 100+% pfba recovery illustrates detection imprecision.

Table 4. Mean Response for Filtrations of Standards

Tracer	3,4-dfba	m-tfmba	3,5-dfba	2,3-dfba	o-tfmba	bromide	2,6-dfba	pfba
mg/L	14.4	10.6	10.1	10.2	10.8	11.2	10.2	17.2
unfiltered	330349.	211801.	190025.	135234.	102507.	47603.4	66863.4	34104.7
8.5 mm centrifugal filt.	306481. (92.8%)	186573. (88.1%)	161009. (84.7%)	122973. (90.9%)	92362.4 (90.1%)	43040.1 (90.4%)	60888.2 (91.1%)	32304.0 (94.7%)
3.0 mm syringe filt.	328452. (99.4%)	211555. (99.9%)	172019. (90.5%)	130309. (96.4%)	97141.5 (94.8%)	45046.7 (94.6%)	63267.8 (94.6%)	34202.0 (100.%)

Peak Height vs. Peak Area

The sample filtration experiments yielded several other subsidiary findings, specifically pertinent to calibration. Because of baseline noise, flow deviations, peak-tailing (inherent to very late eluting compounds or the use of an old column), or peak shouldering with interference effects, peak area integration was less consistent for analytical quantification than peak height. The greater degree of variation in reference points from which peak area could be integrated from run to run produced more variation in peak area. For this reason, peak height was used exclusively as the basis for quantifying detector response.

Precision in Analytical Recoveries

Table 5 is a compilation of normalized standard deviations in the responses to three different eight-component standards. Standards #2 and #3 were derived from 1:2 and 1:10 dilutions, respectively, of standard #1. For each of the four mobile phases, described in Table 3 and Appendix I, the three standards were analyzed in triplicate. The standard deviations about the mean response to a given concentration level in each mobile phase were then normalized to form coefficients of variation. The coefficients of variation for each mobile phase were then averaged for each concentration level to give a mean coefficient of variation.

Table 5. Mean Coefficients of Variation (C.V.)

Tracer	Standard #1 (mg/L)	C.V. %	Standard #2 (mg/L)	C.V. %	Standard #3 (mg/L)	C.V. %
2,3-dfba	20.4	0.7	10.2	0.4	2.04	0.7
2,6-dfba	20.4	0.6	10.2	0.4	2.04	0.7
3,4-dfba	28.8	1.1	14.4	1.0	2.88	0.9
3,5-dfba	20.2	0.8	10.1	0.2	2.02	1.6
Br^-	15.0	0.6	7.5	0.3	1.50	1.3
m-tfmba	21.2	2.3	10.6	0.7	2.12	4.3
o-tfmba	21.6	0.5	10.2	0.5	2.16	0.7
pfba	34.4	0.9	17.2	0.7	3.44	1.2

Response variation could be attributed to slight temporal and spatial variations of sorptive properties, within the column, as functions of temperature and mobile phase properties. The relatively higher variation in response to 3,4-dfba and m-tfmba (Table 5) is a reflection of how close the two tracers elute and interfere with each other. The higher response variation to nearly all tracers in standard #3

shows that proportion of detector imprecision increases with decreasing concentration levels. It should be noted that 4.3% of 2.12 mg/L is only 0.09 mg/L.

Sorption

Bowman (1984), Bowman and Gibbens (1992) found that all the tracers used in this investigation have limited sorptive tendencies in batch sorption studies and field experiments involving sandy soils. Boggs *et al.* (1992) and Benson (1993) further qualified the sorptive tendencies with the caveat that acidic-organic environments rich in humus, peat, or coal invoke hydrophobic sorptive interaction with the fluorobenzoic acids. The specific retention mechanism appears to be similar to that between the tracers and the HPLC column, in that an acidic environment inhibits deprotonation in the fluorobenzoic acid tracers thereby preserving their neutral organic character. The shared organic characteristics of tracers and substrate include hydrophobicity, and thus a motivating force to aggregate in an aquatic medium. No batch sorption testing was undertaken. Fortunately, the site was in a former sand quarry, aquifer pH was 6.8 to 8.0 (Nicholson *et al.*, 1983), and injections entered the subsurface at 2 to 5 m depth and left the subsurface from pumping well intervals at 2 to 8 m depth. All depths mentioned were below the soil cover that had developed at the surface since cessation of quarrying at the site.

Biodegradation

During field testing before the experiment, significant problems were encountered with clogging downstream of the sample collection manifold. It was ascertained (C. Richardson, pers. comm., 1992) that the gelatinous iron stained clogging agent was from bacterial metabolism and colonization by Leptothrix sp. and possibly Thiobacillus. Leptothrix sp. derives metabolic energy principally from oxidation of ferrous iron (Atlas and Bartha, 1987). The lower intervals of the pumping well produced water from a leachate plume with 20 to 30 mg/L iron in reduced form (Nicholson, 1983), which when mixed with oxygenated near-surface waters, downstream of the sample manifold, provided a substrate and conditions amenable for the growth of the above-mentioned bacteria. Thus the iron and bacteria were not exposed to each other in the samples. To inhibit bacterial growth at warmer temperatures, the principal consideration for sample storage was cooling. Syringe filtering of the samples prevented bacterial contamination of HPLC equipment.

Leptothrix sp. is nonacidophilic, suggesting a weak predisposition to degradation of the fluorobenzoic acid tracers. This was confirmed in long-term testing of bacteria-rich aquifer water tracer standards. Although there were some deviations induced by a centrifugal filtering technique used initial-

ly, subsequent testing with low dead-volume disposable filters showed no tracer degradation over a period of three months.

Misidentification of tracers

Since the HPLC methods required frequent redevelopment, there were many different opportunities for tracer coelution with interference effects. If a tracer in a calibration standard eluted at the same time as chloride, nitrite, or nitrate did in the associated interference standard, then the interfered tracer would not be quantified in the five analyses preceding the calibration suite, nor the five following it. A set of samples in which such coelution occurred would be reanalyzed with a method specifically developed to resolve that coelution problem.

Another problem in misidentification arose from retention time drift effects induced by different concentration samples. In a separate observation, background samples were supposed to have background concentrations ranging between 300 mg/L TDS, in the uncontaminated upper intervals, to 3800 mg/L TDS in the leachate plume at the base of the aquifer (Nicholson *et al.*, 1983; background samples from the pumping well in this investigation were acquired but did not survive shipment). The predominant background anions in order of decreasing abundance were carbonate, chloride, and nitrate (Nicholson at al., 1983). Chloride and nitrate generally eluted before 2,6-dfba, pfba, and depending on the separation method, bromide and o-tfmba as well. When a column is saturated with high background concentration of chloride and nitrate, the effect on late eluting tracers would be the same as column deterioration. With fewer retention sites available, normally later eluting tracers would elute earlier. Carbonate, on the other hand, was not detectable in a UV spectrophotometer, thus it would have the same effect as chloride or nitrate but on an unknown selection of tracers.

However, the retention time drift did not consistently place analyte elutions early or late with respect to analytes in calibration standards. It was also observed that almost every other sample chromatogram had minor baseline deviations in conjunction with tracer retention time drift, indicating deviations in flow-rate. A third pertinent observation was that filtered samples with known solute concentrations over 500 mg/L, would plug up the column and induce high-pressure shutdowns. This would suggest that high background concentration samples may have induced intermittent flow conditions and unpredictable retention time drift. Fortunately, no pumping well samples induced column plugging or high-pressure shutdowns, indicating that sample concentrations were not likely to have exceeded 500 mg/L.

As a result of intermittent flow conditions, the most common interferences in samples, nitrate and chloride, had their elutions shifted into tracer elution time brackets, or even overlapped on top of tracer elutions. The most badly affected tracer was bromide, since chloride and nitrate would always elute just before and after bromide, respectively. Depending on the elution sequence of a given method, tracers adjacent to bromide would be similarly affected.

Bromide Recoveries

A mass balance for bromide recovery using the SAX–HPLC results was overbalanced by 200%. Initially, it was thought that a consistent interference effect, or background bromide was involved. Since the SAX–HPLC method used in this investigation was susceptible to misidentification of bromide with nitrate or chloride, ion chromatography (IC) and phenol colorometric analyses, performed independently by the NMBMMR Chemistry Lab, were used for cross verification. The phenol colorometric analysis were eventually qualified by NMBMMR as unreliable due to dilution error and inadequate sample volume. The IC method involved a carbonate/bicarbonate mobile phase (1.8 mM Na_2CO_3 and 1.7 mM $NaHCO_3$), 88 µL sample injections, a Dionex 4000i pump (2.0 mL/min), and a UV detector (set at 208 nm), in conjunction with a 4.6 × 100 mm Hamilton PRP–X100 polyvinyl styrene column, and a Millipore–Waters 745 integrator. The method successfully separated chloride and nitrate from bromide by 2 and 3 minutes of retention time, respectively. The IC results for bromide measurement were consistently 50–60% lower than the SAX–HPLC results. For 64 samples re-analyzed by IC, measurements were reported directly to the time–depth–concentration files (appendix III). From those 64 samples, percentages were obtained for their relationship to original analyses by SAX–HPLC. The percentages were then accumulated and averaged so that the mean response by IC would be 58.6% of that acquired by SAX–HPLC results. Standard deviation was an exasperating 21.3%. The given average percentage was applied to all remaining SAX–HPLC results. The combined results from the subset of 64 and the converted SAX–HPLC results were used to comprise the bromide recoveries and the mass balance in Table 6 (p.28).

While having provided a mass balance that was less than an order of magnitude off, the IC results unfortunately did not increase the resolution of the separate arrivals or resolve the interference effects at the 6, 7, and 8 m pumping well intervals. At this point, it was decided that the apparently high bromide concentrations in the lower levels of the aquifer were a consequence of setting up a groundwater field experiment where many others had already taken place over the last 15 years. The number of bromide injections also contributed to dispersive coalescence that made deconvolution questionable.

IV. CROSS-VERIFICATION MODELING

A random walk 2D particle tracker (Linderfelt, 1993), with a random walk module and a histogram module, was used to help identify and verify arrival mass and character. In the random walk module, particles representing tracer mass were given starting coordinates at an injection point in a 2D flow field.

The analytic solution, in the random walk module, for the flow field velocities was derived from the superposition of a point sink on a gradient, in a transient system (Muskat, 1937; Bear, 1979; Keeley and Tsang, 1983; Wilson and Linderfelt, 1993). Assumptions included a fully penetrating pumping well, receiving essentially horizontal flow, from an isotropic, homogeneous aquifer of constant thickness and infinite domain. The solution was simplified by, among other things, the assumption of essentially horizontal flow. By using a fully penetrating pumping well with a very low pump rate (1.5 L/min), minimal drawdown relative to aquifer thickness facilitated the Dupuit approximation for essentially horizontal flow. Horizontal flow, in turn, allowed vertical integration of flow to a point sink. The conceptualization is given in equation (1), where pumping well potential is expressed in terms of pump-rate (Q_w), the transient well function W(u), hydraulic conductivity (K), and aquifer thickness (b). The ambient gradient (J) is defined by ambient unit discharge (q_o=KJ) divided by conductivity (K). Ambient flow direction components are embodied in θ, the defined ambient flow direction.

$$\text{net potential } (\phi) = \frac{-q_0(x\cos\theta + y\sin\theta)}{K} - \frac{Q_w}{4\pi Kb} W(u) \qquad (1)$$

For input conditions, the well is at x=0 and y=0, with x pointing north, y pointing east, and ambient flow direction θ is measured clockwise from the x-direction. The x-direction velocities are derived by partial differential equations of net potential with respect to the x-direction. The y-direction velocity is calculated by a similar development.

$$\frac{\partial\phi}{\partial x} = \frac{-q_0(\cos\theta)}{K} + \frac{Q_w}{2\pi Kb} \frac{x}{(x^2 + y^2)} \exp\left(\frac{-S(x^2 + y^2)}{4Tt}\right) \qquad (2)$$

The resulting system of equations was further simplified with S=0, thereby excluding storage effects from aquifer response and invoking the assumption that drawdown was at a quasi-steady state. This made the model highly sensitive to aquifer conditions and pump-rate. Fortuitously, the pump-rate, and shifts in ambient flow direction and gradient became significant influences in tracer movement over the duration of the experiment (see figs. 5, 6, and 7).

Figure 5. Pump rate (Q_w) over time. (Q_w in m^3)

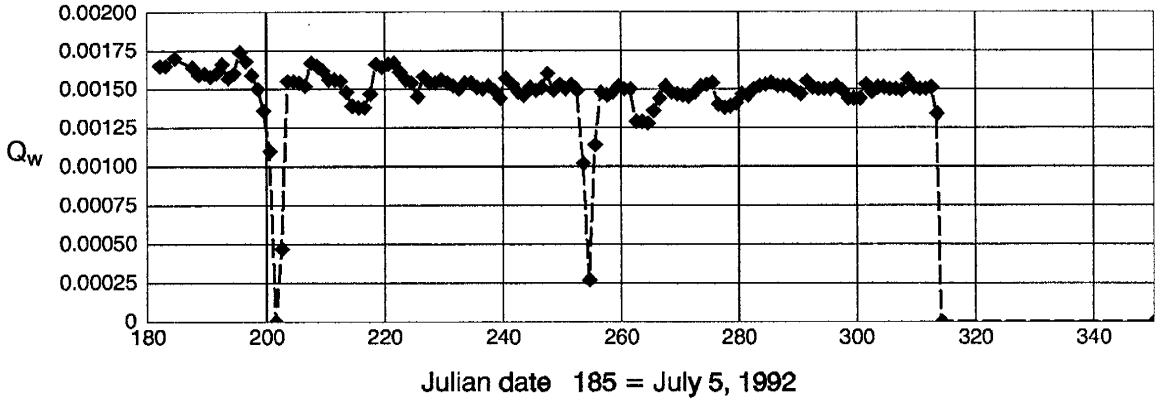

Figure 6. Ambient flow direction (θ) over time. (θ in degrees clockwise from true North).

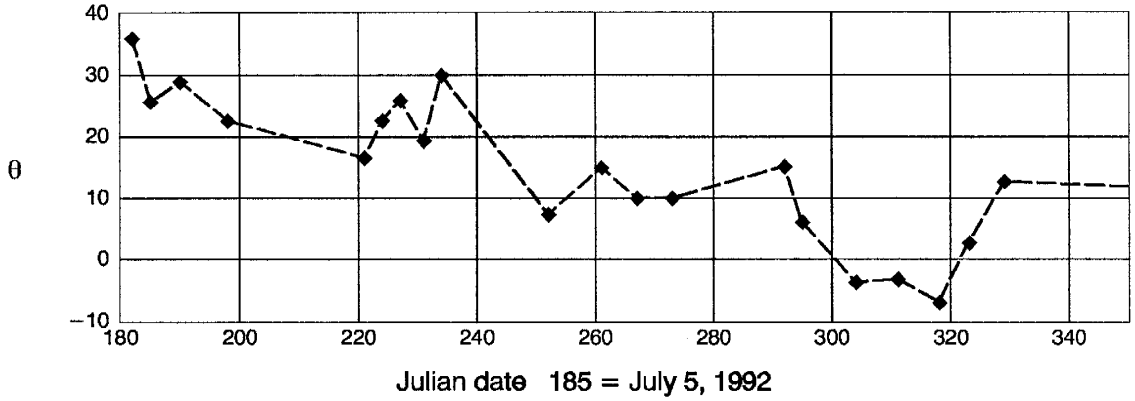

Figure 7. Ambient flow gradient (J) over time

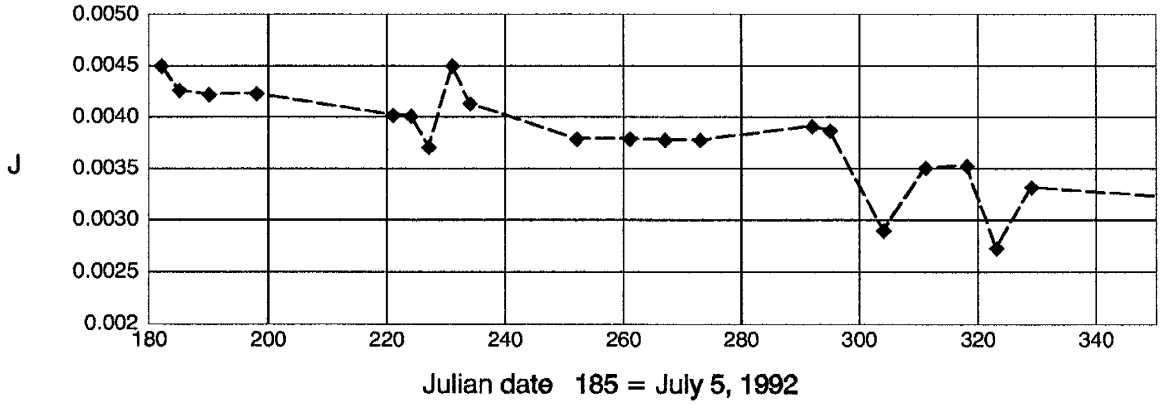

Each particle was iteratively tracked through the flow field by applying time-step duration to positional velocities derived from the analytic solution. To obtain the seepage velocity vectors, Darcy velocities were calculated first (see equations 3 and 4) with the following input constants: initial particle position (x,y), saturated aquifer thickness (b), hydraulic conductivity (K); and the following transient variables for each time-step: pump rate (Q_w, fig. 5), and ambient gradient (J, fig. 6) and flow direction (θ, fig. 7) at the pumping well. Ambient unit discharge (q_o=KJ) was derived from conductivity, which

stayed constant, and ambient gradient, which changed at each time-step. The signs for the terms in equations 3 and 4 are consistent with input conditions. The code however, used opposite signs and modified the input conditions accordingly. Dividing the Darcy velocities by porosity (equation 5) yielded seepage velocity vector components.

$$q_x = -K\frac{\partial\phi}{\partial x} = +q_0\cos\theta - \frac{Q_w}{2\pi b}\frac{x}{(x^2+y^2)} \tag{3}$$

$$q_y = -K\frac{\partial\phi}{\partial y} = +q_0\sin\theta - \frac{Q_w}{2\pi b}\frac{y}{(x^2+y^2)} \tag{4}$$

$$\text{seepage velocity } v_x = q_x / n \tag{5}$$

Dispersive components, derived from Ito Fokker–Planck equation, were then added to the velocity vectors (Uffink, 1989). The random walk aspect was applied by multiplying the transverse and longitudinal dispersivity components by randomized factors and adding the products to both the x and y velocity vectors. Each particle was then iteratively tracked along a randomized path-line. The effective result was the generation of a probabilistic plume of particles for each injection.

For our data conditions, it was found that the maximum time step with sufficiently low truncation error–induced lateral path-line deviation was 0.25 days, compared with tests at 1.0, 0.5, and 0.1 day time-steps (Linderfelt, pers. comm., 1993). A Euler-type time-stepping method was used for the sake of simplicity, and since streamlines converge at the pumping well, the effects of drift inherent in Euler time-stepping methods were minimized (Lee, 1986). No provision was incorporated to maintain equal representation across the probabilistic plume front, in the event of scale–dependent dispersion or a divergent flow field. Hence a large number of particles (1000) were required for each injection (see Appendix III).

The random walk module output consisted of a report of arrival times for particles breaking through at the pumping well. These arrivals were sorted and translated to concentration–time arrival coordinates in a separate histogram module. Apparent concentration was derived from the division of total particle mass per time interval by net pump rate from contributing pumping well intervals. Since the observed recoveries, as mentioned before, were from the 3, 4, 5, and 6 m depth intervals, the input pump–rate (0.857 L/min) was $^4/_7$ of the mean total (1.5 L/min). The resulting output was histograms of average concentration over time (see figs. 8b–15b) from each of the four contributing intervals. The pump–rate in the histogram module was assumed to be constant. Thus generated arrival con-

centrations were subject to dilution error, but arrival times could be used with some confidence to identify and verify observed arrivals.

V. OBSERVED VS. SIMULATED RESULTS

Observed Breakthrough Curves

In verifying the observed tracer arrivals, derived from three dimensional solute behavior, with simulated recoveries of vertically averaged two dimensional tracer behavior, several discrepancies had to be addressed. The model did not account for heterogeneous hydraulic conductivity or vertical tracer movement. The observed tracer arrivals at the pumping well, however, were over 2 to 6 m depth (3 through 6 m intervals inclusive), in relation to injections over 2 to 5 m depth, indicating some degree of sinkage (see Appendix IV). To remove the effects of sinkage and dilution from the observed arrivals at the pumping well, daily observed concentrations (C_x) from contributing intervals were vertically integrated and averaged for each day ($(C_3 + C_4 + C_5 + C_6)/4 = \overline{C}_{day}$). This daily average was used in the actual concentration vs. time breakthrough curves of figs. 8a–15a. For days or intervals without samples or analyses, missing tracer observations were interpolated and any measurements below 0.1 mg/L were discarded as background noise. Pump rate and ambient flow conditions were linearly extrapolated over periods without measurements in order to produce apparent observed concentration.

In calculating a daily mass recovered (M_{day}), total daily observed concentration ($4\overline{C}_{day}$) was multiplied by a subset of daily pumped volume (Q_{day}) for each contributing intervals ($4\overline{C}_{day} \bullet (Q_{day} / 7) = M_{day}$). The mass recoveries in Table 6 were computed by summing M_{day} over the duration of the experiment, since uncertain arrival source identities and overlap thereof in the observed recoveries precluded mass balances for individual injections.

Simulated Breakthrough Curves

In the 2D particle tracker from Linderfelt (1993), injected mass was distributed over a given number of particles. For each one time–step in the random walk module of the 2D particle tracker, each particle was given velocity components and randomized dispersive components, according to its location and transient input conditions (Q_w, J, θ; see p. 24) at that time. With each particle tracked along a randomized path-line, the effective result was the generation of a probabilistic plume of particles. The output from the random walk module was a time report of particles that arrived at the pumping well. A separate histogram module sorted the particle arrival times into sequential intervals, assigned mass to the particles, and determined vertically averaged concentrations as a function of time according to a constant input pump-rate (Q_w) from over the depth of the contributing interval. Since the observed recoveries, as mentioned before, were from the 3, 4, 5, and 6 m depth intervals, the input

pump–rate (0.857 L/min) to the code was $^4/_7$ of the mean total (1.5 L/min). The resulting output was histograms of average concentration over time (see figs. 8b–15b) from each of the four contributing intervals, subject to some dilution error, since the observed pump-rate was actually variable.

The simulated total mass recoveries in Table 6 are not subject to dilution error. To get the arrival masses reported in Table 6, the total injection mass was multiplied by the percentage of arrived particles vs. total used for all injections. Thus, the random walk module results, with their consideration for transient input conditions, were used directly in mass recovery calculation. The simulated mass recoveries are presented in an aggregate form, for the sake of direct comparison with uncertainly resolvable observed arrivals. The injected masses are rounded to the nearest 0.1 g from field measurements (Linderfelt, 1993). The observed recoveries were rounded to the same base for the sake of comparison.

Table 6. Mass Recovery in Observed Results vs. Simulations

Tracer	Injected Mass at all wells (g)	Simulated Recovery at pumping well (g)	Observed Recovery at pumping well (g)
2,3-dfba	120.7	120.5	107.6
2,6-dfba	90.6	30.7	30.7
3,4-dfba	121.1	2.1	18.7
3,5-dfba	120.7	60.4	54.4
Br^-	119.7	94.6	70.6*
m-tfmba	90.5	30.2	29.2
o-tfmba	90.5	30.2	21.7
pfba	150.8	124.0	120.9

* 228.6 g bromide recovered if level 7 was included

Results of Observations and Simulations

The close correspondence of simulated and observed results for particular arrivals, such as the 30 g injections of 2,6-dfba (fig. 9) and m-tfmba (fig. 13) at injection wells I-15 and I-2 respectively, indicated that filter retention, sorption and degradation were at best insignificant influences. The slight discrepancy in simulated vs. observed results for m-tfmba could be attributed to its susceptibility to response variation (4.3% at low concentration levels, see Table 5). Thus most discrepancies could be safely explained in terms of field conditions, such as geologic heterogeneity, differential sinkage, scale-dependent dispersivity, gaps in sampling/analysis frequency, or unpredicted positional variations in capture zone boundaries. On the other hand, observed recoveries of bromide (fig. 12), injected with the two previously mentioned tracers, could not directly support the postulation that most discrepancies could be safely explained in terms of field conditions. In the upper depth intervals, bromide arrivals generally had concentration fronts and peaks travelling slightly ahead of corresponding features for co-injected FBAs. One possible explanation involves the relatively higher aqueous diffusion coefficients for bromide vs. the FBAs (see Table 2). For the following simplified aquifer parameters,

groundwater velocity = 10^{-6} m/s

grain diameter = 10^{-4} m

(both from MacFarlane et al., 1983)

diffusion coefficient = 10^{-9} m^2/s

(from Bowman and Gibbens, 1992)

the Peclet numbers for the tracers in the field experiment would be around 0.1. At that flow regime index value, solute migration would be marginally controlled by diffusion. This implies that bromide, with a relatively higher aqueous diffusion coefficient, may have spread further than the FBAs over given intervals of time or distance. Bromide arrival interpretation was, at the 6, 7, and 8 m depth intervals, complicated by background interferences that were unresolvable by SAX-HPLC, IC, or phenol colorometric analytic methods.

2,3-dfba

2,3-dfba was injected at I-5 and I-8, 3.5 m and 7 m respectively, south of the pumping well (see fig. 2). The simulations (fig. 8b) showed that the I-5 arrival peaked at day 212 (July 30, 1992) and lost some concentration to the monitoring well fence, indicating that I-5 was close to a capture zone boundary. Tracer from I-8 was completely captured in the simulation, with a peak concentration at day 234 (August 21, 1992). The mass balance corresponded by showing 120.5 g recovered in simulation vs. 120.7 g injected. The observed arrival mass of 107.6 g indicated that more mass from I-5 was lost over the boundary than the simulation supposed.

The closeness in sequence and character of the observed arrivals (fig. 8a) compared to the simulated arrivals suggested that the modeling parameters and assumptions were nearly correct. The vertical distribution of both arrivals (Appendix IV) was such that a fast low-concentration arrival component came in at level 3 first, while the bulk of both arrivals was concentrated later in the lower intervals (4, 5, and 6 m) of the pumping well. As the injection plumes sank, they were progressively restrained by apparently lower conductivity below the 3 m interval of the pumping well.

Figure 8a.

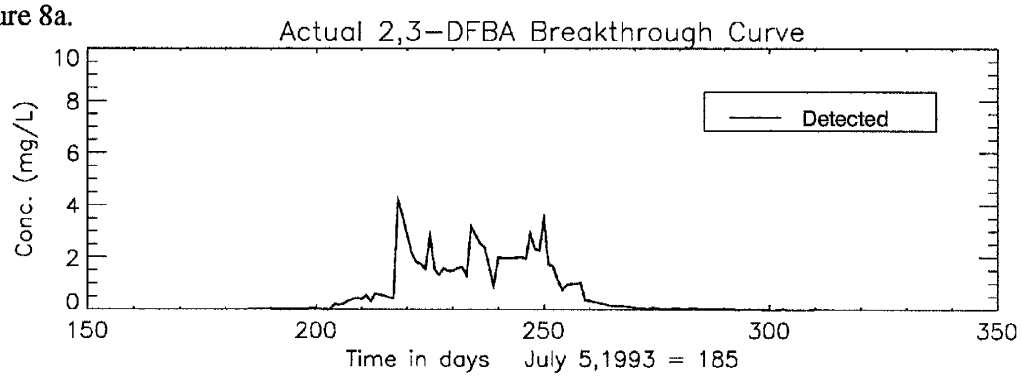

Figure 8b.

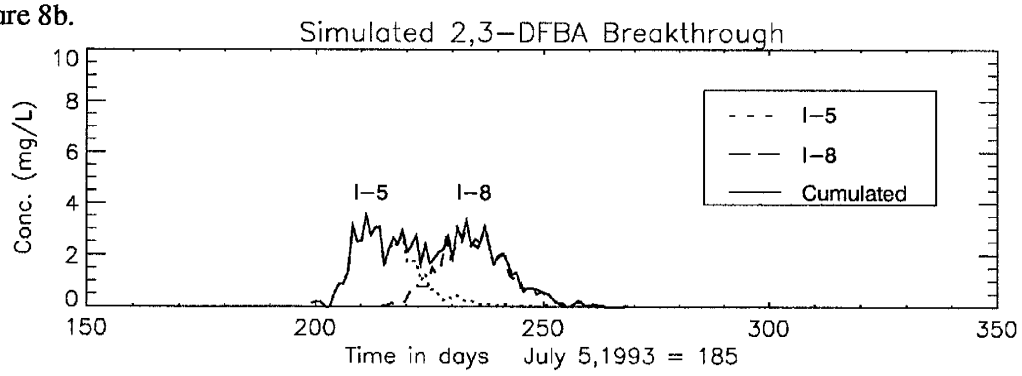

2,6-dfba

2,6-dfba was injected at I-6, 4 m southeast of the pumping well, and at I-15, 9 m south of the pumping well (see fig. 2). The I-15 arrival was matched in simulated vs. analytic recovery, but peaked at day 280 (fig 9a) vs. day 258 in the simulation (fig. 9b). The observed I-6 arrival, however, was matched in arrival time (day 250) and the degree of partial recovery in both the observed and simulated data. This, again was a function of proximity to the pumping well, vertical heterogeneity, and sinkage rate. The component of injection (I-6), that did not go to the fence, had no time to sink to the low conductivity lower intervals and therefore arrived early via the high conductivity upper intervals. The I-15 injection, at 10 m from the pumping well, had more time to sink to the low conductivity intervals (4 and 5 m) by which it arrived, later than predicted.

Figure 9a.

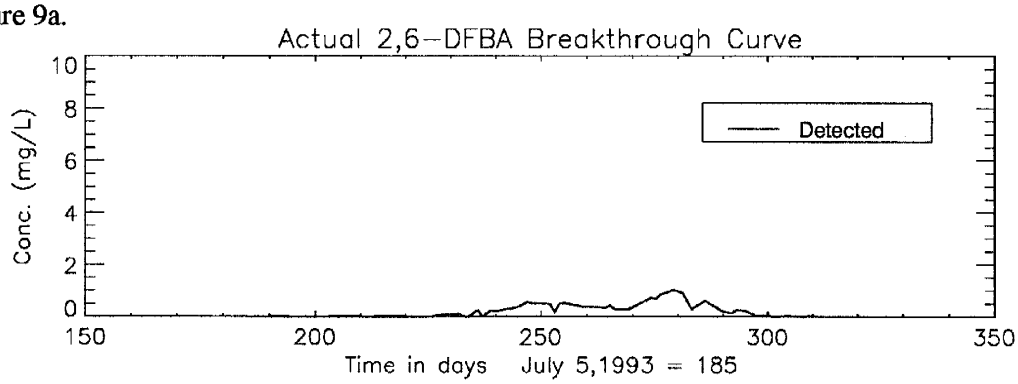

Figure 9b.

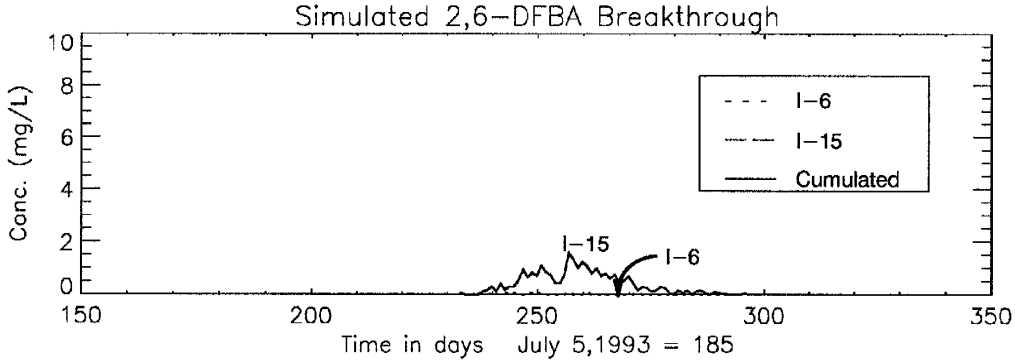

3,4–dfba

3,4–dfba was injected at I–10, 3.5 m west of the pumping well, and at I–3, 9 m southwest of the pumping well (see fig. 2). I–3 was not recovered in the simulations, and was outside of the group of wells that made correlatable contributions to the pumping well in both observed and simulated arrivals. I–10 was partially recovered (2.1 g) in the simulation (fig. 10b), but to a greater extent in the observed data (18.7 g; figs. 10a). The recovery of 3,4–dfba was unusual in being largely confined to the 6 m interval of the pumping well. If all the measured 3,4–dfba was from the I–10 injection, only 3.5 m from the pumping well, it would have required extra time in the subsurface in order to sink to 6 m depth. The extra time could have arisen from stagnation and cycling near the downstream side of the capture zone, which would support the conclusion that west and northwest of the pumping well, the conductivity zonation was inversed, in that a high conductivity zone was below a low conductivity zone. An alternative interpretation stems from model conceptualization, in that the model did not incorporate dynamic particle tracking, whereby additional particles would be inserted in regions of divergent flow. The under-representation of 3,4–dfba from I–10 in the simulation (fig. 10b) could simply be due to under-representation of particles tracked through the downstream stagnation area of the capture zone.

Figure 10a.

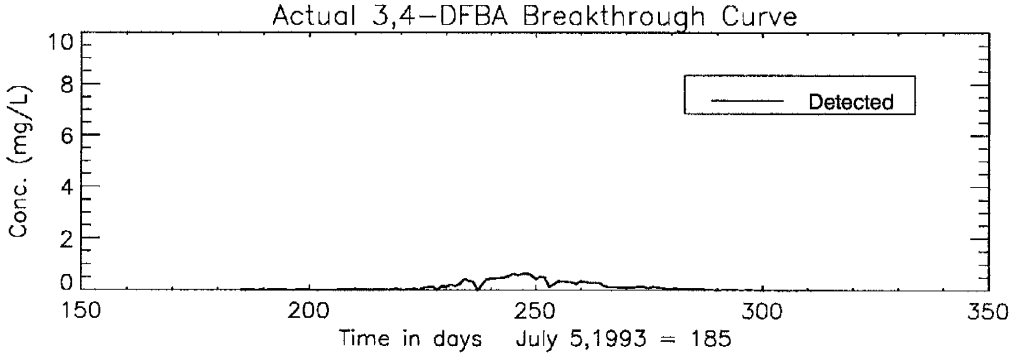

Figure 10b.

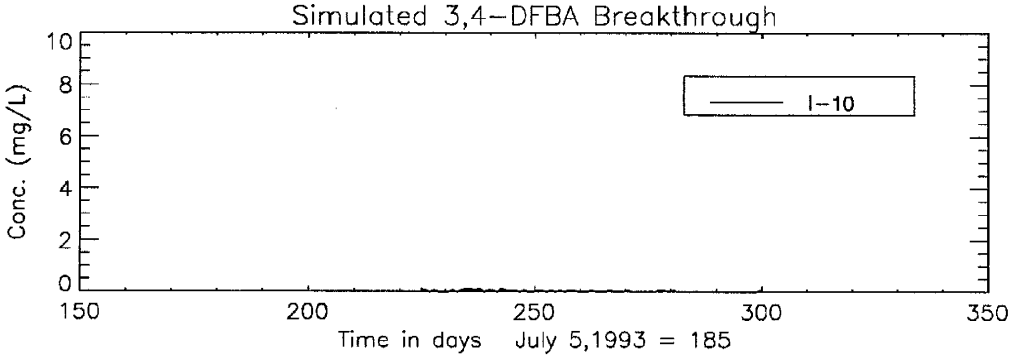

3,5-dfba

3,5-dfba was injected at I-11, 4.5 m northwest of the pumping well, and at I-7, 7 m south of the pumping well (see fig. 2). In the simulations (fig. 11b) I-7 was completely recovered (60.4 g) while I-11 was missed. The observed recovery (fig. 11a) corresponded with such a scenario, but was lower (54.3 g) and more spread out, substantiating that I-7 was just inside a capture zone, while I-11 was outside. The spreading of the observed arrivals was, again due to the interaction of sinkage rate, proximity to the well, and the effect of low conductivity lower intervals. The arrival component of I-7 at the 3 m depth interval arrived earlier than the larger proportion of the arrival component, which had time to sink to, and arrived via, levels 4, 5, and 6.

Figure 11a.

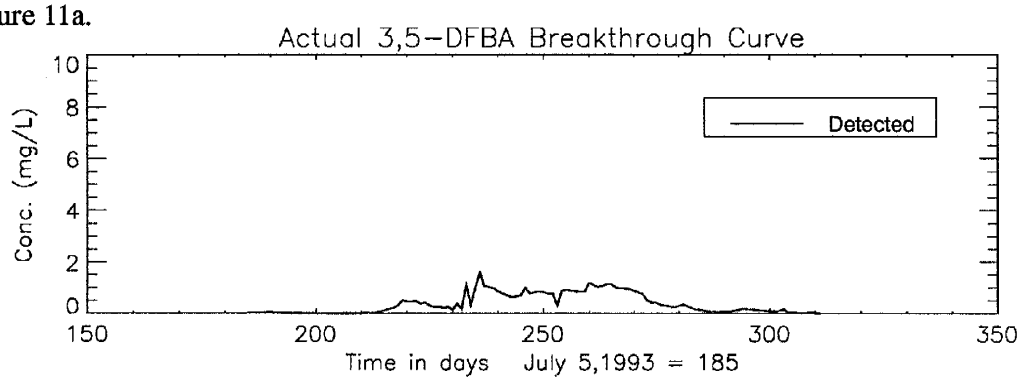

Figure 11b.

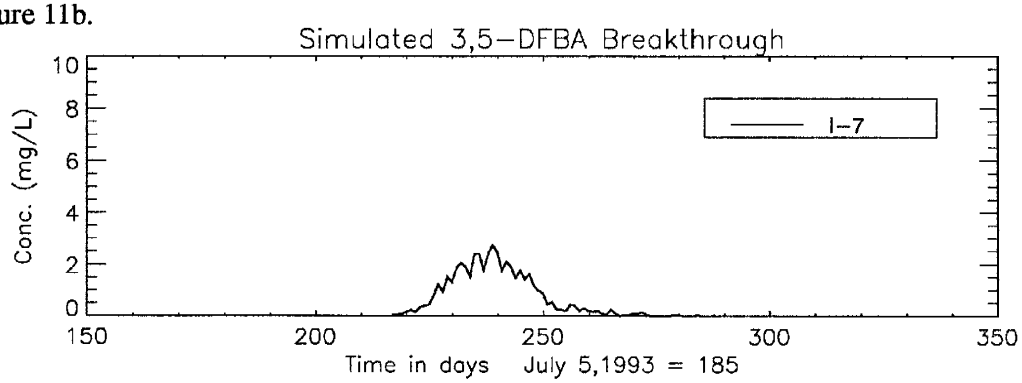

Potassium Bromide

Potassium bromide was injected at I-1 and I-2, 1 and 5 m southwest of the pumping well, respectively. It was also injected at I-9, 6.5 m southeast of the pumping well, and at I-15, 9 m south of the pumping well (see fig. 2). In the measurements, only the dissociated bromide was detectable. Accordingly, the simulations involved dissociated bromide mass (see Table 6). The mass balance of bromide is unfortunately wide open to question. In the simulations (fig. 12b), all of the arrivals from I-1, I-2, and I-15 were fully captured (30.3 + 29.4 + 30.0 g respectively = 89.7g), while I-9 was only partially recovered (4.9 g) just after I-15. The observed arrivals did not clearly support any of the predicted arrivals after I-1. A mass balance using the HPLC-SAX results for bromide recoveries from levels 3, 4, 5, and 6 was overbalanced by 200%. If the 70.588 g observed recovery from IC results of levels 3, 4, 5, and 6 is accepted from Appendix IV, it would indicate bromide was lost, possibly to lower levels.

Figure 12a.

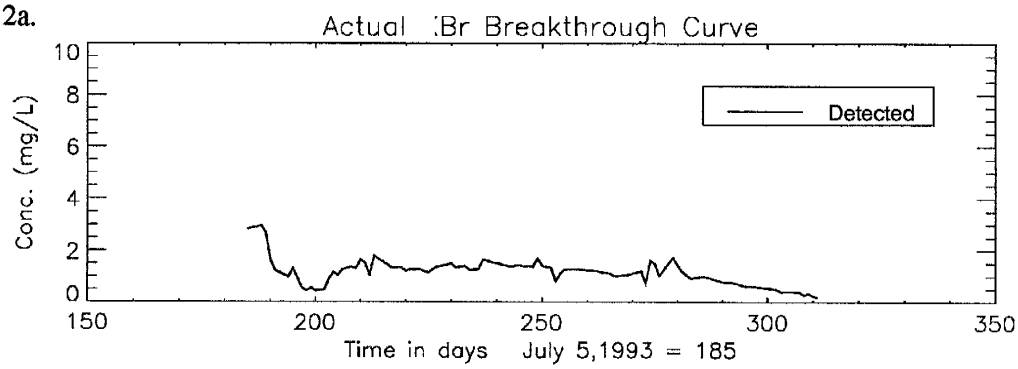

Figure 12b.

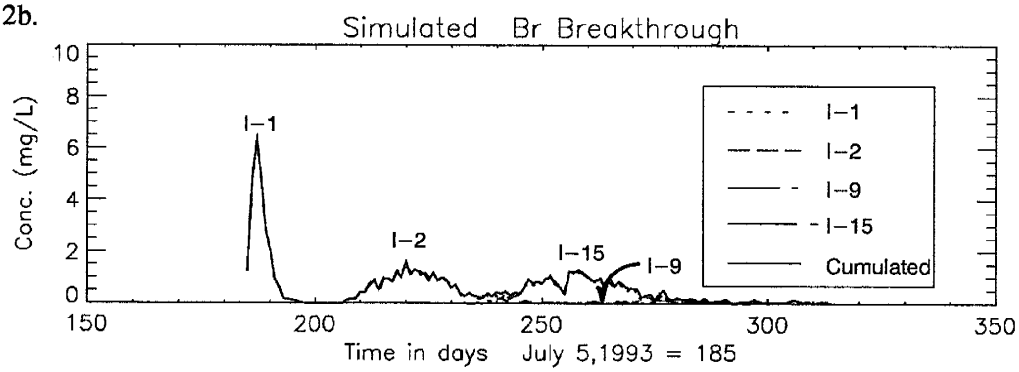

The IC results unfortunately did not increase the resolution of the separate arrivals or resolve the interference effects at the 6, 7, and 8 m intervals. At this point, it was decided that the apparently high bromide concentrations in the lower levels of the aquifer could be a consequence of setting up a groundwater field experiment where many others had already taken place over the last 15 years. The

number of bromide injections also contributed to dispersive coalescence that made deconvolution questionable.

The peak values in the simulations did manage to come close to minor peak values convoluted in the observed data. The simulated arrivals (fig. 12b) for I-1, I-2, I-9, and I-15 were at days 186, 220, 266, and 252 respectively. The observed data (fig. 12a) showed highest peaks at 188, 231, 249, and 279. The observed arrivals for co-injected tracers peaked as follows: o-tfmba from I-1 at day 185, m-tfmba from I-2 at day 235, pfba from I-9 at day 240, and 2,6-dfba from I-15 at day 280. Inspection of the time-depth-concentration data from Appendix IV, as well as the actual breakthrough curves of bromide arrivals vs. co-injected FBA arrivals, shows that the bromide arrivals in levels 3, 4, and 5 started sooner than the arrivals of any co-injected FBA, indicating that bromide probably diffused farther and faster than the FBAs.

m-tfmba

Injections of m-tfmba were at I-2, 5 m southwest of the pumping well, and at I-14, 7 m west of the pumping well (see fig. 2). All of I-2 was captured and all of I-14 was lost in the simulations (fig. 13b). This scenario was adequately supported by the observed arrivals (fig. 13a), the mass balance in Table 6, and the context of previous simulations. As previously mentioned the I-2 arrival had a slow high-concentration front in the in the upper intervals, and a fast low-concentration front in the lower intervals. Since this relative velocity distribution was observed in the 3,4-dfba I-10 arrival as well, the injection points west of the pumping well probably all had a low conductivity upper zone and a high conductivity lower zone. The limited sinkage of I-2 could be due to its proximity to the pumping well, implying that the injection plume did not spend enough time in the aquifer to sink completely to the high conductivity lower zone.

The 1 g difference between analytic vs. simulated recoveries was within detection error, and could have also been lost in a sampling/analysis frequency gap.

Figure 13a.

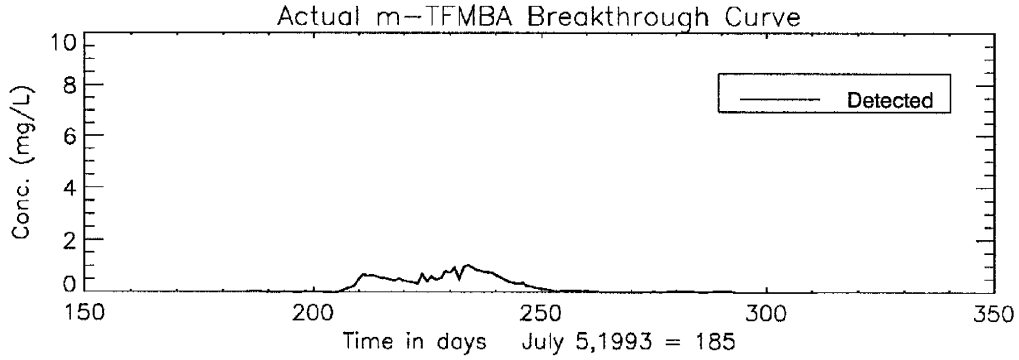

Figure 13b.

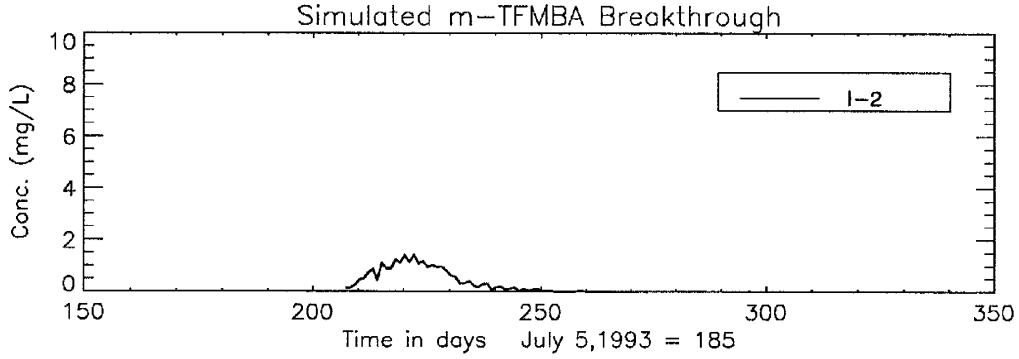

o-tfmba

Injections of o-tfmba were at I-1, 1 m southwest of the pumping well, and at I-13, 7 m southwest of the pumping well (see fig. 2). All of I-1 was captured and all of I-13 was lost in the simulations (fig. 14b). This scenario was adequately supported by the observed arrivals (fig. 14a) and the context of previous simulations. The proximity of I-1 to the pumping well did not allow fast enough sinkage of the injection plume to clearly define any vertical heterogeneity differences. It is apparent, however, that the 4 m depth interval restrained the injection plume somewhat, and that levels 4 and 5 contributed the most concentration.

The character of the I-1 arrival was further complicated by a two-day lag between injection and the commencement of sampling, which explained the 21.7 g observed recovery vs. the 30.2 g simulated recovery. Clearly, this sampling gap allowed some tracer to pass through the system undetected.

Figure 14a.

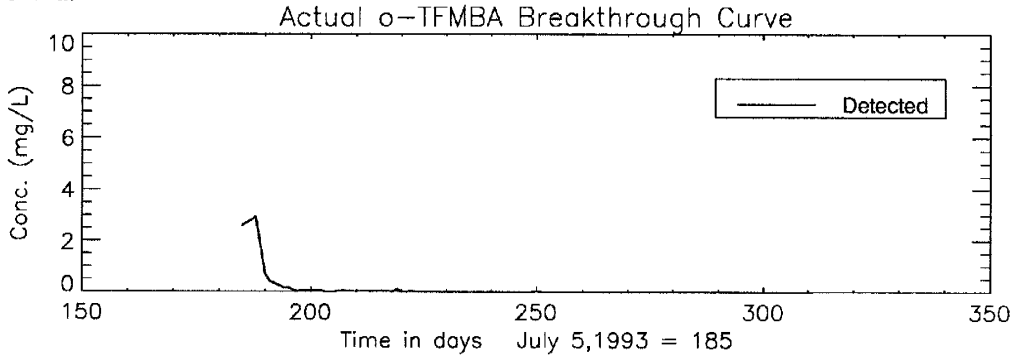

Figure 14b.

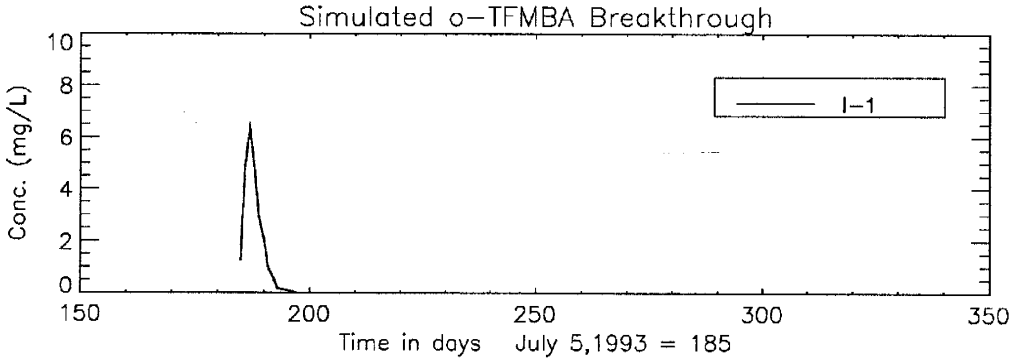

pfba

Injections of pfba were at I-4 and I-12, 3.5 and 10 m south of the pumping well, respectively. It was also injected at I-9, 6.5 m southeast of the pumping well (see fig. 2). I-4 and I-12 were completely captured in the simulations (fig. 15b) and well represented in the observed recoveries (fig. 15a). The character of the observed I-4 arrival was most comparable to the I-1 o-tfmba arrival, with a fast low-concentration arrival in interval 3, a slower and significantly higher-concentration arrival in level 4, and a slightly faster high-concentration arrival in level 5. This would suggest that the arrivals were laterally displaced to reflect a stratigraphic sequence with conductivity decreasing with increasing depth, except for a much lower conductivity unit in between, at level 4. The discontinuity in the observed I-4 (fig. 15a) arrival reflected a pump shutdown; not in the lack of samples, but in the dilution event associated with a flow regime transition from a forced gradient to a natural gradient and back. The I-12 injection had the longest travel path of all pfba injections; accordingly, it underwent the most sinkage. In comparison to the simulation data, the observed I-12 arrival, at levels 4, 5, and 6, was later and more spread out, indicating that those levels had lower conductivity and higher dispersivity than the input values of the simulation.

Figure 15a.

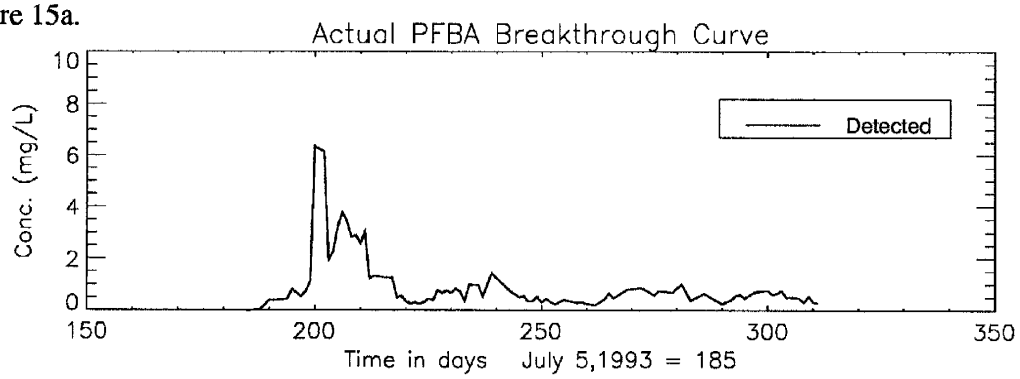

Figure 15b.

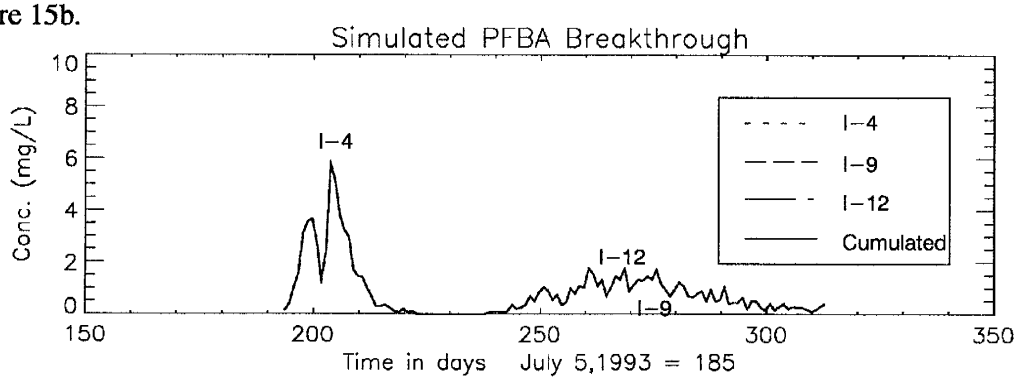

The I-9 arrival was partially recovered from day 264 to 271 in the simulation (3.4 g) if the 120.6 g total injected at I-4 and I-12 were completely captured. In the observed data, the I-9 identity was even weaker, but was assigned to an arrival that extended from day 225 to day 250, which was accompanied by its co-injected bromide arrival, peaking coincidentally near day 240. All other bromide arrivals were clearly linked with the arrivals of their FBA co-injections. The I-9 arrival character was such that the pfba did not sink very much and arrived via the high conductivity zone in level 3 (east of the pumping well), while a small later component arrived through level 4. The observed arrival of bromide that was time-linked with the I-9 pfba arrival (see Appendix IV) was thinly spread and under-represented relative to the pfba arrival in the upper intervals. The high bromide concentrations in the lower intervals (6, 7, and 8) are masked to some extent by background interference but closer in arrival time to the co-injected pfba This would suggest that bromide diffusion spread laterally and downwards to a further extent than pfba. By spreading to the low conductivity zone in the lower intervals, the bromide plume component at those depths was thereby delayed to closer correspondence to its co-injected pfba arrival.

Discussion

General Trends

In every plot of arrivals (see figs. 8 - 15), the observed recoveries were more spread out than the simulation results. Since the varying flow field was accounted for, spreading due to dispersivity or heterogeneity were thus inadequately accounted for in the simulations. Spreading was not notable for injections closest to the pumping well, such as o-tfmba (fig. 14a) from injection I-1. Recalling fig. 2, as we move progressively further from the pumping well to injections I-2 (m-tfmba and bromide) and I-4 (pfba), more spreading in the observed data vs. the simulations became apparent (figs. 12a, 13a, and 15a, respectively). This may indicate the need for scale-dependent dispersivity input as distance between an injection point and the pumping well increases.

A common characteristic in the spreading became apparent in the comparison of arrivals from I-2 (m-tfmba and bromide, figs. 12a and 13a), I-4 (pfba, fig. 15a), I-5 (2,3-dfba, fig. 8a), I-6 (2,6-dfba, fig. 9a), and I-7 (3,5-dfba, fig. 11a). The arrivals in each of those cases started with a subdued low peak relative to the simulation, and finished with a late high secondary peak. In reference to the time-depth-concentration data in Appendix III, those particular arrivals had fast low-concentration fronts at upper levels (3 and 4 m) and slow high-concentration fronts at lower levels (5 and 6 m). The above-mentioned injection points, east of the pumping well, therefore had a high conductivity zone at 2 to 3+ m depth and a low conductivity zone at 4 to 6 m depth. To further substantiate this position, Linderfelt (1993) noted that injections into the 4-5m interval in injection wells I-3 (3,4-dfba) and I-12 (pfba) took 45 to 60 minutes, as opposed to 30 minutes or less for all other injections. The splitting of concentration fronts in time, space, and proportion, showed that vertical averaging and integration of solute concentration in transport may adequately ignore sinkage effects, but could not correctly account for segregation of layered arrival components due to vertical heterogeneity.

The m-tfmba and associated bromide arrival of injection I-2 (m-tfmba and bromide) distinguished itself from the previously mentioned group by having a slow high-concentration front in the upper intervals (3 and 4 m), and a fast low-concentration front in the lower intervals (5 and 6 m). In support of this anomaly, it was observed that the arrivals of injections I-1 (o-tfmba and bromide) and I-10 (3,4-dfba) were similar in having a slow upper interval and a faster lower interval. The concentration distributions for those two arrivals, however, had a larger concentration component towards the lower intervals of the aquifer. A second conclusion concerning heterogeneity would be that the injection points west of the pumping well had a low conductivity upper zone, a high conductivity lower zone,

and possibly a discontinuous but very low conductivity lamina separating the two. Such a lamina could help explain the restrained sinkage of injection I-2 (m-tfmba and bromide).

There were several considerations by which to anticipate discrepancies between actual and modeled recoveries of tracer plume breakthrough at the pumping well. Since the tracers are anionic, and spent most of their time in a neutral pH subsurface or cold storage, we could disqualify: cationic exchange, degradation by heat or photochemical reaction, and precipitative losses through evaporation. Furthermore, the addition of potassium hydroxide to the injection solutions ensured that solute-solute interactions would not produce insolubility problems close to the injection points.

Infrastructure

Time gaps in the pumping well sampling schedule could allow peak values of arrivals to pass through the system undetected.

Subsurface Filtration

Brusseau (1993) found size exclusion effects to be apparent on a molecular scale, using data sets generated by Gibbens (1989) with the fluorobenzoic acid tracers used in this investigation. Gibbens (1989) found that pfba migrated faster than water-bound tritium through aggregated clay-rich geologic matrices. Brusseau's postulation was that solute-surface layer interactions produced a thinner diffuse double layer (DDL) for larger diameter anion complexes than for tritiated water, thereby explaining the consistently later arrival of tritium vs. pfba. Anionic size exclusion, associated with aggregated clay-rich geologic matrices, was not effective in the silicate sand matrix of our field site. In our case, the preferential spreading and marginally faster arrival times for bromide vs. the FBAs (see Appendix IV) indicated that the higher aqueous diffusion coefficient of bromide (Table 2) may have had a controlling influence on its migration. As mentioned before (p. 29) the Peclet numbers for the tracers were around 0.1, indicating that solute migration would be marginally controlled by diffusion.

Losses Directed by Geologic Heterogeneity

Since the investigation involved a phreatic aquifer over a seasonal change with frequent local precipitation events, the problem of mobile-immobile flow was potentially significant. Given that the injections were from 2 to 5 m depth and the water table cycled between 1 to 2 m depth, the tracers had minimal chance of being isolated above the water table. It was more likely that tracers could be lost in water bound to the geologic matrix or stuck in dead-end pores. An estimate of effective porosity could be obtained by inverse modeling a porosity value to fit observed seepage velocity.

It would be difficult, however, to isolate the effects of mobile–immobile flow from tracer partitioning between the two flow regimes, and the effects of cyclical inclusion/exclusion of tracer position with respect to a variable capture zone position.

VI. CONCLUSIONS AND RECOMMENDATIONS

Conclusions

In testing various SAX–HPLC analytic methodologies on resolving multiple tracer arrivals, three trends were apparent. 1) At low mobile phase pH conditions, when the FBAs are for the most part neutral and undissociated, the retention mechanism was degree of dissociation. 2) As mobile phase pH approached higher tracer pK_a values, polarity effects influenced separation more than degree of ionic dissociation. 3) Retention time drift, or gradual coelution of tracers and background anions, as a function of column deterioration, indicated that the use of acidic pH mobile phases produced method instability.

Cross verification by a vertically averaged 2D solute transport model (Linderfelt, 1993) helped not only to guide interpretation and recognition of gross errors in analytic methodology, but helped also to separate the identity, sequence, and character of coalescing arrivals of identical tracers from different injection points.

The close correspondence of simulated and observed results for particular arrivals, such as the 30 g injections of 2,6–dfba (fig. 9) and m–tfmba (fig. 13) at injection wells I–15 and I–2 respectively, indicated that filter retention, sorption and degradation were at best insignificant influences. The slight discrepancy in simulated vs. observed results for m–tfmba could be attributed to its susceptibility to response variation (4.3% at low concentration levels, see Table 5). Thus most discrepancies could be safely explained in terms of physical conditions, such as geologic heterogeneity, differential spreading, scale–dependent dispersivity, gaps in sampling/analysis frequency, or unpredicted positional variations in capture zone boundaries. On the other hand, observed recoveries of bromide (fig. 12), injected with the two previously mentioned tracers, could not directly support the postulation that most discrepancies could be safely explained in terms of physical conditions. Although bromide has a higher aqueous diffusion coefficient than any FBA (Table 2), and thus spread faster than any FBA, bromide arrival interpretation was badly complicated by background interferences that were unresolvable by SAX–HPLC, IC, or phenol colorometric analytic methods.

Field conditions were, fortunately, very well geostatistically characterized. Heterogeneity, or facies variation, was limited to two conductivity zonations, vertically and laterally. East of the pumping well, conductivity decreased with depth, while west of the pumping well, conductivity increased with depth. The vertical transition occurred between the 3 and 4 m depth intervals of the pumping

well. The lateral transition zone occurred near the pumping well and the two closest injection wells (I-1 and I-2). The field experiment was luckily installed so as to have the lateral conductivity transition paralleling most flow lines, rather than crossing them. Since the simulation arrivals generally coincided with the actual arrival components from the high conductivity zones, the geometric mean of 9.23×10^{-5} m/s (Woodbury and Sudicky, 1991) was locally overstated, but then indicative of the high conductivity zones.

The most important discrepancies between observed tracer behavior and model behavior, attributable to analytic methodology, were due to the effects of tracer misidentification, background interferences (especially in the case of bromide), and detector imprecision. Geologic heterogeneity, gaps in acquisition or analysis of samples, and preferential migration rates of bromide vs. FBAs were the main sources of discrepancy outside of analytic methodology. Aside from the inability to account for segregated arrival components due to vertical heterogeneity, influences from model conceptualization such as using a transient pump rate in the random walk module and a constant pump rate in the histogram module, turned out to be indistinguishable.

Recommendations for HPLC

There are two recommendations, given the constraints of four basic components in this project: isocratic phosphate-based mobile phase, constant flow rate, Strong Anion eXchange (SAX) chromatographic column, and UV detector using external calibrations for concentration vs. response.

The pH-pK_a relationship can effectively invoke separation of fluorobenzoic acids with similar elution times only if the pH is numerically lower than the highest pK_a involved. Using the constraints of SAX chromatography and UV-detection, an optimal separation of a maximum number of fluorobenzoic acids would therefore involve pK_a separations of 0.1 or more, the widest possible pK_a range overall, and the highest possible mobile phase pH within that range. Furthermore, given that chloride and nitrate were always very close to bromide in elution time, a good selection of tracers would exclude bromide.

Cleaning a column with a 0.3 ml/min solvent flush of distilled-deionized water for more than 3 hours would render a just previous separation unreproducible, even after 3 hours re-equilibration with mobile phase. This pointed out the susceptibility of the SAX bonded phase to hydrolysis and necessitated minimizing solvent flushes to 3 column volumes, and using column reversals more

frequently. To further alleviate this condition, water for flushing was mixed to include 10% acetonitrile.

If new directions for separation methodology are sought, one could probably investigate the use of another salt for the mobile phase, or build on the use of a C18 column as Stensrud *et al.* (1990) did. Phosphate is apparently more deleterious to silane-modified packings than acetate, borate, nitrate, or sulfate (Snyder and Kirkland, 1979). Octadecyl silane (C18) columns are relatively more stable than SAX (C4 with quaternary amine) columns, but then again, not as selective in retentive capability.

Recommendations for Modeling

The principal modeling considerations were to match actual flow-field and pump-rate conditions to model time-steps, and to anticipate the effects of local zones of high conductivity. The splitting of concentration fronts in time, space, and proportion, showed that vertical averaging and integration of solute concentration in transport may adequately mask sinkage effects, but can not correctly account for lateral segregation of layered arrival components due to vertical heterogeneity.

Since both the random walk process and the Ito Fokker-Planck extra terms (Uffink, 1989) incorporated dispersivity, the need for dispersivity input is valid. However, most of the spreading in observed data was due to lateral segregation of layered arrival components by vertical heterogeneity. Scale-dependent dispersivity could mask, or be equated to, the segregating effects of heterogeneity. Dispersivity determinations, however, are constrained by experimental or empirical data availability. Conductivity measurements, on the other hand, could be measured or interpreted from geological or geophysical data, even from observed qualitative geologic information. Efforts at matching simulated to observed tracer behavior would be most productively focussed on incorporating consideration for spatial variation of hydraulic conductivity.

One other recommendation for modeling would be to incorporate dynamic particle tracking, whereby additional particles would be inserted in regions of divergent flow. The under-representation of 3,4-dfba from I-10 in the simulation (fig. 10b) could simply be due to under-representation of particles tracked through the downstream stagnation area of the capture zone.

REFERENCES

Atlas, R.M. and R. Bartha, 1987, Microbial ecology: Fundamentals and applications, Benjamin/ Cummings Publ. Co., 352–353.

Bair, E.S. and G.S. Roadcap, 1992, Comparison of flow models used to delineate capture zones of wells: 1. Leaky–confined fractured–carbonate aquifer, Ground Water, 30(2), 199–211.

Bair, E.S., C.M. Safreed and E.A. Stasny, 1991, A Monte Carlo based approach for determining traveltime-related capture zones of wells using convex hulls as confidence regions, Ground Water, 29(6), 849–855.

Bear, J., 1979, Groundwater Hydraulics, McGraw–Hill, New York.

Benson, C., 1993, An evaluation of several fluorinated benzoic acids for use as soil and ground water tracers, Unpublished M.S. thesis (in progress), Hydrology Program, New Mexico Inst. of Mining and Tech., Socorro, NM.

Bowman, R.S., 1984, Analysis of soil extracts for inorganic and organic tracer anions via high performance liquid chromatography, J. Chromatogr., v. 285, 467–477.

Bowman, R.S. and J.F. Gibbens, 1992, Difluorobenzoates as nonreactive tracers in soil and ground water, Ground Water, 30(1), 8–14.

Boggs, J.M. and E.E. Adams, 1992, Field study of dispersion in a heterogeneous aquifer 4. Investigation of adsorption and sampling bias, Water Resour. Res., 28(12), 3325–3336.

Brusseau, M.L., 1993, The influence of solute size, pore–water velocity, and intra-particle porosity on solute dispersion and transport in soil, Water Resour. Res., (in press).

Environmental Protection Agency, 1990, WHPA, An integrated semi–analytical model for the delineation of Well-Head Protection Areas, Office of Ground–Water Protection, Washington, D.C.

Gibbens, J.F., 1989, An evaluation of several fluorinated benzoic acids for use as soil and ground water tracers, Unpublished M.S. thesis, Hydrology Program, New Mexico Inst. of Mining and Tech., Socorro, NM.

Guven, O., R.W. Falta, F.J. Molz, and J.G. Melville, 1985, Analysis and interpretation of single–well tracer tests in stratified aquifers, Water Resour. Res., 21(5), 676–684.

Hantush, M.S. and C.E. Jacob, 1954, Plane potential flow of ground-water with linear leakage, Trans. Amer. Geophys. Union, Washington D.C., v. 35, 917–936.

Hoeksema, R.J. and R.B. Clapp, 1990, Calibration of groundwater flow models using Monte Carlo simulations; Calibration and Reliability in Groundwater Modelling, Int'l Assoc. of Hydrological Sciences ModelCARE 90, ed.: K. Kovar; IAHS Press, Oxfordshire, UK; 33–42

Howe, L., 1988, Tennessee Valley Authority – Quality Assurance Procedure, No. NRS–LB–AP–30.418.8, section 8.3.

Huyakorn, P.S., P.F. Andersen, F.J. Molz, O. Guven, and J.G. Melville, 1986, Simulations of two-well tracer tests in stratified aquifers at the Chalk River and the Mobile sites, Water Resour. Res., 22(7), 1016–1030.

Javendel, I. and C-F Tsang, 1984, Capture-zone type curves: A tool for aquifer cleanup, Ground Water, 24(5), 616–625.

Keeley, J.F. and C-F. Tsang, 1983, Velocity plots and capture zones of pumping centers for ground water investigations, in Proceedings of the Third National Symposium on Aquifer Restoration and Ground-Water Monitoring, Natl. Water Well Assoc.

Kinzelbach, W., 1988, The random walk method in pollutant transport simulation, Groundwater Flow and Quality Modeling, ed.: E. Castidio *et al.*, D. Reidel Publ. Co., 227–245

Lee, K., 1986, Pollution capture zones for pumping wells in aquifers with ambient flow, M.S. Thesis, Hydrology Program, New Mexico Institute of Mining and Technology, Socorro, New Mexico.

Leppert, S.C., 1990, Capture zones in transient flow fields: simulations and analysis, M.S. Independent Study, available as Open File Report 90–7, Hydrology Program, New Mexico Institute of Mining and Technology, Socorro, New Mexico.

Linderfelt, W.L., 1993, Capture zone delineation in a shallow sand aquifer: Models and experiments, Ph.D. Thesis, Department of Geoscience, Mexico Institute of Mining and Technology, Socorro, New Mexico.

MacFarlane, D.S., J.A. Cherry, R.W. Gillham, and E.A. Sudicky, 1983, Migration of contaminants in groundwater at a landfill: A case study 1. Groundwater flow and plume delineation, J. Hydrol., v. 63, 1–29

Molz, F.J., O. Guven, J.G. Melville, R.D. Crocker, and K.T. Matteson, 1986, Performance, analysis, and simulation of a two-well tracer test at the Mobile site, Water Resour. Res., 22(7), 1031–1037.

Morrisey, D.J., 1987, Estimation of the recharge area contributing to a pumped well in a glacial drift river valley aquifer, USGS Open File Rpt. 86–543.

Muskat, M., 1937, The Flow of Homogeneous Fluids Through Porous Media, McGraw-Hill Book Co., New York.

Nelken, L.H., and J.C. Birkett, 1982, Dipole moments, Handbook of Chemical Property Estimation Methods; (eds.)W.J. Lyman, W.F. Reehl, and D.H. Rosenblatt, McGraw-Hill, N.Y., 17-1 to 17-25.

Nelson, R.W., E.A. Jacobsen, and W. Conbere, 1987, Uncertainty assessment for fluid flow and contaminant transport modeling in heterogeneous groundwater systems, Advances in Transport Phenomena in Porous Media, ed.: J. Bear and M.Y. Corapcioglu, Martinus Nijhoff Publ., Boston, 701–726

Nicholson, R.V., J.A. Cherry, and E.J. Reardon, 1983, Migration of contaminants in groundwater at a landfill: A case study 6. Hydrogeochemistry, J. Hydrol., v. 63, 131–176.

Pearson, R.J., S.D. Comfort, and W.P. Inskeep, 1992, Analysis of fluorobenzoate tracers by ion chromatography, Soil Science Society of America Journal, 56(6), 1794–1796.

Schafer–Perini, A., 1990, Numerical study of the influence of permeability heterogeneity in non-uniform steady-state flow systems, Ph.D. Thesis, New Mexico Institute of Mining and Technology, Socorro, New Mexico.

Schafer–Perini, A.L. and J.L. Wilson, 1991, Efficient and accurate front tracking for two–dimensional groundwater flow models, Water Resour. Res., 27(7), 1471–1485.

Snyder, L.R., and J.J. Kirkland, 1979, Introduction to Modern Liquid Chromatography, 2nd ed., John Wiley & Sons Inc., New York, 863p.

Springer, A.E. and E.S. Bair, 1992, Comparison of methods used to delineate capture zones of wells: 2. Stratified–drift buried–valley aquifer, Ground Water, 30(6), 908–917.

Stensrud, W.A., M.A. Bame, K.D. Lantz, and G.J. Saulnier, Jr., 1990, WIPP Hydrology Program, Waste Isolation Pilot Plant, southeastern New Mexico, hydrologic data report #8. Sandia National Laboratories, Contractor Report SAND89–7056

Sudicky, E.A., 1986, A natural gradient experiment on solute transport in a sand aquifer: Spatial variability of hydraulic conductivity and its role in the dispersion process, Water Resour. Res., 22(13), 2069–2082.

Teutsch, G., 1990, A variable scale approach for the delineation of ground–water protection zones using field and numerical modelling techniques; Selected papers on hydrogeology from the 28th Int'l Geological Congress: Washington D.C., USA, July 9–19, 1989, Int'l Assoc. of Hydrogeologists, ed.: E.S. Simpson and J.M. Sharp Jr.; Verlag Henz Heise Publ., Hannover, West Germany; 393–404.

Teutsch, G. and B. Hofmann, 1990, The delineation of ground–water protection zones using forced gradient tracer tests: a model validation case study; Calibration and Reliability in Groundwater Modelling, Int'l Assoc. of Hydrological Sciences ModelCARE 90, ed.: K. Kovar; IAHS Press, Oxfordshire, UK; 351–362.

Theis, C.V., 1935, The relation between the lowering of the piezometric surface and the rate and duration of discharge of a well using ground water storage, Trans. Amer. Geophys. Union, Washington D.C., 518–524.

Thiem, G., 1906, Hydrologische Methoden, Leipzig, 56 p.

Tucker, W.A. and L.H. Nelken. 1982. Diffusion coefficients in air and water, Handbook of Chemical Property Estimation Methods; (eds.)W.J. Lyman, W.F. Reehl, and D.H. Rosenblatt, McGraw-Hill, N.Y., 17-1 to 17-25.

Uffink, G.J.M., 1989, Application of Kolmogorov's backward equation in random walk simulations of groundwater contaminant transport, Contaminant Transport in Groundwater, (eds.) Kobus and Kinzelbach, Balkema, Rotterdam, p.283–289.

Wilson, J.L. and W.L. Linderfelt, 1991, Groundwater quality in pumping wells located near surface water bodies, New Mexico Water Resources Research Inst. Technical Completion Report No. 261., 144 p.

Woodbury, A.D. and E.A. Sudicky, 1991, The geostatistical characteristics of the Borden aquifer, Water Resour. Res., 27(4), 533-546.

APPENDIX I
SAMPLE CHROMATOGRAMS

The following four chromatograms show the principal separations developed and used for the EPA capture zone project on which this independent study is based. The principle difference to focus on is the change in elution order caused by a change in mobile phase pH.

Table I-1. Analytic Conditions

file	date	wavelength (nm)	flow-rate (mL/min)	column mftr.	column #	mobile phase pH	molarity	%ACN
CPW.15R	09/01/92	205	2.0	Phenomenex	33204	2.60	0.01	18
CPW.29R	09/04/92	205	2.0	Phenomenex	30687	2.80	0.02	18
BPWI.15R	09/01/92	205	1.0	Regis	290138	3.47	0.008	18
36b*	09/04/92	205	1.0	Phenomenex	40217	3.52	0.02	18

* page number in lab notebook.

File=e:\lc\CPW.15R Date printed = 04-15-1993 Time = 14:19:36
1.00 to 22.00 min. Low Y = -10.31065 mv High Y = 882.16626 mv Span = 892.47687 mv

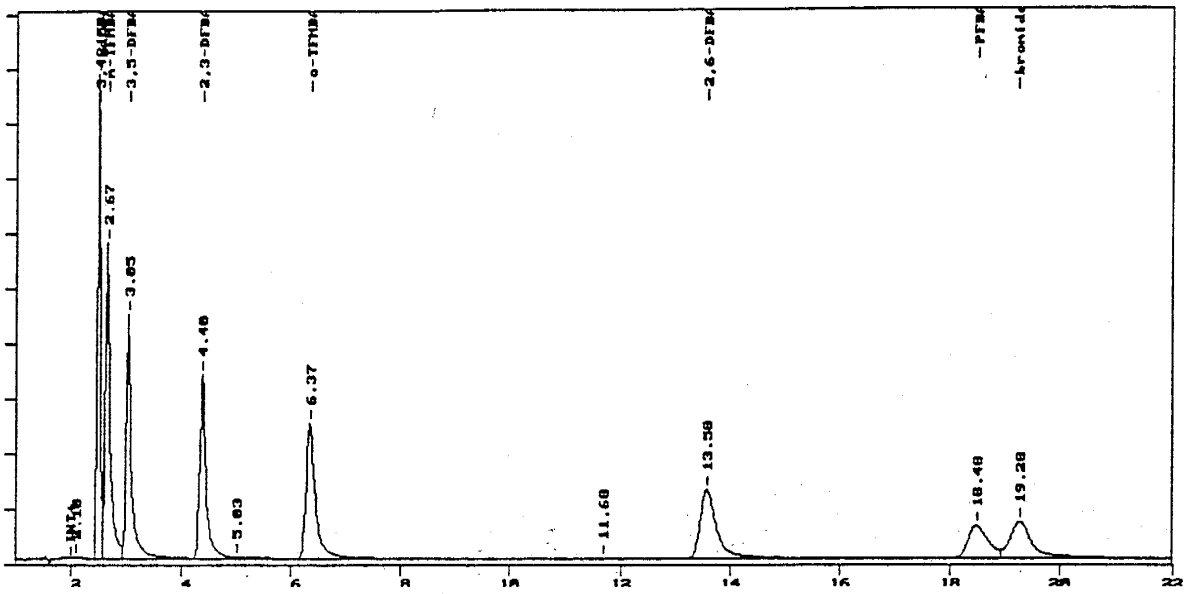

Test
e:\blue\Q51CF0D6.BNC
Data file = e:\lc\CPW.15R
Date stamp = 09/01/92 Time = 20:55:42
Sample name = 20%b12
Collected on SEP 1, 1992 20:32:21 from port # 2
Operator = R. TerBerg
Reference file name = Q51CF0D6.BNC
Instrument = com port 2
Method name = e:\lc\rat.MET version # 141
Date method last modified = 04/15/93 Time = 14:18:46
Calibration file = E:\LC\RAT.CAL version # 31
Date cal file last modified = 04/15/93 Time = 13:59:58
Run time = 22.02 minutes Area reject = 0
Amount injected = 1 Dilution Factor = 1
Sample Weight = 1 Internal Standard Amount = 1
Sampling rate = 1 per second Starting peak width = .1 minutes
Peak detect threshold = 1.59
Chrom-Perfect Software Serial number = 9110 Version = 4.01 For New Mexico Tec
Today's date = 04-15-1993 Time = 14:19:47

PK	Ret Time	Name	Amount	Amount %	Area	Area %	Type	Width	Height	Height %
1	2.100		0.0000	0.0000%	10,115.5	0.051%	BB	0.282	598.63	0.0248%
2	2.500	3,4-dfba	28.8000	15.2059%	3,034,317.8	15.414%	BV	0.065	777,993.13	32.2919%
3	2.667	m-TFMBA	21.2000	11.1932%	3,181,518.5	16.162%	VV	0.105	506,299.91	21.0148%
4	3.050	3,5-DFBA	20.2000	10.6653%	2,820,815.5	14.330%	VV	0.120	391,549.78	16.2519%
5	4.400	2,3-DFBA	20.4000	10.7709%	2,525,481.0	12.829%	VV	0.143	294,442.34	12.2213%
6	5.033		0.0000	0.0000%	79,474.7	0.404%	VV	0.391	3,389.13	0.1407%
7	6.367	o-TFMBA	21.6000	11.4044%	2,698,766.8	13.710%	VV	0.208	216,485.00	8.9856%
8	11.683		0.0000	0.0000%	1,653.7	0.008%	VB	0.296	92.97	0.0039%
9	13.583	2,6-DFBA	20.4000	10.7709%	2,364,919.0	12.014%	SBB	0.359	109,722.37	4.5542%
11	18.483	PFBA	34.4000	18.1626%	1,318,120.8	6.696%	BV	0.434	50,652.47	2.1024%
12	19.283	bromide	22.4000	11.8268%	1,649,997.0	8.382%	VB	0.474	58,027.35	2.4085%

Total area = 1.968518E+07 Total amount = 189.4 Sample units = mg/L Total height = 2409253

File=e:\lc\CPW.29R Date printed = 09-09-1992 Time = 22:07:54
1.00 to 14.00 min. Low Y = -12.95885 mv High Y = 638.75922 mv Span = 651.71808 mv

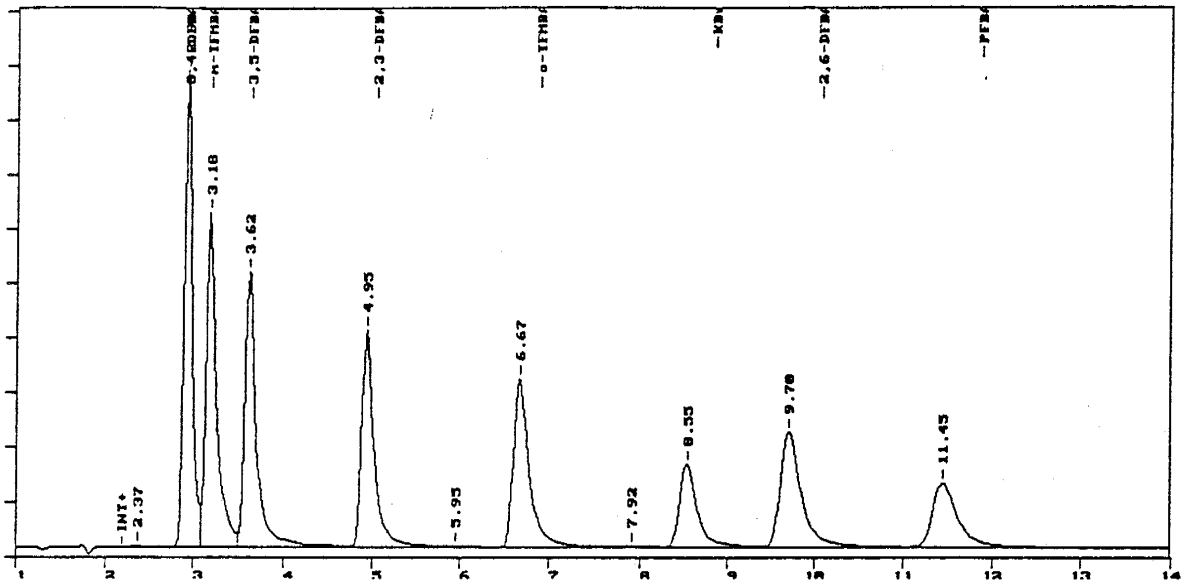

pumping well samples
e:\blue\Q5202566.BNC
Data file = e:\lc\CPW.29R
Date stamp = 09/04/92 Time = 07:08:36
Sample name = 20%b12
Collected on SEP 4, 1992 06:53:25 from port # 2
Operator = R. TerBerg
Reference file name = Q5202566.BNC
Instrument = com port 2
Method name = E:\LC\RAT.MET version # 26
Date method last modified = 09/09/92 Time = 22:06:32
Calibration file = E:\LC\RT3PT.CAL version # 9
Date cal file last modified = 09/09/92 Time = 21:16:52
Run time = 14.02 minutes Area reject = 4,000
Amount injected = 1 Dilution Factor = 1
Sample Weight = 1 Internal Standard Amount = 1
Sampling rate = 1 per second Starting peak width = .1 minutes
Peak detect threshold = 1.59
Chrom-Perfect Software Serial number = 9110 Version = 4.01 For New Mexico Tec
Today's date = 09-09-1992 Time = 22:08:05

PK	Ret Time	Name	Amount	Amount %	Area	Area %	Type	Width	Height	Height %
1	2.367		0.0000	0.0000%	13,432.5	0.067%	BB	0.191	1,173.15	0.0573%
2	2.933	3,4-DFBA	28.8000	15.2059%	3,568,526.3	17.697%	BV	0.106	563,452.06	27.5030%
3	3.183	m-TFMBA	21.2000	11.1932%	3,209,871.0	15.918%	VV	0.135	395,242.47	19.2924%
4	3.617	3,5-DFBA	20.2000	10.6653%	2,890,062.5	14.332%	VV	0.148	324,667.56	15.8476%
5	4.950	2,3-DFBA	20.4000	10.7709%	2,555,307.0	12.672%	VV	0.167	254,967.02	12.4454%
6	5.950		0.0000	0.0000%	45,530.2	0.226%	VV	0.483	1,571.13	0.0767%
7	6.667	o-TFMBA	21.6000	11.4044%	2,526,135.0	12.527%	VV	0.213	198,059.00	9.6676%
8	7.917		0.0000	0.0000%	38,281.0	0.190%	VV	0.521	1,223.93	0.0597%
9	8.550	KBr	22.4000	11.8268%	1,437,676.9	7.130%	VV	0.247	97,132.66	4.7412%
10	9.700	2,6-DFBA	20.4000	10.7709%	2,341,538.3	11.612%	VV	0.288	135,610.53	6.6194%
11	11.450	PFBA	34.4000	18.1626%	1,538,431.9	7.629%	VB	0.339	75,590.53	3.6897%

l area = 2.016479E+07 Total amount = 189.4 Sample units = mg/L Total height = 2048690

File=e:\lc\BPWI.80R Date printed = 04-14-1993 Time = 15:25:50
1.00 to 19.00 min. Low Y = -9.48918 mv High Y = 14.63430 mv Span = 24.12348 mv

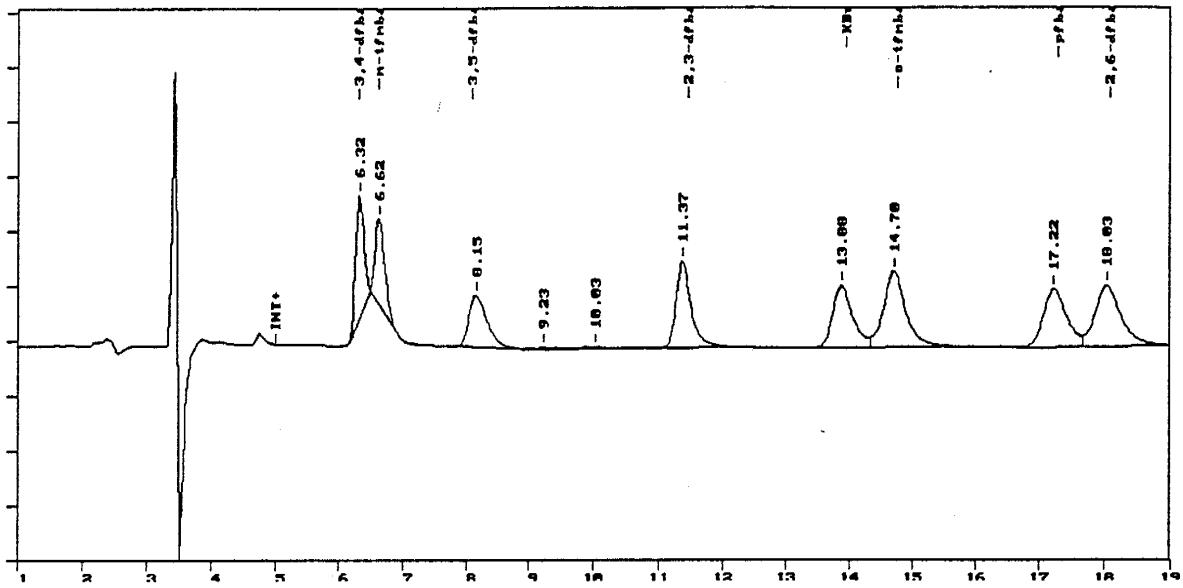

pumping well samples
e:\blue\Q617B27E.BNC
Data file = e:\lc\BPWI.80R
Date stamp = 03/06/93 Time = 01:45:38
Sample name = 1%b12
Collected on MAR 6, 1993 01:25:17 from port # 2
Operator = R. TerBerg
Reference file name = Q617B27E.BNC
Instrument = com port 2
Method name = e:\lc\rat.MET version # 130
Date method last modified = 04/13/93 Time = 13:33:28
Calibration file = E:\LC\RT3PT.CAL version # 335
Date cal file last modified = 04/14/93 Time = 15:14:08
Run time = 19.02 minutes Area reject = 0
Amount injected = 1 Dilution Factor = 1
Sample Weight = 1 Internal Standard Amount = 1
Sampling rate = 1 per second Starting peak width = .1 minutes
Peak detect threshold = 1.59
Chrom-Perfect Software Serial number = 9110 Version = 4.01 For New Mexico Tec
Today's date = 04-14-1993 Time = 15:26:02

PK	Ret Time	Name	Amount	Amount %	Area	Area %	Type	Width	Height	Height %
1	6.317	3,4-dfba	1.4400	15.2059%	48,352.8	10.233%	BB	0.152	5,310.36	20.1330%
2	6.617	m-tfmba	1.0600	11.1932%	38,539.6	8.156%	BB	0.171	3,764.86	14.2736%
3	8.150	3,5-dfba	1.0100	10.6653%	46,645.2	9.872%	BB	0.347	2,240.56	8.4946%
4	9.233		0.0000	0.0000%	1,477.1	0.313%	BV	0.261	94.48	0.3582%
5	10.033		0.0000	0.0000%	1,647.7	0.349%	VB	0.347	79.11	0.2999%
6	11.367	2,3-dfba	1.0200	10.7709%	62,559.8	13.240%	BB	0.278	3,750.16	14.2178%
7	13.883	KBr	1.1200	11.8268%	58,896.9	12.465%	BV	0.365	2,690.54	10.2005%
8	14.700	o-tfmba	1.0800	11.4044%	79,535.3	16.832%	VB	0.400	3,312.33	12.5579%
9	17.217	pfba	1.7200	18.1627%	62,432.4	13.213%	BV	0.415	2,506.83	9.5040%
10	18.033	2,6-dfba	1.0200	10.7708%	72,429.7	15.328%	VB	0.459	2,627.21	9.9605%

Total area = 472516.5 Total amount = 9.469996 Sample units = mg/L Total height = 26376.45

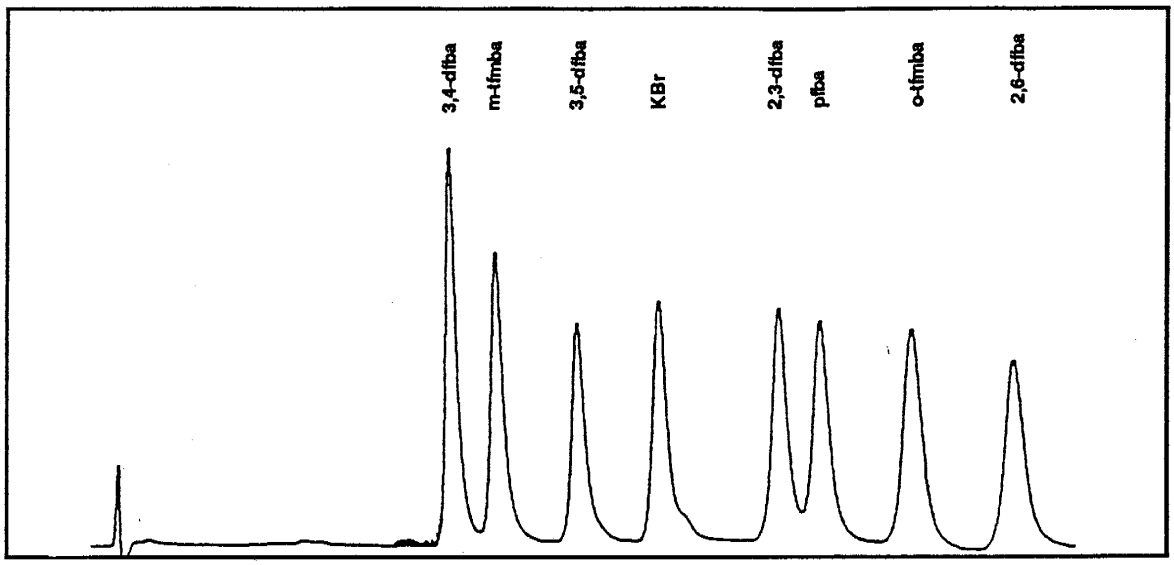

Sample name: 10%b12
Collected on DEC 2, 1992 17:20
Operator = R. TerBerg
Instrument = Waters 745 HPLC Data Recorder

PK	Name
1	3,4-dfba
2	m-tfmba
3	3,5-dfba
4	KBr
5	2,3-dfba
6	pfba
7	o-tfmba
8	2,6-dfba

APPENDIX II
Input Data for Pump Rate, Ambient Flow Direction, and Gradient

The following tabulated data comprises the transient input conditions (see figs. 5, 6, and 7; p.25) for the cross-verification modeling used to help identify and verify arrival mass and character.

Julian Date	Pump Rate (m^3)
182.00	.00165
183.00	.00165
184.50	.00170
187.50	.00164
188.50	.00159
189.50	.00160
190.50	.00158
191.50	.00160
192.50	.00166
193.50	.00157
194.50	.00160
195.50	.00174
196.50	.00168
197.50	.00159
198.50	.00150
199.50	.00136
200.50	.00110
201.50	.00000
202.50	.00047
203.50	.00155
204.50	.00155
205.50	.00154
206.50	.00152
207.50	.00167
208.50	.00165
209.50	.00162
210.50	.00156
211.50	.00156
212.50	.00155
213.50	.00148
214.50	.00139
215.50	.00138
216.50	.00138
217.50	.00147
218.50	.00166
219.50	.00164
220.50	.00166
221.50	.00167
222.50	.00161
223.50	.00156
224.50	.00154
225.50	.00145
226.50	.00158
227.50	.00154
228.50	.00154
229.50	.00156
230.50	.00154
231.50	.00152
232.50	.00150
233.50	.00154
234.50	.00154
235.50	.00151
236.50	.00150
237.50	.00152
238.50	.00149
239.50	.00144
240.50	.00157
241.50	.00153
242.50	.00148
243.50	.00146
244.50	.00151
245.50	.00149
246.50	.00151
247.50	.00160
248.50	.00149
249.50	.00153
250.50	.00150
251.50	.00153
252.50	.00149
253.50	.00102
254.50	.00027
255.50	.00114
256.50	.00148
257.50	.00146
258.50	.00148
259.50	.00152
260.50	.00150
261.50	.00150
262.50	.00129
263.50	.00129
264.50	.00128
265.50	.00136
266.50	.00144
267.50	.00152
268.50	.00148
269.50	.00147
270.50	.00146
271.50	.00145
272.50	.00148
273.50	.00152
274.50	.00153
275.50	.00154
276.50	.00140
277.50	.00138
278.50	.00139
279.50	.00141
280.50	.00147
281.50	.00146
282.50	.00150
283.50	.00152
284.50	.00153
285.50	.00154
286.50	.00152
287.50	.00152
288.50	.00152
289.50	.00149
290.50	.00147
291.50	.00155
292.50	.00151
293.50	.00150
294.50	.00150
295.50	.00150
296.50	.00152
297.50	.00149
298.50	.00144
299.50	.00144
300.50	.00144
301.50	.00153
302.50	.00148
303.50	.00151
304.50	.00151
305.50	.00150
306.50	.00150
307.50	.00149
308.50	.00156
309.50	.00151
310.50	.00150
311.50	.00150
312.50	.00151
313.38	.00134
314.17	.00000
400.00	.00000

Julian Date	Ambient Flow Gradient	Ambient Flow Direction
182	.00450	35.90
185	.00426	25.68
190	.00422	28.96
198	.00423	22.57
221	.00402	16.61
224	.00401	22.63
227	.00370	25.88
231	.00450	19.42
234	.00413	29.97
252	.00379	7.28
261	.00379	15.00
267	.00378	10.00
273	.00378	10.00
292	.00391	15.16
295	.00387	6.09
304	.00290	-3.68
311	.00351	-3.19
318	.00353	-6.89
323	.00273	2.70
329	.00330	12.72
358	.00320	11.6
372	.00320	5.7

APPENDIX III
SIMULATION SUMMARIES

The following summaries are checklists that accompany particle-time reports output by the particle tracker (Linderfelt, 1993). The checklist items in order of appearance are:

1). Tracer and injection location
2). Number of release periods - in each case, only one pulse injection was used
3). Number of sources - Multi-source particle tracking capability was bypassed in order to isolate particle behavior for each injection
4). Number of particles going to the well - total particles that travelled from the injection point to the pumping well
5). Well recovery - fraction of total particles injected, which were recovered at the pumping well
6). Number of particles going to the fence - total particles that travelled from the injection point, across a set of coordinates defining up to two monitoring well fences
7). Fence recovery - fraction of total particles injected, which crossed the coordinates defining up to two monitoring well fences
8). Total number of particles - total particles tracked from the injection point
9). TOTAL - total run time for the simulation (in seconds on a SUN 4-330 with 40MB of memory)

2,3-dfba I-5

Number of release periods: 1
Number of sources: 1
Number of particles going to well: 997
Well recovery: 1.00
Number of particles going to fence:
Fence # 1: 2
Fence # 2: 0
Fence recovery:
Fence # 1: 0.00
Fence # 2: 0.00
Total number of particles = 1000
TOTAL: 69.010 secs

3,4-dfba I-3

Number of release periods: 1
Number of sources: 1
Number of particles going to well: 0
Well recovery: 0.00
Number of particles going to fence:
Fence # 1: 0
Fence # 2: 0
Fence recovery:
Fence # 1: 0.00
Fence # 2: 0.00
Total number of particles = 1000
TOTAL: 224.580 secs

2,3-dfba I-8

Number of release periods: 1
Number of sources: 1
Number of particles going to well: 1000
Well recovery: 1.00
Number of particles going to fence:
Fence # 1: 0
Fence # 2: 0
Fence recovery:
Fence # 1: 0.00
Fence # 2: 0.00
Total number of particles = 1000
TOTAL: 95.730 secs

2,6-dfba I-6

Number of release periods: 1
Number of sources: 1
Number of particles going to well: 8
Well recovery: 0.01
Number of particles going to fence:
Fence # 1: 872
Fence # 2: 694
Fence recovery:
Fence # 1: 0.87
Fence # 2: 0.69
Total number of particles = 1000
TOTAL: 228.570 secs

3,5-dfba I-7

Number of release periods: 1
Number of sources: 1
Number of particles going to well: 1000
Well recovery: 1.00
Number of particles going to fence:
Fence # 1: 0
Fence # 2: 0
Fence recovery:
Fence # 1: 0.00
Fence # 2: 0.00
Total number of particles = 1000
TOTAL: 97.350 secs

2,6-dfba I-15

Number of release periods: 1
Number of sources: 1
Number of particles going to well: 500
Well recovery: 1.00
Number of particles going to fence:
Fence # 1: 0
Fence # 2: 0
Fence recovery:
Fence # 1: 0.00
Fence # 2: 0.00
Total number of particles = 500
TOTAL: 63.560 secs

3,4-dfba I-10

Number of release periods:	1
Number of sources:	1
Number of particles going to well:	34
Well recovery:	0.03
Number of particles going to fence:	
Fence # 1:	635
Fence # 2:	34
Fence recovery:	
Fence # 1:	0.63
Fence # 2:	0.03
Total number of particles =	1000

TOTAL: 232.710 secs

m-tfmba I-2

Number of release periods:	1
Number of sources:	1
Number of particles going to well:	1000
Well recovery:	1.00
Number of particles going to fence:	
Fence # 1:	0
Fence # 2:	0
Fence recovery:	
Fence # 1:	0.00
Fence # 2:	0.00
Total number of particles =	1000

TOTAL: 78.850 secs

m-tfmba I-14

Number of release periods:	1
Number of sources:	1
Number of particles going to well:	0
Well recovery:	0.00
Number of particles going to fence:	
Fence # 1:	0
Fence # 2:	0
Fence recovery:	
Fence # 1:	0.00
Fence # 2:	0.00
Total number of particles =	1000

TOTAL: 220.480 secs

3,5-dfba I-11

Number of release periods:	1
Number of sources:	1
Number of particles going to well:	0
Well recovery:	0.00
Number of particles going to fence:	
Fence # 1:	106
Fence # 2:	0
Fence recovery:	
Fence # 1:	0.11
Fence # 2:	0.00
Total number of particles =	1000

TOTAL: 226.980 secs

o-tfbma I-1

Number of release periods:	1
Number of sources:	1
Number of particles going to well:	1000
Well recovery:	1.00
Number of particles going to fence:	
Fence # 1:	0
Fence # 2:	0
Fence recovery:	
Fence # 1:	0.00
Fence # 2:	0.00
Total number of particles =	1000

TOTAL: 23.621 secs

o-tfmba I-13

Number of release periods:	1
Number of sources:	1
Number of particles going to well:	0
Well recovery:	0.00
Number of particles going to fence:	
Fence # 1:	0
Fence # 2:	0
Fence recovery:	
Fence # 1:	0.00
Fence # 2:	0.00
Total number of particles =	1000

TOTAL: 225.480 secs

bromide I-1

Number of release periods:	1
Number of sources:	1
Number of particles going to well:	1000
Well recovery:	1.00
Number of particles going to fence:	
Fence # 1:	0
Fence # 2:	0
Fence recovery:	
Fence # 1:	0.00
Fence # 2:	0.00
Total number of particles =	1000

TOTAL: 23.621 secs

bromide I-2

Number of release periods:	1
Number of sources:	1
Number of particles going to well:	1000
Well recovery:	1.00
Number of particles going to fence:	
Fence # 1:	0
Fence # 2:	0
Fence recovery:	
Fence # 1:	0.00
Fence # 2:	0.00
Total number of particles =	1000

TOTAL: 78.850 secs

pfba I-4

Number of release periods:	1
Number of sources:	1
Number of particles going to well:	1000
Well recovery:	1.00
Number of particles going to fence:	
Fence # 1:	0
Fence # 2:	0
Fence recovery:	
Fence # 1:	0.00
Fence # 2:	0.00
Total number of particles =	1000

TOTAL: 49.300 secs

bromide I-9

Number of release periods:	1
Number of sources:	1
Number of particles going to well:	160
Well recovery:	0.16
Number of particles going to fence:	
Fence # 1:	225
Fence # 2:	67
Fence recovery:	
Fence # 1:	0.22
Fence # 2:	0.07
Total number of particles =	1000

TOTAL: 226.280 secs

bromide I-15

Number of release periods:	1
Number of sources:	1
Number of particles going to well:	1000
Well recovery:	1.00
Number of particles going to fence:	
Fence # 1:	0
Fence # 2:	0
Fence recovery:	
Fence # 1:	0.00
Fence # 2:	0.00
Total number of particles =	1000

TOTAL: 130.550 secs

pfba I-12

Number of release periods:	1
Number of sources:	1
Number of particles going to well:	970
Well recovery:	0.97
Number of particles going to fence:	
Fence # 1:	0
Fence # 2:	0
Fence recovery:	
Fence # 1:	0.00
Fence # 2:	0.00
Total number of particles =	1000

TOTAL: 150.500 secs

pfba I-9

Number of release periods:	1
Number of sources:	1
Number of particles going to well:	87
Well recovery:	0.17
Number of particles going to fence:	
Fence # 1:	115
Fence # 2:	33
Fence recovery:	
Fence # 1:	0.23
Fence # 2:	0.07
Total number of particles =	500

TOTAL: 110.409 secs

APPENDIX IV
TIME-DEPTH-CONCENTRATION BREAKTHROUGH DATA

The following data is a tracer by tracer tabulation of HPLC analytic results. For each tracer the Julian date of acquisition, from July 5, 1992 (185) to November 7, 1992 (311), references the pumping well intervals for which samples were analyzed. The 1 m intervals are denoted by the basal depth of each interval. Of the seven intervals in the pumping well, only those bottoming at 3, 4, 5, and 6 m depth yielded tracer recoveries from the in samples. For the purpose of consistent comparison with the vertically averaged 2D simulations, the recoveries from the four producing intervals were totalled and averaged for a recovery per producing-meter-interval, or a recovery normalized by interval pump-rate.

xyz time-depth-conc. bt data for depth	normalized conc. from gps. of levels					Br-					
					2	3*	4*	5*	6*	7*	8
Julian day	3 to 6	3 to 7	3 to 8	all							
185	2.0543	2.8421	2.5643	2.2825	0.5920	3.5984	0.0212	4.1621	0.4354	5.9936	1.1750
186	2.3624	2.9659	2.6216	2.2621	0.1055	0.8937	5.0558	1.8798	1.7000	5.3000	0.9000
189	1.5526	2.6820	2.3434	2.0236	0.1060	0.1320	1.9658	1.4124	2.7000	7.2000	0.6500
190	0.6721	1.6777	1.5614	1.3720	0.1160	0.0809	1.3355	0.3919	0.9000	5.7000	1.1000
191	0.3224	1.2379	1.1966	1.0366	0.0905	0.0707	0.4343	0.1844	0.8000	4.9000	0.9900
194	0.1802	0.9841	0.9297	0.8166	0.1380	0.0518	0.2596	0.1763	0.2331	4.2000	0.8573
195	0.2189	1.3055	1.2199	1.0851	0.1361	0.0490	0.1073	0.2683	0.4512	5.6516	0.7923
197	0.1301	0.5477	0.5729	0.5157	0.1721	0.0576	0.0396	0.1919	0.2315	2.2179	0.6982
198	0.0836	0.4532	0.4905	0.4330	0.0884	0.0276	0.0217	0.0671	0.2186	1.9309	0.6768
199	0.0782	0.5540	0.5673	0.5155	0.0844	0.0244	0.0190	0.0488	0.2206	2.4572	0.7539
200	0.0848	0.4478	0.5049	0.4475	0.1032	0.0146	0.0120	0.0626	0.2500	1.9000	0.7900
202	0.1107	0.4868	0.5611	0.4959	0.1051	0.0356	0.0205	0.1405	0.2462	1.9913	0.9323
203	0.0993	0.9141	0.9869	0.8682	0.1424	0.0499	0.0000	0.0000	0.3472	4.1734	1.3507
204	0.1545	1.1688	1.1795	1.0343	0.1629	0.0900	0.0311	0.0564	0.4375	5.2151	1.2440
205	0.1483	1.0420	1.0815	0.9482	0.1341	0.0324	0.0464	0.0849	0.4316	4.6128	1.2782
206	0.1884	1.2702	1.2962	1.1296	0.1312	0.0691	0.0983	0.1256	0.4605	5.5974	1.4263
207	0.2298	1.3143	1.3282	1.1555	0.1311	0.1137	0.1705	0.1883	0.4467	5.6523	1.3859
208	0.3039	1.3475	1.3245	1.1535	0.1272	0.1585	0.2125	0.2347	0.6100	5.5218	1.2086
209	0.3275	1.3070	1.2552	1.0983	0.1570	0.2143	0.2590	0.3783	0.4581	5.2250	0.9961
210	0.4328	1.8462	1.8052	1.4034	0.1929	0.3054	0.5690	0.2468	0.6100	6.5000	1.4000
211	0.5748	1.5199	1.4499	1.2621	0.1351	0.5630	0.8513	0.8850	0.2000	5.3000	1.1000
212	0.4862	1.0617	1.1041	0.9709	0.1722	0.3705	0.4524	0.8347	0.2872	3.3638	1.3157
213	0.6003	1.7931	1.7113	1.4869	0.1405	0.3686	0.7435	0.7008	0.5685	6.5641	1.3025
217	0.4752	1.3186	1.2236	1.0640	0.1053	0.2216	0.6296	0.4251	0.6245	4.6932	0.7488
218	0.5099	1.3260	1.2151	1.0627	0.1482	0.1460	0.7162	0.4813	0.6961	4.5906	0.6604
219	0.5926	1.3441	1.2313	1.0712	0.1111	0.1589	0.7921	0.6791	0.7404	4.3500	0.6870
220	0.4467	1.1974	1.1100	0.9657	0.1000	0.1256	0.7136	0.4976	0.4500	4.2000	0.6730
221	0.5629	1.2704	1.1720	1.0177	0.0920	0.1101	0.8333	0.5184	0.9900	4.1000	0.6800
222	0.5262	1.2635	1.1786	1.0218	0.0806	0.1147	0.6913	0.4835	0.8154	4.2128	0.7540
223	0.5230	1.2604	1.1753	1.0195	0.0650	0.1373	0.6600	0.4781	0.8164	4.2100	0.7500
224	0.4448	1.2003	1.1290	0.9798	0.0650	0.1600	0.6557	0.4636	0.5000	4.2220	0.7725
225	0.3741	1.1461	1.0878	0.9444	0.0650	0.1806	0.7511	0.5648	0.0000	4.2340	0.7950
226	0.5524	1.2911	1.2122	1.0511	0.0650	0.1950	0.7107	0.5468	0.7573	4.2480	0.8175
227	0.6645	1.3832	1.2926	1.1201	0.0650	0.2119	0.9189	0.7009	0.8261	4.2580	0.8400
228	0.6851	1.4021	1.3121	1.1368	0.0650	0.2127	0.9674	0.7001	0.8600	4.2700	0.8625
229	0.7436	1.4513	1.3569	1.1760	0.0902	0.2331	1.0981	0.7476	0.8958	4.2820	0.8850
230	0.7947	1.4958	1.4015	1.2141	0.0900	0.2686	0.7500	0.9400	1.2000	4.3000	0.9300
231	0.8568	1.3471	1.2076	1.0476	0.0877	0.2956	1.2000	0.8400	1.1000	3.3000	0.5100
232	0.7158	1.3726	1.2872	1.1155	0.0854	0.2931	0.6900	0.7800	1.1000	4.0000	0.8600
233	0.6760	1.4008	1.2357	1.0710	0.0831	0.2940	1.0000	0.6200	0.7900	4.3000	0.4100
234	0.8079	1.2464	1.0836	0.9404	0.0808	0.2964	0.5500	0.7854	0.8000	3.8000	0.2700
235	0.5167	1.2733	1.2078	1.0464	0.0785	0.2968	0.8900	0.2000	0.6800	4.3000	0.8800
237	0.7800	1.8480	1.5400	1.3309	0.0762	0.3500	0.9700	0.3200	1.4000	5.2000	1.0000
238	0.8560	1.5448	1.4507	1.2540	0.0739	0.4069	0.8958	0.3176	1.0038	5.1000	0.9800
240	0.8350	1.5080	1.4166	1.2245	0.0716	0.4667	0.8704	0.2556	0.9470	5.0000	0.9800
243	0.4681	1.3708	1.3012	1.1252	0.0693	0.4330	0.6206	0.1553	0.8556	4.9696	0.9530
245	0.4978	1.4309	1.3507	1.1673	0.0670	0.3982	0.6478	0.1407	0.8164	5.1632	0.9500
246	0.4565	1.3668	1.3160	1.1373	0.0647	0.3600	0.7322	0.0680	0.6776	5.0850	0.9633
247	0.5065	1.3965	1.3262	1.1473	0.0624	0.3371	0.5279	0.1255	1.0356	4.9682	0.9766
248	0.4786	1.3701	1.3068	1.1287	0.0601	0.3359	0.4826	0.1158	0.9851	4.9314	0.9899
249	0.8743	1.7002	1.5841	1.3680	0.0578	0.2900	2.0686	0.1127	1.0257	5.0041	1.0032
250	0.4415	1.4180	1.3494	1.1645	0.0555	0.2494	0.4204	0.1089	0.9893	5.3137	1.0165
251	0.4450	1.3806	1.3054	1.1265	0.0532	0.2300	0.3984	0.1461	1.0054	5.0229	1.0298
252	0.3969	1.3354	1.2667	1.1102	0.0509	0.2029	0.3516	0.1157	0.9256	5.0814	1.0431
253	0.1603	0.8151	0.8553	0.7401	0.0486	0.1200	0.0937	0.1496	0.2778	3.4346	1.0564
254	0.3241	1.1106	1.1038	0.9527	0.0463	0.0317	0.1497	0.1492	0.9656	4.2568	1.0697
255	0.4130	1.2684	1.2375	1.0670	0.0440	0.3327	0.2647	0.1870	0.8675	4.6900	1.0830
256	0.3565	1.2738	1.2471	1.0749	0.0417	0.3149	0.2055	0.1973	0.7162	4.9352	1.1136
259	0.3475	1.2567	1.2347	1.0640	0.0394	0.3026	0.1886	0.2590	0.6399	4.9082	1.1100
260	0.3293	1.2228	1.2080	1.0407	0.0371	0.2771	0.1629	0.2956	0.5815	4.7969	1.1337
262	0.3214	1.2151	1.2055	1.0363	0.0348	0.2819	0.1735	0.3654	0.4348	4.7900	1.1574
264	0.2683	1.1337	1.1416	0.9831	0.0325	0.2451	0.1757	0.3995	0.2530	4.5950	1.1811
265	0.2921	1.1137	1.1289	0.9720	0.0307	0.2419	0.2124	0.5116	0.2025	4.4000	1.2048
266	0.2613	1.0120	1.0481	0.9026	0.0300	0.1922	0.2400	0.4151	0.1978	4.0146	1.2285
269	0.2563	1.0565	1.0908	0.9392	0.0297	0.1102	0.3646	0.3298	0.2285	4.2596	1.2522
272	0.3969	1.2057	1.2174	1.0477	0.0293	0.0871	0.5389	0.7176	0.2441	4.4409	1.2759
273	0.5342	0.7274	0.8228	0.7094	0.0290	0.0689	0.6300	1.1000	0.3400	1.5000	1.3000
274	0.8096	1.6077	1.5396	1.3239	0.0286	0.0985	0.7800	1.4000	0.1600	5.6000	1.2000
275	0.6814	1.4851	1.4376	1.2363	0.0283	0.0557	0.6700	1.8000	0.2000	4.7000	1.2000
276	0.5104	1.0283	1.0903	0.9385	0.0280	0.0816	0.5400	1.3000	0.1200	3.1000	1.4000
279	0.8925	1.7140	1.7117	1.4711	0.0276	0.0000	0.1000	3.4000	0.0700	5.0000	1.7000
281	0.5399	1.1920	1.1933	1.0268	0.0276	0.0586	0.5100	1.5000	0.0900	3.8000	1.2000
283	0.1996	0.9197	0.9864	0.8323	0.0276	0.0596	0.4360	0.1725	0.1300	3.6000	1.2000
286	0.3491	1.0003	1.0296	0.8864	0.0273	0.0300	0.5046	0.6838	0.1779	3.8050	1.1763
290	0.1402	0.7942	0.8539	0.7358	0.0269	0.0000	0.3485	0.1793	0.0319	3.4100	1.1526
292	0.1544	0.7865	0.8269	0.7126	0.0266	0.0000	0.3559	0.1742	0.0674	3.2150	1.1289
293	0.1614	0.7331	0.7951	0.6853	0.0262	0.0000	0.3525	0.1786	0.1144	3.0200	1.1052
294	0.1343	0.6724	0.7406	0.6385	0.0259	0.0000	0.2847	0.1583	0.0942	2.8250	1.0815
295	0.1268	0.6275	0.6992	0.6029	0.0256	0.0264	0.2304	0.1566	0.0918	2.6300	1.0578
297	0.1462	0.6056	0.6770	0.5839	0.0252	0.0279	0.2652	0.2126	0.0873	2.4350	1.0341
300	0.1317	0.5533	0.6295	0.5431	0.0249	0.0000	0.1709	0.2532	0.1026	2.2400	1.0104
301	0.1544	0.5325	0.6082	0.5248	0.0245	0.0000	0.2626	0.2849	0.0701	2.0450	0.9867
302	0.1514	0.4911	0.5698	0.4918	0.0242	0.0367	0.1923	0.2807	0.0958	1.8500	0.9630
303	0.0921	0.4047	0.4936	0.4266	0.0239	0.0000	0.0000	0.2769	0.0914	1.6550	0.9393
304	0.1577	0.4182	0.5011	0.4329	0.0235	0.0269	0.2291	0.3100	0.0650	1.4600	0.9156
307	0.1868	0.4024	0.4840	0.4182	0.0232	0.0332	0.3205	0.3496	0.0438	1.2650	0.8919
308	0.0748	0.2738	0.3729	0.3229	0.0228	0.0000	0.1389	0.0667	0.0934	1.0700	0.8682
309	0.2050	0.3390	0.4233	0.3660	0.0225	0.0511	0.3483	0.3221	0.0986	0.8750	0.8445
310	0.1383	0.2466	0.3423	0.2966	0.0222	0.0396	0.0906	0.3365	0.0864	0.6800	0.8208
311	0.1144	0.1885	0.2899	0.2516	0.0218	0.0252	0.3428	0.0639	0.0256	0.4850	0.7971

xyz time-depth-conc. bt data for 2,3-dfba in pumping well

depth Julian day	normalized conc.*	2	3*	4*	5*	6*	7	8
185	0.0170	0.0172	0.0168	0.0191	0.0135	0.0184	0.0164	0.0158
188	0.0167	0.0149	0.0165	0.0169	0.0178	0.0157	0.0161	0.0184
189	0.0163	0.0152	0.0169	0.0188	0.0174	0.0122	0.0133	0.0162
190	0.0156	0.0157	0.0137	0.0181	0.0171	0.0157	0.0000	0.0000
191	0.0000	0.0000	0.0000	0.0000	0.0000	0.0000	0.0000	0.0000
194	0.0038	0.0000	0.0043	0.0000	0.0109	0.0000	0.0233	0.0000
195	0.0000	0.0307	0.0000	0.0000	0.0000	0.0000	0.0000	0.0000
197	0.0106	0.0423	0.0000	0.0000	0.0000	0.0423	0.0000	0.0000
198	0.0000	0.0000	0.0000	0.0000	0.0000	0.0000	0.0000	0.0000
199	0.0837	0.0000	0.3349	0.0000	0.0000	0.0000	0.0000	0.0000
200	0.0239	0.0000	0.0957	0.0000	0.0000	0.0000	0.0000	0.0000
201	0.0000	0.0000	0.0000	0.0000	0.0000	0.0000	0.0000	0.0000
202	0.0094	0.0000	0.0319	0.0000	0.0065	0.0000	0.0000	0.0000
203	0.2064	0.0068	0.7946	0.0000	0.0000	0.0308	0.0000	0.0000
204	0.1854	0.0081	0.7415	0.0000	0.0000	0.0000	0.0355	0.0000
205	0.2185	0.0000	0.8661	0.0000	0.0000	0.0000	0.0000	0.0000
206	0.3468	0.0000	1.3872	0.0000	0.0000	0.0000	0.0111	0.0450
207	0.4060	0.0000	1.5632	0.0000	0.0175	0.0232	0.0239	0.0000
208	0.4281	0.0000	1.6993	0.0000	0.0130	0.0000	0.0000	0.0000
209	0.4041	0.0000	1.5802	0.0286	0.0000	0.0076	0.0000	0.0156
210	0.5448	0.0000	1.5117	0.1187	0.0033		0.0000	0.0000
211	0.3112	0.0000	0.5419	0.4650	0.2377	0.0000		0.0000
212	0.6170	0.0000	0.5842	0.3582	1.5154	0.0000	0.0000	0.0000
213	0.4289	0.0000	0.5781	0.9360	0.0000	0.1995	0.0000	0.1277
217	4.1973	0.0000	0.8308	4.3908	5.4852	6.0824	0.0000	0.0000
218	3.8095	0.0000	0.9061	5.2489	4.2286	4.0525	0.0000	0.0000
219	2.8566	0.0000	0.8210	4.6964	3.7484	2.1613		
220	2.1724	0.0000	0.6441	3.6744	3.3504	1.0206		
221	1.8103	0.0000	0.4055	3.5964	3.0227	0.2146	0.0000	0.0000
222	1.7454	0.0000	0.4167	3.8310	2.5661	0.1478	0.0000	0.0000
223	1.5451		0.5192	3.5639	2.0871	0.0000		
224	2.8468			3.7436	1.9498			
225	1.5429		0.9483	3.4345	1.5580	0.2310		
226	1.3352			2.4381	1.5446	0.0228		
227	1.5884		1.6419	2.6578	1.7962	0.1776		
228	1.4782		1.5377	2.2362	2.1367	0.0000		
229	1.4740	0.0000	1.3246	2.1401	2.3610	0.0704	0.0000	
230	1.5761		1.1312	2.2789	2.6367	0.2578		
231	1.6363		0.7421	2.4162	2.3538	1.0330		
232	1.2954		0.5997	2.9876		1.5943	0.0000	
233	3.1699			3.0715	4.7033	1.7948	0.0000	
234	2.5238		0.4685	3.0573	4.5646	1.9646	0.0000	
236	2.3718		0.4489	2.6259	4.8253	1.5691	0.1150	0.0223
237	0.9083		0.0000	2.7248			0.0000	
239	1.9834		0.6811	2.6851	2.4389	1.9284		
240	1.9621		0.9007	2.8027	1.6592	2.4656		
243	2.0075		0.4881	2.7940	0.8403	3.8074	0.1035	0.0000
245	1.9273		0.2034	2.7039	1.1929	3.6088	0.0000	
246	2.9178			2.8254	1.8086	4.0198	0.0294	
247	2.3313		0.0000	2.7981	2.8236	3.7034	0.2273	
248	2.2541		0.0000	2.8359	3.2143	3.1861	0.0708	
249	3.4738			3.4927	3.8421	3.0870	0.0843	
250	1.7221		0.0000	2.0877	2.8416	1.9561	0.0000	
251	1.6567		0.0000	2.1518	2.8800	1.6028	0.0266	0.0000
252	1.1365		0.0000	1.5325	1.9204	1.1012	0.0170	
253	0.7560			0.3935	1.6461	0.2285	0.0000	
254	0.9363		0.0000	0.6207	1.4448	1.8798	0.0383	
255	1.0236		0.0000	1.7567	1.3125	1.0250		
258	0.3614		0.0000	0.5403	0.3791	0.5261	0.0246	0.0000
259	0.3381		0.0179	0.5772	0.3083	0.4490	0.0000	
260	0.2652		0.0000	0.3842	0.2493	0.4274	0.0000	
261								
262	0.1852		0.0000	0.2579	0.1638	0.3191		
264	0.1625		0.0000	0.1881	0.1391	0.3228		
265	0.1410	0.0000	0.0000	0.1681	0.1129	0.2831		
266	0.0963		0.0000	0.1325	0.0445	0.2200	0.0000	
269	0.0462		0.0000	0.0000	0.0374	0.1474	0.0000	
272	0.0300		0.0000	0.0000	0.0357	0.0845	0.0000	
273	0.0930		0.0000	0.0370	0.2112	0.1238	0.0000	
274	0.0429		0.0000	0.0246	0.0586	0.0865		
275	0.0156		0.0000	0.0000	0.0253	0.0370		
276	0.0481		0.0000	0.0563	0.0508	0.0854		
279	0.0327		0.0000	0.0000	0.0364	0.0943		
281	0.0486	0.0000	0.0000	0.0000	0.0446	0.1497	0.0091	0.0000
283	0.0211		0.0000	0.0000	0.0000	0.0842		
286	0.0248			0.0000	0.0302	0.0442	0.0000	
290	0.0211		0.0000	0.0000	0.0000	0.0842		
291								
292	0.0000		0.0000	0.0000	0.0000	0.0000		
293	0.0200		0.0000	0.0000	0.0000	0.0799		
294	0.0142		0.0000	0.0000	0.0000	0.0567		
295	0.0187		0.0000	0.0000	0.0000	0.0749		
297	0.0000		0.0000	0.0000	0.0000	0.0000		
300	0.0000		0.0000	0.0000	0.0000	0.0000		
301	0.0000		0.0000	0.0000	0.0000	0.0000		
302	0.0226		0.0905	0.0000	0.0000	0.0000		
303	0.0000		0.0000	0.0000	0.0000	0.0000		
304	0.0000		0.0000	0.0000	0.0000			
305								
306								
307	0.0000		0.0000	0.0000	0.0000	0.0000		
308	0.0000		0.0000	0.0000	0.0000	0.0000		
309	0.0154		0.0000	0.0000	0.0000	0.0617		
310	0.0123		0.0000	0.0000	0.0493	0.0000		
311	0.0000		0.0000	0.0000	0.0000	0.0000		

xyz time-depth-conc. bt data for 2,6-dfba in pumping well

depth Julian day	normalize conc.*	2	3*	4*	5*	6*	7	8
185	0.0000	0.0000	0.0000	0.0000	0.0000	0.0000	0.0000	0.0000
188	0.0000	0.0000	0.0000	0.0000	0.0000	0.0000	0.0000	0.0876
189	0.0000	0.0000	0.0000	0.0000	0.0000	0.0000	0.0000	0.0000
190	0.0000	0.0000	0.0000	0.0000	0.0000	0.0000	0.0000	0.0000
191	0.0054	0.0548	0.0215	0.0000	0.0000	0.0000	0.0000	0.0000
194	0.0000	0.0000	0.0000	0.0000	0.0000	0.0000	0.0000	0.0000
195	0.0000	0.0132	0.0000	0.0000	0.0000	0.0000	0.0000	0.0000
197	0.0000	0.0000	0.0000	0.0000	0.0000	0.0000	0.0000	0.0000
198	0.0000	0.0000	0.0000	0.0000	0.0000	0.0000	0.0000	0.0000
199	0.0000	0.0000	0.0000	0.0000	0.0000	0.0000	0.0000	0.0000
200	0.0000	0.0000	0.0000	0.0000	0.0000	0.0000	0.0000	0.0000
202	0.0000	0.0000	0.0000	0.0000	0.0000	0.0000	0.0000	0.0000
203	0.0000	0.0000	0.0000	0.0000	0.0000	0.0000	0.0000	0.0000
204	0.0320	0.0000	0.0000	0.0000	0.1278	0.0000	0.0000	0.0000
205	0.0099	0.0000	0.0000	0.0190	0.0208	0.0000	0.0000	0.0000
206	0.0062	0.0203	0.0000	0.0000	0.0246	0.0000	0.0000	0.0000
207	0.0043	0.0000	0.0000	0.0000	0.0172	0.0000	0.0000	0.0000
208	0.0000	0.0000	0.0000	0.0000	0.0000	0.0000	0.0000	0.0000
209	0.0100	0.0000	0.0000	0.0401	0.0000	0.0000	0.0000	0.0000
210	0.0000	0.0000	0.0000	0.0000	0.0000		0.0000	0.0000
211	0.0000	0.0000	0.0000	0.0000	0.0000	0.0000	0.0000	0.0000
212	0.0000	0.0000	0.0000	0.0000	0.0000	0.0000	0.0000	0.0000
213	0.0000	0.0000	0.0000	0.0000	0.0000	0.0000	0.0000	0.0000
217	0.0093	0.0000	0.0371	0.0000	0.0000	0.0000	0.0000	0.0000
218	0.0000	0.0000	0.0000	0.0000	0.0000	0.0000	0.0000	0.0000
219	0.0094	0.0000	0.0375	0.0000	0.0000	0.0000		
220	0.0000		0.0000	0.0000	0.0000	0.0000		
221	0.0000	0.0000	0.0000	0.0000	0.0000	0.0000	0.0000	0.0000
222	0.0000	0.0000	0.0000	0.0000	0.0000	0.0000	0.0000	0.0000
223	0.0000		0.0000	0.0000	0.0000	0.0000		
224	0.0000			0.0000	0.0000			
225	0.0000		0.0000	0.0000	0.0000	0.0000		
226	0.0000			0.0000	0.0000	0.0000		
227	0.0540		0.2158	0.0000	0.0000	0.0000		
228	0.0603		0.2410	0.0000	0.0000			
229	0.0753	0.0000	0.2712	0.0000	0.0000	0.0301	0.0000	
230	0.0788		0.3150	0.0000	0.0000	0.0000		
231	0.0901		0.3603	0.0000	0.0000	0.0000		
232	0.0800		0.3200	0.0000		0.0000	0.0000	
233	0.0000			0.0000	0.0000	0.0000	0.0000	
234	0.0000		0.0000	0.0000	0.0000	0.0000	0.0000	
236	0.2444		0.4489	0.1693	0.3008	0.0585	0.0000	0.0000
237	0.0000			0.0000			0.0000	
239	0.2400		0.8039	0.0520	0.1040	0.0000		
240	0.2083		0.7593	0.0000	0.0740	0.0000		
243	0.2950		0.6839	0.2484	0.2475	0.0000	0.0000	0.0000
245	0.3713		0.5216	0.1405	0.1460	0.6770	0.0000	
246	0.4636			0.2550	0.1039	1.0320	0.0000	
247	0.5691		0.4416	0.1690	0.1064	1.5592	0.0000	
248	0.5161		0.4341	0.1737	0.1227	1.3340	0.0000	
249	0.5109			0.2328	0.1202	1.1797	0.0000	
250	0.4998		0.2748	0.2206	0.1210	1.3828	0.0000	
251	0.5093			0.2409	0.1084	1.1785	0.0000	
252	0.4735		0.2362	0.2301	0.1058	1.3220	0.0000	
253	0.1714			0.0403	0.1324	0.3414	0.0000	
254	0.4857		0.0000	0.1322	0.1237	1.6868	0.0000	
255	0.5272		0.4514	0.1594	0.1861	1.3120		
258	0.4221		0.4500	0.1104	0.2282	0.8997	0.0000	0.0000
259	0.3680		0.3940	0.0582	0.3185	0.7813	0.0000	
260	0.3688		0.3917	0.0000	0.4200	0.7435	0.0000	
261								
262	0.3739		0.4078	0.0922	0.6080	0.3877		
264	0.3339		0.3123	0.1474	0.5923	0.2834		
265	0.4351	0.0000	0.3158	0.1736	0.6989	0.5520		
266	0.2992		0.2529	0.2502	0.4838	0.2100	0.0000	
269	0.2774		0.1100	0.4900	0.3436	0.1658	0.0000	
272	0.5451		0.1031	0.8387	0.8689	0.3695	0.0000	
273	0.6305		0.0705	0.7722	1.4561	0.2231	0.0000	
274	0.7311		0.0597	0.9710	1.6557	0.2379		
275	0.6700		0.0671	0.7748	1.6416	0.1965		
276	0.8481		0.0413	0.9263	2.1937	0.2312		
279	1.0291		0.0000	0.4945	3.4230	0.1987		
281	0.9240	0.0000	0.0521	0.7718	2.6533	0.2188	0.0000	0.0000
283	0.2870		0.0000	0.6476	0.3608	0.1395		
286	0.6112			0.6083	1.0986	0.1266		
290	0.1944		0.0000	0.6145	0.1632	0.0000		
291								
292	0.1399		0.0000	0.4389	0.1206	0.0000		
293	0.2699		0.1295	0.5281	0.2926	0.1313		
294	0.2344		0.1334	0.3825	0.2851	0.1367		
295	0.2224		0.1684	0.3236	0.3976	0.0000		
297	0.0611		0.0000	0.2444	0.0000	0.0000		
300	0.0501		0.0000	0.0000	0.0000	0.2005		
301	0.0000		0.0000	0.0000	0.0000	0.0000		
302	0.0000		0.0000	0.0000	0.0000	0.0000		
303	0.0158		0.0000	0.0000	0.0633	0.0000		
304	0.0533		0.0000	0.1065				
305								
306								
307	0.0155		0.0000	0.0621	0.0000	0.0000		
308	0.0000		0.0000	0.0000	0.0000	0.0000		
309	0.0446		0.0000	0.0977	0.0808	0.0000		
310	0.0199		0.0000	0.0000	0.0795	0.0000		
311	0.0163		0.0000	0.0652	0.0000	0.0000		

xyz time-depth-conc. bt data fo 3,4-dfba in pumping well

depth	normalize	2	3*	4*	5*	6*	7	8
Julian da	conc.*							
185	0.0085	0.0140	0.0188	0.0000	0.0151	0.0000	0.0230	0.0491
188	0.0029	0.0126	0.0117	0.0000	0.0000	0.0000	0.0000	0.0516
189	0.0032	0.0000	0.0000	0.0127	0.0000	0.0000	0.0000	0.0437
190	0.0000	0.0000	0.0000	0.0000	0.0000	0.0000	0.0000	0.0494
191	0.0000	0.0000	0.0000	0.0000	0.0000	0.0000	0.0000	0.0000
194	0.0100	0.0000	0.0000	0.0000	0.0320	0.0080	0.0000	0.0210
195	0.0031	0.0000	0.0000	0.0000	0.0000	0.0123	0.0000	0.0000
197	0.0037	0.0000	0.0148	0.0000	0.0000	0.0000	0.0000	0.0000
198	0.0000	0.0000	0.0000	0.0000	0.0000	0.0000	0.0000	0.0000
199	0.0104	0.0000	0.0000	0.0000	0.0000	0.0414	0.0495	0.0000
200	0.0000	0.0000	0.0000	0.0000	0.0000	0.0000	0.0000	0.0000
202	0.0000	0.0177	0.0000	0.0000	0.0000	0.0000	0.0000	0.0000
203	0.0000	0.0000	0.0000	0.0000	0.0000	0.0000	0.0000	0.0000
204	0.0015	0.0000	0.0000	0.0060	0.0000	0.0000	0.0000	0.0000
205	0.0000	0.0000	0.0000	0.0000	0.0000	0.0000	0.0000	0.0000
206	0.0000	0.0000	0.0000	0.0000	0.0000	0.0000	0.0000	0.0102
207	0.0084	0.0000	0.0000	0.0127	0.0000	0.0208	0.0000	0.0133
208	0.0000	0.0000	0.0000	0.0000	0.0000	0.0000	0.0000	0.0053
209	0.0112	0.0065	0.0000	0.0283	0.0000	0.0166	0.0498	0.0069
210	0.0048	0.0025	0.0095	0.0050	0.0000		0.0000	0.0222
211	0.0000	0.0066	0.0000	0.0000	0.0000	0.0000		0.0153
212	0.0028	0.0040	0.0026	0.0000	0.0000	0.0087	0.0000	0.0000
213	0.0000	0.0000	0.0000	0.0000	0.0000	0.0000	0.0000	0.0000
217	0.0120	0.0000	0.0116	0.0103	0.0138	0.0123	0.0119	0.0115
218	0.0090	0.0033	0.0112	0.0102	0.0000	0.0144	0.0000	0.0106
219	0.0535	0.0109	0.0000	0.0102	0.2037	0.0000		
220	0.0000		0.0000	0.0000	0.0000	0.0000		
221	0.0209	0.0214	0.0000	0.0000	0.0371	0.0463	0.0209	0.0310
222	0.0239	0.0108	0.0000	0.0000	0.0000	0.0957	0.0226	0.0326
223	0.0468		0.0000	0.0000	0.0000	0.1871		
224	0.0106			0.0000	0.0211			
225	0.0802		0.0000	0.0000	0.0000	0.3208		
226	0.1179			0.0000	0.0431	0.3106		
227	0.1402		0.0000	0.0000	0.1072	0.4535		
228	0.0112		0.0000	0.0000	0.0448			
229	0.1513	0.0178	0.0257	0.0259	0.0648	0.4888	0.0154	
230	0.1353		0.0246	0.0000	0.0407	0.4757		
231	0.2119		0.0000	0.0000	0.0355	0.8119		
232	0.1603		0.0000	0.0000		0.6411	0.0000	
233	0.2396			0.0000	0.0000	0.7186	0.0000	
234	0.4305		0.0000	0.0000	0.1198	1.6020	0.0000	
236	0.3092		0.0000	0.0000	0.0572	1.1795	0.0542	0.0375
237	0.0000			0.0000			0.0204	
239	0.4204		0.0000	0.0000	0.0000	1.6817		
240	0.4584		0.0000	0.0000	0.0000	1.8334		
243	0.4878		0.0130	0.0171	0.0251	1.8960	0.0377	0.0000
245	0.6278		0.0000	0.0000	0.0000	2.5111	0.0000	
246	0.5823			0.0000	0.0000	1.7468	0.0000	
247	0.6208		0.0000	0.0000	0.0000	2.4832	0.0000	
248	0.6553		0.0000	0.0000	0.0000	2.6212	0.0000	
249	0.5943			0.0000	0.0000	1.7829	0.0000	
250	0.4299		0.0000	0.0500	0.0103	1.6592	0.0152	
251	0.5260			0.0000	0.0185	1.5595	0.0000	
252	0.4962		0.0000	0.0000	0.0000	1.9848	0.0000	
253	0.1191			0.0000	0.0000	0.3573	0.0000	
254	0.2292		0.0000	0.0000	0.0000	0.9167	0.0000	
255	0.3438		0.0000	0.0000	0.0000	1.3752		
258	0.3100		0.0000	0.0000	0.0000	1.2399	0.0113	0.0000
259	0.2448		0.0000	0.0000	0.0000	0.9791	0.0000	
260	0.3425		0.0000	0.0000	0.0219	1.3479	0.0000	
261								
262	0.2912		0.0000	0.0000	0.0000	1.1649		
264	0.2921		0.0000	0.0000	0.0166	1.1519		
265	0.1871	0.0000	0.0000	0.0000	0.0000	0.7484		
266	0.1197		0.0000	0.0000	0.0000	0.4788	0.0341	
269	0.1056		0.0000	0.0000	0.0000	0.4225	0.0000	
272	0.1074		0.0000	0.0000	0.0000	0.4296	0.0000	
273	0.1427		0.0000	0.0000	0.0762	0.4945	0.0000	
274	0.1174		0.0000	0.0000	0.0000	0.4695		
275	0.0910		0.0000	0.0000	0.0000	0.3641		
276	0.1214		0.0760	0.0000	0.0000	0.4095		
279	0.0718		0.0000	0.0000	0.0000	0.2872		
281	0.0836	0.0156	0.0000	0.0000	0.0152	0.3192	0.0226	0.0417
283	0.0593		0.0000	0.0000	0.0000	0.2371		
286	0.0518			0.0000	0.0338	0.1215		
290	0.0034		0.0000	0.0000	0.0000	0.0135		
291								
292	0.0364		0.0000	0.0000	0.0000	0.1456		
293	0.0322		0.0000	0.0000	0.0000	0.1287		
294	0.0241		0.0000	0.0000	0.0000	0.0965		
295	0.0115		0.0000	0.0000	0.0000	0.0458		
297	0.0238		0.0000	0.0000	0.0000	0.0953		
300	0.0000		0.0000	0.0000	0.0000	0.0000		
301	0.0172		0.0000	0.0000	0.0000	0.0686		
302	0.0156		0.0000	0.0000	0.0000	0.0622		
303	0.0186		0.0000	0.0000	0.0000	0.0745		
304	0.0000		0.0000	0.0000				
305								
306								
307	0.0000		0.0000	0.0000	0.0000	0.0000		
308	0.0121		0.0000	0.0000	0.0000	0.0482		
309	0.0164		0.0000	0.0000	0.0000	0.0655		
310	0.0201		0.0240	0.0231	0.0000	0.0331		
311	0.0035		0.0000	0.0141	0.0000	0.0000		

xyz time-depth-conc. bt data for 3,5-dfba in pumping well

depth	normalized	2	3*	4*	5*	6*	7	8
Julian day	conc.*							
185	0.0365	0.0426	0.0364	0.0407	0.0363	0.0365	0.0370	0.0401
188	0.0368	0.0313	0.0352	0.0358	0.0381	0.0369	0.0421	0.1516
189	0.0388	0.0353	0.0410	0.0365	0.0450	0.0326	0.0399	0.0423
190	0.0856	0.0413	0.0349	0.0336	0.1513	0.0427	0.0379	0.0331
191	0.0161	0.0000	0.0000	0.0844	0.0000	0.0000	0.0000	0.0000
194	0.0068	0.0000	0.0000	0.0000	0.0270	0.0000	0.0000	0.0000
195	0.0056	0.0000	0.0089	0.0000	0.0136	0.0000	0.0000	0.0000
197	0.0000	0.0000	0.0000	0.0000	0.0000	0.0000	0.0000	0.0000
198	0.0038	0.0000	0.0000	0.0000	0.0152	0.0000	0.0101	0.0000
199	0.0077	0.0000	0.0306	0.0000	0.0000	0.0000	0.0000	0.0000
200	0.0007	0.0000	0.0000	0.0028	0.0000	0.0000	0.0000	0.0000
202	0.0000	0.0000	0.0000	0.0000	0.0000	0.0000	0.0000	0.0000
203	0.0018	0.0000	0.0073	0.0000	0.0000	0.0000	0.0000	0.0000
204	0.0000	0.0000	0.0000	0.0000	0.0000	0.0000	0.0173	0.0102
205	0.0000	0.0000	0.0000	0.0000	0.0000	0.0000	0.0000	0.0000
206	0.0000	0.0000	0.0000	0.0000	0.0000	0.0000	0.0164	0.0085
207	0.0080	0.0101	0.0124	0.0000	0.0044	0.0070	0.0351	0.0000
208	0.0044	0.0000	0.0102	0.0000	0.0000	0.0074	0.0074	0.0134
209	0.0125	0.0051	0.0179	0.0000	0.0242	0.0078	0.0163	0.0266
210	0.0000	0.0000	0.0000	0.0000	0.0000		0.0000	0.0000
211	0.0375	0.0000	0.0136	0.0343	0.0506	0.0514		0.0062
212	0.0127	0.0000	0.0224	0.0000	0.0284	0.0000	0.0000	0.0000
213	0.0135	0.0000	0.0540	0.0000	0.0000	0.0000	0.0000	0.0000
217	0.2104	0.0000	0.8865	0.1087	0.0882	0.0000	0.0000	0.0000
218	0.3155	0.0000	0.9368	0.2253	0.1000	0.0000	0.0000	0.0000
219	0.5054	0.0000	1.3604	0.3123	0.3488	0.0000		
220	0.4780		1.0052	0.6234	0.2794	0.0000		
221	0.4748	0.0000	1.0080	0.6582	0.2329	0.0000	0.0000	0.0000
222	0.4956	0.0000	0.6871	0.9964	0.3189	0.0000	0.0000	0.0000
223	0.3640		0.3151	0.9269	0.2918	0.3000		
224	0.4218			0.5960	0.2475			
225	0.3074		0.1842	0.6721	0.3734	0.0000		
226	0.2550			0.4424	0.2869	0.0338		
227	0.2732		0.1959	0.4936	0.4032	0.0000		
228	0.2184		0.1290	0.2866	0.4561	0.0000		
229	0.2613	0.0000	0.1861	0.4562	0.4029	0.0000	0.0000	
230	0.1440		0.0116	0.3656	0.1988	0.0000		
231	0.3942		0.0000	0.6722	0.9045	0.0000		
232	0.1746		0.0000	0.6863		0.0122	0.0000	
233	1.1304			0.9322	2.3740	0.0848	0.0000	
234	0.3356		0.0000	1.2232	0.1198	0.0000	0.0000	
236	1.6088		0.0259	1.3170	5.0922	0.0000	0.0860	0.0000
237	1.0601			1.0601			0.0000	
239	0.9951		0.0000	0.5301	3.4502	0.0000		
240	0.8530		0.0000	0.3144	2.9666	0.1311		
243	0.8321		0.0000	0.4006	2.0132	0.1144	0.0000	0.0000
245	0.7077		0.0000	0.8037	1.7761	0.2509	0.0000	
246	0.9923			0.9362	1.6842	0.3764	0.0000	
247	0.7811		0.0000	1.1443	1.4961	0.4841	0.0000	
248	0.8198		0.0000	1.3452	1.3734	0.5606	0.0000	
249	0.8610			1.2634	0.9779	0.3417	0.0000	
250	0.8265		0.0000	1.6041	1.1508	0.5512	0.0000	
251	0.7830			1.2775	0.7611	0.3105	0.0000	
252	0.7863		0.0000	1.8434	0.8171	0.4847	0.0000	
253	0.3038			0.4364	0.3852	0.0878	0.0000	
254	0.8917		0.0000	2.5473	0.3243	0.6951	0.0000	
255	0.9159		0.0000	2.5883	0.4973	0.5781		
258	0.8469		0.0536	2.7076	0.2542	0.3722	0.0000	0.0000
259	0.6326		0.0000	2.7694	0.1787	0.3823	0.0000	
260	1.1940		0.0000	3.8423	0.2422	0.8914	0.0000	
261								
262	1.0254		0.0000	3.1502	0.1437	0.8078		
264	1.1417		0.0000	3.3212	0.0965	1.1470		
265	1.1417		0.0409	3.1078	0.1392	1.2789		
266	1.0050		0.0000	2.6756	0.0443	1.3000	0.0000	
269	0.9500		0.0000	2.0400	0.0630	1.6969	0.0000	
272	0.7574		0.0000	1.6801	0.0000	1.3494	0.0000	
273	0.5117		0.0000	1.0870	0.1464	0.8135	0.0000	
274	0.4352		0.0000	1.0044	0.0000	0.7363		
275	0.4133		0.0000	0.9354	0.0000	0.7179		
276	0.3372		0.0000	0.6557	0.0000	0.4930		
279	0.2512		0.0000	0.5528	0.0000	0.4519		
281	0.3521	0.0000	0.0000	0.8335	0.0266	0.5482	0.0488	0.0749
283	0.1973		0.0000	0.4982	0.0000	0.2911		
286	0.0818			0.2755	0.0000	0.0000		
290	0.0489		0.0000	0.1955	0.0000	0.0000		
291								
292	0.1058		0.0000	0.1765	0.0000	0.2468		
293	0.1288		0.0286	0.1936	0.0754	0.2173		
294	0.1903		0.2475	0.1983	0.1547	0.1607		
295	0.1833		0.0788	0.1925	0.2530	0.2089		
297	0.1303		0.0000	0.2176	0.0000	0.3037		
300	0.0899		0.0000	0.0000	0.0000	0.3597		
301	0.0840		0.0000	0.0000	0.0000	0.3361		
302	0.0979		0.0000	0.0832	0.0000	0.3082		
303	0.1623		0.0000	0.2916	0.0000	0.3575		
304	0.0354		0.0000	0.0707				
305								
306								
307	0.0094		0.0000	0.0374	0.0000	0.0000		
308	0.0125		0.0000	0.0000	0.0000	0.0500		
309	0.0397		0.0000	0.0000	0.0000	0.1589		
310	0.0056		0.0000	0.0000	0.0000	0.0224		
311	0.0000		0.0000	0.0000	0.0000	0.0000		

xyz time-depth-conc. bt data for m-tfmba in pumping well

depth Julian day	normalize conc.*	2	3*	4*	5*	6*	7	8
185	0.0173	0.0124	0.0351	0.0000	0.0340	0.0000	0.0000	0.0000
188	0.0240	0.6567	0.0166	0.0457	0.0209	0.0127	0.0209	0.0516
189	0.0157	0.0142	0.0105	0.0170	0.0199	0.0153	0.0000	0.0000
190	0.0032	0.0000	0.0000	0.0128	0.0000	0.0000	0.0000	0.0000
191	0.0000	0.4622	0.0000	0.0000	0.0000	0.0000	0.0000	0.0000
194	0.0175	0.0000	0.0000	0.0000	0.0480	0.0220	0.0000	0.0110
195	0.0119	0.0152	0.0225	0.0000	0.0249	0.0000	0.0000	0.0145
197	0.0021	0.0258	0.0083	0.0000	0.0000	0.0000	0.0000	0.0106
198	0.0230	0.0229	0.0207	0.0224	0.0224	0.0264	0.0178	0.0164
199	0.0173	0.0220	0.0177	0.0200	0.0186	0.0151	0.0200	0.0150
200	0.0145	0.0070	0.0054	0.0065	0.0162	0.0295	0.0071	0.0108
202	0.0093	0.0193	0.0171	0.0068	0.0059	0.0073	0.0244	0.0195
203	0.0024	0.0097	0.0097	0.0000	0.0000	0.0000	0.0000	0.0000
204	0.0000	0.0000	0.0000	0.0000	0.0000	0.0000	0.0000	0.0000
205	0.0000	0.0000	0.0000	0.0000	0.0000	0.0000	0.0000	0.0000
208	0.0250	0.0000	0.0000	0.0500	0.0500	0.0000	0.0000	0.0000
207	0.1140	0.0000	0.0634	0.1875	0.2049	0.0000	0.0000	0.0000
208	0.1745	0.0000	0.1684	0.2405	0.2718	0.0172	0.0000	0.0203
209	0.2388	0.0000	0.2048	0.3233	0.4177	0.0093	0.0790	0.0498
210	0.4936	0.0084	0.3436	0.7487	0.3684		0.0000	0.0000
211	0.6816	0.0075	0.4821	0.8954	1.3489	0.0000		0.0000
212	0.8114	0.0189	0.3999	0.6223	1.4236	0.0000	0.0000	0.0000
213	0.8356	0.0040	0.3815	1.0394	1.1215	0.0000	0.0000	0.0000
217	0.4802	0.0000	0.2397	1.0388	0.6422	0.0000	0.0000	0.0000
218	0.4591	0.0000	0.1584	1.0140	0.6458	0.0183	0.0000	0.0000
219	0.5189	0.0079	0.1259	1.2177	0.7320	0.0000		
220	0.4245		0.0221	1.0378	0.6382	0.0000		
221	0.3969	0.0000	0.0360	0.9637	0.5546	0.0333	0.0000	0.0000
222	0.3762	0.0000	0.0286	0.9497	0.5266	0.0000	0.0000	0.0000
223	0.3311		0.0000	0.8932	0.4689	0.1623		
224	0.6799			0.8068	0.5530			
225	0.4174		0.0000	0.7757	0.8309	0.2629		
226	0.6040			0.9274	0.6816	0.2231		
227	0.4735		0.1414	1.0218	0.7306	0.0000		
228	0.5265		0.0000	1.3061	0.7997			
229	0.8075	0.0000	0.0138	1.6606	0.8906	0.8848	0.0000	
230	0.7327		0.0000	1.5454	0.9049	0.4804		
231	0.9359		0.0000	1.9338	1.0781	0.7318		
232	0.5048		0.0000	1.4844		0.5346	0.0000	
233	0.9662			1.3746	0.8714	0.6526	0.0000	
234	1.0347		0.0000	1.8620	0.9546	1.3220	0.0000	
236	0.8383		0.0000	1.3060	0.8021	1.2452	0.0639	0.0000
237	0.7952			0.7952			0.0000	
239	0.7495		0.0000	1.3062	0.4575	1.2341		
240	0.6629		0.0000	1.2293	0.3651	1.0571		
243	0.3894		0.0100	0.8268	0.0912	0.6295	0.0000	0.0000
245	0.3142		0.0000	0.8909	0.0000	0.3659	0.0000	
246	0.3496			0.5488	0.0000	0.5000	0.0000	
247	0.2244		0.0000	0.6767	0.0529	0.1678	0.0000	
248	0.2094		0.0000	0.6189	0.0000	0.2186	0.0000	
249	0.1616			0.4847	0.0000	0.0000	0.0000	
250	0.1172		0.0000	0.4689	0.0000	0.0000	0.0000	
251	0.1017			0.2927	0.0124	0.0000	0.0000	
252	0.0824		0.0000	0.3297	0.0000	0.0000	0.0000	
253	0.0167			0.0501	0.0000	0.0000	0.0000	
254	0.0333		0.0308	0.1024	0.0000	0.0000	0.0000	
255	0.0597		0.0418	0.1970	0.0000	0.0000		
258	0.0584		0.0000	0.2232	0.0104	0.0000	0.0000	0.0611
259	0.0363		0.0000	0.1452	0.0000	0.0000	0.0000	
260	0.0436		0.0000	0.1745	0.0000	0.0000	0.0000	
261								
262	0.0259		0.0000	0.1037	0.0000	0.0000		
264	0.0000		0.0000	0.0000	0.0000	0.0000		
265	0.0000		0.0000	0.0000	0.0000	0.0000		
266	0.0000		0.0000	0.0000	0.0000	0.0000	0.0000	
269	0.0000		0.0000	0.0000	0.0000	0.0000	0.0000	
272	0.0000		0.0000	0.0000	0.0000	0.0000	0.0000	
273	0.0201		0.0283	0.0519	0.0000	0.0000	0.0000	
274	0.0000		0.0000	0.0000	0.0000	0.0000		
275	0.0284		0.0252	0.0409	0.0320	0.0157		
276	0.0036		0.0000	0.0000	0.0143	0.0000		
279	0.0305		0.0244	0.0537	0.0261	0.0179		
281	0.0335	0.0377	0.0000	0.0531	0.0152	0.0658	0.0434	0.0519
283	0.0269		0.0309	0.0342	0.0228	0.0195		
286	0.0000			0.0000	0.0000	0.0000		
290	0.0376		0.0183	0.0814	0.0212	0.0294		
291								
292	0.0262		0.0285	0.0286	0.0000	0.0476		
293	0.0000		0.0000	0.0000	0.0000	0.0000		
294	0.0000		0.0000	0.0000	0.0000	0.0000		
295	0.0000		0.0000	0.0000	0.0000	0.0000		
297	0.0000		0.0000	0.0000	0.0000	0.0000		
300	0.0000		0.0000	0.0000	0.0000	0.0000		
301	0.0000		0.0000	0.0000	0.0000	0.0000		
302	0.0000		0.0000	0.0000	0.0000	0.0000		
303	0.0000		0.0000	0.0000	0.0000	0.0000		
304	0.0000		0.0000	0.0000	0.0000			
305								
306								
307	0.0000		0.0000	0.0000	0.0000	0.0000		
308	0.0000		0.0000	0.0000	0.0000	0.0000		
309	0.0000		0.0000	0.0000	0.0000	0.0000		
310	0.0000		0.0000	0.0000	0.0000	0.0000		
311	0.0000		0.0000	0.0000	0.0000	0.0000		

xyz time-depth-conc. bt data for o-tfmba in pumping well

depth Julian day	normalize conc.*	2	3*	4*	5*	6*	7	8
185	2.5914	0.0409	4.6628	0.0256	5.6353	0.0418	0.0160	0.0000
188	2.9240	0.0101	1.1177	6.6427	2.2606	1.6750	0.0000	0.3084
189	1.8264	0.0000	0.1796	2.5193	2.1517	2.4548	0.0074	0.0097
190	0.6994	0.0000	0.0649	1.7912	0.5691	0.3725	0.0061	0.0000
191	0.4102	0.0000	0.0375	1.1610	0.3830	0.0590	0.0131	0.0000
194	0.1690	0.0215	0.0174	0.6585	0.0000	0.0000	0.0000	0.0000
195	0.1575	0.0064	0.0333	0.1550	0.4418	0.0000	0.0000	0.0000
197	0.0076	0.0099	0.0000	0.0302	0.0000	0.0000	0.0000	0.0198
198	0.0486	0.0248	0.0224	0.0181	0.1539	0.0000	0.0106	0.0164
199	0.0462	0.0102	0.0116	0.0340	0.1230	0.0160	0.0230	0.0144
200	0.0600	0.0000	0.0000	0.0266	0.1918	0.0215	0.0292	0.0239
202	0.0536	0.0290	0.0134	0.0116	0.1779	0.0115	0.0165	0.0200
203	0.0000	0.0112	0.0000	0.0000	0.0000	0.0000	0.0000	0.0000
204	0.0000	0.0000	0.0000	0.0000	0.0000	0.0000	0.0000	0.0000
205	0.0000	0.0000	0.0000	0.0000	0.0000	0.0000	0.0000	0.0000
208	0.0234	0.0000	0.0378	0.0000	0.0557	0.0000	0.0155	0.0576
207	0.0434	0.0139	0.0290	0.0457	0.0825	0.0162	0.0301	0.0000
208	0.0282	0.0231	0.0497	0.0162	0.0189	0.0282	0.0330	0.0465
209	0.0257	0.0250	0.0609	0.0229	0.0189	0.0000	0.0000	0.0000
210	0.0073	0.0536	0.0000	0.0000	0.0220		0.0312	0.0343
211	0.0218	0.0472	0.0293	0.0000	0.0577	0.0000		0.0243
212	0.0200	0.0326	0.0182	0.0000	0.0421	0.0216	0.1221	0.1220
213	0.0354	0.0620	0.0000	0.1115	0.0000	0.0300	0.0180	0.0000
217	0.0212	0.0000	0.0000	0.0286	0.0000	0.0562	0.0280	0.0544
218	0.0000	0.0000	0.0000	0.0000	0.0000	0.0000	0.0000	0.0159
219	0.1032	0.0560	0.0484	0.0519	0.3123	0.0000		
220	0.0000		0.0000	0.0000	0.0000	0.0000		
221	0.0000	0.0000	0.0000	0.0000	0.0000	0.0000	0.0000	0.0000
222	0.0373	0.0000	0.0000	0.0648	0.0844	0.0000	0.0000	0.0188
223	0.0000		0.0000	0.0000	0.0000	0.0000		
224	0.0000			0.0000	0.0000			
225	0.0000		0.0000	0.0000	0.0000	0.0000		
226	0.0163			0.0000	0.0651	0.0000		
227	0.0000		0.0000	0.0000	0.0000	0.0000		
228	0.0000		0.0000	0.0000	0.0000			
229	0.0000	0.0000	0.0000	0.0000	0.0000	0.0000	0.0000	
230	0.0000		0.0000	0.0000	0.0000	0.0000		
231	0.0000		0.0000	0.0000	0.0000	0.0000		
232	0.0000		0.0000	0.0000		0.0000	0.0000	
233	0.0000			0.0000	0.0000	0.0000	0.0000	
234	0.0000		0.0000	0.0000	0.0000	0.0000	0.0000	
236	0.0000		0.0000	0.0000	0.0000	0.0000	0.0000	0.0603
237	0.0000			0.0000			0.0000	
239	0.0000		0.0000	0.0000	0.0000	0.0000		
240	0.0000		0.0000	0.0000	0.0000	0.0000		
243	0.0000		0.0000	0.0000	0.0000	0.0000	0.0000	0.0000
245	0.0000		0.0000	0.0000	0.0000	0.0000	0.0000	
246	0.0000			0.0000	0.0000	0.0000	0.0000	
247	0.0000		0.0000	0.0000	0.0000	0.0000	0.0000	
248	0.0000		0.0000	0.0000	0.0000	0.0000	0.0000	
249	0.0000			0.0000	0.0000	0.0000	0.0000	
250	0.0163		0.0000	0.0650	0.0000	0.0000	0.0000	
251	0.0000			0.0000	0.0000	0.0000	0.0000	
252	0.0000		0.0000	0.0000	0.0000	0.0000	0.0000	
253	0.0000			0.0000	0.0000	0.0000	0.0000	
254	0.0000		0.0000	0.0000	0.0000	0.0000	0.0000	
255	0.0000		0.0000	0.0000	0.0000	0.0000		
258	0.0018		0.0000	0.0000	0.0070	0.0000	0.0000	0.0000
259	0.0000		0.0000	0.0000	0.0000	0.0000	0.0000	
260	0.0000		0.0000	0.0000	0.0000	0.0000	0.0000	
261								
262	0.0000		0.0000	0.0000	0.0000	0.0000		
264	0.0000		0.0000	0.0000	0.0000	0.0000		
265	0.0000		0.0000	0.0000	0.0000	0.0000		
266	0.0000		0.0000	0.0000	0.0000	0.0000	0.0000	
269	0.0000		0.0000	0.0000	0.0000	0.0000	0.0000	
272	0.0000		0.0000	0.0000	0.0000	0.0000	0.0000	
273	0.0000		0.0000	0.0000	0.0000	0.0000	0.0000	
274	0.0000		0.0000	0.0000	0.0000	0.0000		
275	0.0000		0.0000	0.0000	0.0000	0.0000		
278	0.0000		0.0000	0.0000	0.0000	0.0000		
279	0.0000		0.0000	0.0000	0.0000	0.0000		
281	0.0000	0.0000	0.0000	0.0000	0.0000	0.0000	0.0000	0.0000
283	0.0000		0.0000	0.0000	0.0000	0.0000		
286	0.0000			0.0000	0.0000	0.0000		
290	0.0000		0.0000	0.0000	0.0000	0.0000		
291								
292	0.0000		0.0000	0.0000	0.0000	0.0000		
293	0.0000		0.0000	0.0000	0.0000	0.0000		
294	0.0000		0.0000	0.0000	0.0000	0.0000		
295	0.0000		0.0000	0.0000	0.0000	0.0000		
297	0.0000		0.0000	0.0000	0.0000	0.0000		
300	0.0000		0.0000	0.0000	0.0000	0.0000		
301	0.0000		0.0000	0.0000	0.0000	0.0000		
302	0.0000		0.0000	0.0000	0.0000	0.0000		
303	0.0000		0.0000	0.0000	0.0000	0.0000		
304	0.0000		0.0000	0.0000				
305								
306								
307	0.0000		0.0000	0.0000	0.0000	0.0000		
308	0.0000		0.0000	0.0000	0.0000	0.0000		
309	0.0000		0.0000	0.0000	0.0000	0.0000		
310	0.0000		0.0000	0.0000	0.0000	0.0000		
311	0.0000		0.0000	0.0000	0.0000	0.0000		

xyz time-depth-conc. bt data, f			pfba	in pumping well				
depth	normalize	2	3*	4*	5*	6*	7	8
Julian da	conc.*							
185	0.0000	0.0000	0.0000	0.0000	0.0000	0.0000	0.0000	0.0000
188	0.0330	0.0000	0.1321	0.0000	0.0000	0.0000	0.0820	0.0585
189	0.1889	0.1895	0.5738	0.0000	0.1819	0.0000	0.0000	0.0000
190	0.3871	0.0000	1.5483	0.0000	0.0000	0.0000	0.0000	0.0000
191	0.3841	0.0000	1.5363	0.0000	0.0000	0.0000	0.0000	0.0000
194	0.4438	0.0000	1.2233	0.0000	0.5520	0.0000	0.0230	0.0000
195	0.8107	0.0000	2.9493	0.0906	0.2031	0.0000	0.0000	0.0000
197	0.5391	0.0000	1.6298	0.0453	0.4811	0.0000	0.0000	0.0000
198	0.7231	0.0000	1.2025	0.1318	1.5580	0.0000	0.0000	0.0000
199	1.0984	0.0000	0.9094	0.1283	3.3560	0.0000	0.0000	0.0000
200	6.3433	0.0344	2.4459	0.4868	22.4404	0.0000	0.0000	0.0000
202	6.1303	0.0000	2.3845	0.4819	21.6547	0.0000	0.0000	0.0000
203	1.9486	0.0000	0.5626	0.7521	5.4797	0.0000	0.0000	0.1614
204	2.2545	0.0000	0.4546	2.2228	6.3405	0.0000	0.0000	0.0000
205	3.2157	0.0363	0.4560	4.4139	7.9926	0.0000	0.0000	0.0000
206	3.7771	0.0000	0.3539	6.2998	8.1051	0.3498	0.0000	0.0000
207	3.4509	0.0000	0.4538	6.3619	5.2327	1.7550	0.0000	0.0000
208	2.8344	0.0000	0.3321	5.6530	2.6702	2.6821	0.0000	0.0000
209	2.8904	0.0550	0.3085	6.2985	1.5183	3.4363	0.0000	0.0000
210	2.5823	0.0000	0.2503	7.1455	0.3513		0.0000	0.0000
211	3.0270	0.0000	0.3550	6.6810	0.7361	4.3360		0.0000
212	1.2134	0.0000	0.4642	2.5793	0.3582	1.4520	0.0000	0.0000
213	1.3187	0.0000	0.1109	3.0338	0.0624	2.0676	0.0000	0.0000
217	1.2380	0.0000	0.1595	4.0000	0.0000	0.7925	0.0000	0.0000
218	0.4989	0.0000	0.0000	1.4373	0.0000	0.5585	0.0000	0.0000
219	0.5633	0.0000	0.0000	1.2500	0.5532	0.4500		
220	0.3517		0.0467	1.0001	0.0000	0.3598		
221	0.2657	0.0000	0.0000	0.7279	0.0000	0.3349	0.0000	0.0000
222	0.3057	0.0000	0.0821	0.7670	0.0000	0.3738	0.0000	0.0000
223	0.2584		0.0000	0.6552	0.0000	0.3782		
224	0.3157			0.8313	0.0000			
225	0.4528		0.6330	0.5785	0.0000	0.5997		
226	0.3926			0.5142	0.0000	0.6636		
227	0.7878		2.0420	0.5054	0.0000	0.6038		
228	0.6678		2.2674	0.4039	0.0000	0.0000		
229	0.7627	0.1209	2.2524	0.3321	0.0000	0.4662	0.0000	
230	0.6734		1.9319	0.3109	0.0000	0.4506		
231	0.8278		2.2567	0.5320	0.0000	0.5227		
232	0.7183		1.9350	0.5418		0.3962	0.0000	
233	0.3558			0.6930	0.0000	0.3743	0.0000	
234	0.9806		3.0011	0.8322	0.0000	0.2892	0.0000	
236	0.9722		3.2064	0.5561	0.1261	0.0000	0.0000	0.0000
237	0.5360			0.5360			0.0000	
239	1.4298		5.0033	0.4493	0.2665	0.0000		
240	1.2400		4.2088	0.4825	0.2686	0.0000		
243	0.7549		0.8855	1.6852	0.2779	0.1909	0.0000	0.0000
245	0.5131		0.0000	1.6685	0.3839	0.0000	0.0000	
246	0.5861			1.4125	0.2859	0.0000	0.0000	
247	0.3528		0.0000	1.1806	0.2304	0.0000	0.0000	
248	0.3605		0.0000	1.2108	0.2313	0.0000	0.0000	
249	0.5303			1.3531	0.2379	0.0000	0.0000	
250	0.3150		0.0000	0.9712	0.2888	0.0000	0.0000	
251	0.4536			0.9431	0.3600	0.0576	0.0000	
252	0.3266		0.0000	0.8971	0.4091	0.0000	0.0000	
253	0.2354			0.2236	0.4825	0.0000	0.0000	
254	0.3208		0.0000	0.8967	0.3864	0.0000	0.0000	
255	0.4057		0.0000	0.9813	0.6413	0.0000		
258	0.3051		0.0000	0.4361	0.7844	0.0000	0.0000	0.0000
259	0.3293		0.1751	0.1637	0.8846	0.0937	0.0000	
260	0.2508		0.1498	0.0000	0.8532	0.0000	0.0000	
261								
262	0.2139		0.0000	0.0000	0.8554	0.0000		
264	0.4239		0.0000	0.2904	1.1818	0.2232		
265	0.6572	0.0000	0.0000	0.2721	2.3565	0.0000		
266	0.4671		0.0000	0.2896	1.4873	0.0914	0.0000	
269	0.7975		0.0000	0.3000	2.5685	0.3213	0.0000	
272	0.8747		0.0000	0.9335	2.2268	0.3384	0.0000	
273	0.7868		0.0000	0.8230	1.9502	0.3740	0.0000	
274	0.8877		0.0000	1.1487	1.1343	0.4678		
275	0.5737		0.0000	0.9223	0.9505	0.4221		
276	0.7576		0.0000	1.2177	1.1967	0.6167		
279	0.6868		0.0000	0.8478	1.2691	0.6302		
281	1.0083	0.0000	0.0000	1.3779	1.8670	0.7883	0.0000	0.0000
283	0.3834		0.0000	0.8721	0.2179	0.4435		
286	0.6500			0.7820	0.7682	0.3998		
290	0.2526		0.0000	0.6162	0.3942	0.0000		
291								
292	0.4037		0.0000	0.7700	0.4690	0.3756		
293	0.5757		0.0000	1.1255	0.6488	0.5286		
294	0.6066		0.0000	1.2368	0.6204	0.5690		
295	0.4653		0.0000	1.2604	0.6008	0.0000		
297	0.7036		0.0000	1.4900	0.5233	0.8011		
300	0.7735		0.0000	1.0975	0.8225	1.1740		
301	0.6143		0.0000	1.0732	0.4653	0.9188		
302	0.6521		0.0000	1.1015	0.4769	1.0300		
303	0.7735		0.0000	1.5282	0.4637	1.1021		
304	0.5326		0.0000	1.0652				
305								
306								
307	0.4689		0.0000	1.0556	0.4741	0.3458		
308	0.3186		0.0000	0.3807	0.0661	0.8277		
309	0.5429		0.0000	0.9955	0.4216	0.7546		
310	0.3356		0.0000	0.2174	0.4593	0.6656		
311	0.2828		0.0000	0.9383	0.0628	0.1300		